

POLITECNICO DI TORINO

Mechanical Engineering

Master's Thesis

CNG-H₂ engine model in CONVERGE



Candidate:

Mirko Di Battista

Supervisors:

Daniela Misul

Mirko Baratta

Academic Year

2020/2021

*Ai miei genitori,
alla mia famiglia,
a me.*

Abstract

This thesis follows the study and development of the CFD model of H₂ engines using a previous CNG engine model. To do our research, a CFD commercial code CONVERGE was used, which has allowed us to reduce the time for the model pre-processing, thanks to the independent meshing tools its sophisticated algorithms that can refine the mesh locally. All our study was conducted on the Fiat FIRE 1400 16V engine, which is installed in the test bench of DENERG laboratories. In this thesis, the models ECFM and ISSIM were used, which allowed the combustion described by splitting the chemical parameters from the physical one, reducing the numerical cost, and avoiding reproducing all the combustion kinematics. Using 0D and 1D combustion simulator software DARS, the laminar flame speed table was introduced in the converge model. The work can be divided into two main phases: in the first one, we have increased the load in a CNG engine model previously developed and studied in Paolo De Angelis' thesis. Since experimental data weren't available for the full load, we used the 0D 1D software GT-POWER to obtain intake and exhaust pressure. Later, we developed a CNG DI engine model in CONVERGE using the SOURCE CELL METHOD and using the previous results in the PFI engine.

Contents

Abstract	I
1 Introduction	1
2 Experimental data	2
2.1 Experimental layout	2
2.1.1 Engine Main Characteristics	2
2.1.2 Intake system	3
2.1.3 Fuel supply system	3
2.1.4 Sensors	3
2.2 Data acquisition system and data conditioning and parameters for model validation	5
2.2.1 Parameters for model validation	5
2.2.1.1 Mean intake pressure, pressure at the spark advance, fuel mass in the chamber and trapped mass in the chamber	5
2.2.1.2 Peak pressure, peak angle, mass fraction burned and heat release rate	7
2.2.2 Data conditioning	8
3 CFD Model Setup	11
3.1 Boundaries and initial conditions	11
3.1.1 Initial conditions	11
3.1.2 Boundary conditions	12
3.1.3 Law of the wall (y^+)	13
3.2 Meshing in CONVERGE	16
3.2.1 Fixed Embedding	16
3.2.2 Adaptive Mesh Refinement (AMR)	17
3.2.3 Mesh adopted	21
3.3 Combustion model	22
3.3.1 ISSIM (Imposed Stretch Spark Ignition Model)	22
3.3.2 ECFM (Extended Coherent Flamelet Model)	30

3.4 Injector model (Source Cell method)	35
4 GT-POWER Model Setup	39
4.1 Editing of the previous PFI model	39
4.2 DI model	43
5 Simulation results	46
5.1 2000x12 and 2000x14 simulations	46
5.2 PFI engine load increase on GT-POWER	49
5.3 PFI Full load simulation	53
5.4 DI engine studies on GT-POWER	58
6 Conclusions	66
Nomenclature	II
Bibliography	VI

Chapter 1

Introduction

The pollution restriction introduced in 2021 led the automotive research field to develop new engines, increasingly sophisticated, introducing direct injection, EGR dilutes, variable valve opening, etc. And also the automotive research is step by step moving from the gasoline to new fuel as methane and hydrogen. It is quite important to consider that H₂ ICE vehicles can reach an efficiency almost equal to the FC vehicles at full load. Also H₂ produced for ICE has not to be perfectly pure, this is one of the main advantages of H₂ for ICE: it is less expensive than H₂ for FC. Hydrogen is a very interesting solution, it has a high laminar speed flame and its combustion produces nearly zero CO₂, HC, and CO emissions. In order to develop a proper engine model, a CFD model has to be used. To simulate the combustion process the ECFM model was used. The PFI model was previously developed using experimental data of a CNG engine installed on the DENERG test bench. My thesis aims to develop an H₂ engine model using the previously validated CNG engine model and to compare their performances. It can be observed in the literature that bmep of an H₂ PFI engine is really low compared to the bmep of a CNG PFI engine due to the low density of hydrogen and the risk of backfiring, which is the combustion of the hydrogen in the intake port. This problem leads us to study and develop a DI model; in fact, thanks to the direct injection in the chamber the problem of the very low density of hydrogen were eliminated, also the risk of backfiring was deleted, due to the absence of H₂ in the intake port in an H₂ engine. Also, using the SOURCE CELL METHOD, it was possible to simulate a DI engine model without defining the geometry and mechanics of the injector. In the last phase of the work, a rudimental H₂ DI engine model was developed.

Chapter 2

Experiment data

In this section is quickly described the engine Fiat FIRE 1400, with particular attention on how the data has been processed using a Matlab script, since all the data get from the experiment has to be synthesize in information useful for the model setup and validation.

2.1 Experimental layout

First of all we're going to describe the main characteristic of the Fiat FIRE 1400 and the sensors used in the test bench. This was already studied and analized by Marco Mina[1] and Paolo De Angelis[2] in their thesis, indeed all the reported information are taken from their thesis.

2.1.1 Engine main characteristics

The engine studied is a Fiar FIRE 1.4 16V Turbo CNG, which is installed in the DENERG, *Figure 2.1*, and made by Centro Ricerche Fiat in Orbassano, with the aim to develop a new generation engine with reduced sizes and with higher, or at least equal, power, following the “downsizing” logic, and optimized for the methane and NG combustion. In the *table 2.1* are reported the main characteristics of the engine.

Engine main characteristics (Tab 2.1)	
Cycle	Otto, four-stroke
Fuel supply	Metatron METAFUEL 6AO.PNT injector
Valves	16V, two crankshaft in head
Intake valve opening (IVO)	TDC -3°
Intake valve closing (IVC)	BDC $+37^{\circ}$
Exhaust valve opening (EVO)	BDC $+37^{\circ}$
Exhaust valve closing (EVC)	TDC -3°
Cylinders	4 (inline)
Bore	72 mm
Stroke	84 mm
Displacement	1368 cm ³
Connencting rod length	129 mm
Compression ratio	9.8



Figure 2.1: Engine and test bench under construction

2 Experimental data

2.1.2 Intake system

The engine intake system for the fiat FIRE it is made by: (listed following the nearness to the engine)

- indirect air mass flow rate meter Speed Density - Lambda type;
- wired controlled butterfly valve, for load regulation;
- idle air control actuator;
- intercooler air-water;
- centrifugal radial compressor.

2.1.3 Fuel supply system

The fuel supply system mounted on the engine is consisting by three main components:

- *Tartarini Meta M* pressure regulator;
- injectors rail;
- gas electro-injectors per cylinder.

2.1.4 Sensors

In *Figure 2.2*, is reported the complete experiment layout, it can be observed that there are many sensors and measuring instruments to monitor the main physical quantities, temperature, pressure, mass flow rate, gas components mass fraction. We can split these sensors in four groups:

- on engine sensors:
 - pressure and temperature in inlet manifold;
 - pressure in the chamber for each cylinder;
 - pressure in the 4 intake runners and in the exhaust ones;
 - additional pressure sensor at the inlet runner of cylinder 2 to analyse the pressure wave in the manifold;
 - temperature in the inlet and outlet runners;
 - pressure and temperature in the compressor inlet and outlet;
 - pressure and temperature in the turbine inlet and outlet;
 - water and temperature at the inlet and outlet of engine cooling system;
 - pressure and temperature of lubrication oil.
- intake system sensors:
 - environment temperature and pressure;
 - air mass flow rate;
 - pressure and temperature in the setting chamber;
 - fuel mass flow rate, consumption and temperature;
 - pressure and temperature after the intercooler;
 - water temperature at the intercooler inlet and outlet.
- exhaust system sensors:
 - air to fuel ratio (A/F);
 - pollutants;
- on brake sensors:
 - Engine torque and speed;
 - High accuracy speed from additional encoder.

2 Experimental data

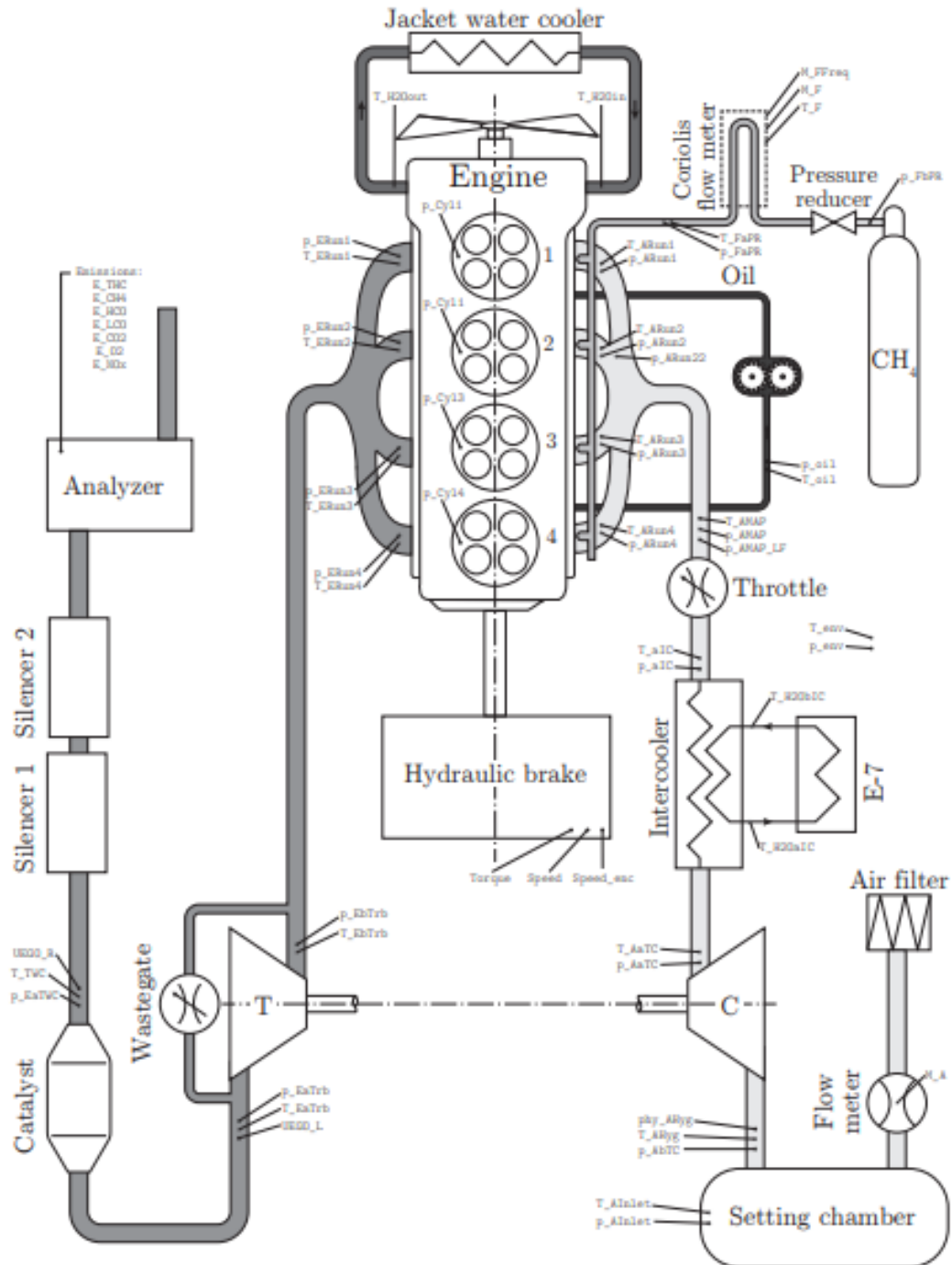


Figure 2.2: Experimental layout

2.2 Data acquisition system and data conditioning and parameters for model validation

The DAQ system is used to collect the signal from all the trasducers. In this thesis it won't be described, to know more: [1, pp 76-113] [2, pp 19-24].

2.2.1 Parameters for model validation

A CFD model can be splitted in 3 main problems:

- Fluid dynamic problem: it is governed by Navier-Stokes equations and give us the velocity field \mathbf{v} and the pressure distribution \mathbf{p} ;
- Thermal problem: it is described by the law of conservation of energy, and give us the temperature T ;
- Combustion problem: it is modelled by a set of Arrhenius and diffusion equations, that give us the concentration of the various species and the heat realise by each reaction. (actually it is a subpart of the thermal problem, but, since the importance of the combustion process we analyze it as a separated problem).

The CFD model of an ICE is validated considering the goodness of the velocity field, the pressure distribution and the combustion model.

In order to validate the model experimental data have to be considered:

- $p_{cyl}(\theta)$: average pressure in cylinder 1 [bar];
- \dot{m}_f : fuel mass flow rate [kg/h];
- α : air-fuel ratio [-].

For the fluid dynamics problem we focus on the turbulnce, the transport of the fresh charge during the intake phase (where there isn't an interference with the combustion process). We compare the following data:

- $\langle p \rangle_{int}$: mean intake pressure in cylinder 1 [bar];
- $\langle p \rangle_{SA}$: pressure at the spark advance [bar];
- m_f : fuel mass in the chamber [mg];
- m_{cyl} : trapped mass in the chamber [mg].

2.2.1.1 Mean intake pressure, pressure at the spark advance, fuel mass in the chamber and trapped mass in the chamber

To evaluate the mean intake pressure a range of angles, in which the intake phase happens, has to be identified. We properly choose a thresold $h_{v,min}$ beyond which we consider that the valve is opened. We identify this range as: $Range = \{\theta \in R | h_{v,int}(\theta) \geq h_{v,min}\}$.

The mean intake pressure can be obtained making an arithmetic average of the cylionder pressure during that range.

$$\langle p \rangle_{int} = \frac{1}{N} \sum_{i=1}^N p_{cyl}(\theta_i) \text{ where } \theta_i \in Range \quad (2.1).$$

To calculate the pressure at the spark we consider the value of the pressure inside the combustion chamber during the spark advance.

2 Experimental data

The fuel mass in the chamber is the amount of fuel entered in the chamber during the suction phase. CONVERGE provide us an output of this value (species_mass_region_0.out in kg).

$$m_{f,model}[mg] = mf(\theta_0)[kg]10^3 \text{ where } \theta_{IVC} < \theta_0 < \theta_{SA} \quad (2.2).$$

For the experimental data we obtain it from the fuel mass flow rate:

$$m_{f,exp}[mg] = \frac{\frac{mf[\frac{kg}{h}]}{\frac{3600}{n[rpm]}} \frac{10^3}{2}}{\frac{60}{2}} \quad (2.3).$$

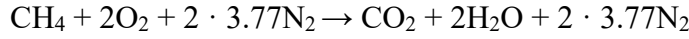
Trapped mass in the chamber can be evaluated in two different ways:

- It can be evaluated using the air-fuel ratio α and the fuel mass previously calculated m_f
 $m_{cyl} = (1 + \alpha)m_f \quad (2.4).$
- It can be calculated taking into account the residues of combustion. First of all we consider the total mass trapped in the cylinder between IVC and EVO and the mass of CO₂ trapped in the cylinder between IVC and SA (CONVERGE save them in the species_mass_region0.out).

$$m_{cyl,model}[mg] = m(\theta_0)[kg]10^3 \text{ where } \theta_{IVC} < \theta_0 < \theta_{EVO} \quad (2.5).$$

$$m_{r,CO_2}[mg] = m_{CO_2}(\theta_0)[kg]10^3 \text{ where } \theta_{IVC} < \theta_0 < \theta_{SA} \quad (2.6).$$

Considering the balance equation of the combustion the mass fraction of CO₂ in the exhaust (x_{CO_2}) can be calculated.



$$\begin{aligned} \rightarrow m_f(1 + \alpha) &= \frac{m_f}{M_{CH_4}} (M_{CO_2} + 2M_{H_2O} + 7.54M_{N_2}) = m_{exh} \\ \rightarrow \frac{m_{CO_2}}{m_{exh}} &= x_{CO_2} = \frac{M_{CO_2}}{M_{CH_4}(1 + \alpha)} = \frac{44.01 \text{ kg/kmol}}{16.04 \frac{\text{kg}}{\text{kmol}} (1 + 17.09)} = 0.152 \end{aligned}$$

Dividing the mass of carbon dioxide, the total mass of residues is calculated, then by dividing for the total mass the mass fraction of residue is obtained ($x_{r,model}$) that are present in the cylinder.

$$x_r = \frac{m_{r,CO_2}}{x_{CO_2} m_{cyl,exp}}. \quad (2.7).$$

Using the 2.3 the trapped mass for is calculated, assuming that the percentage of residues in the model is close to the experimental one.

$$\begin{aligned} x_{r,exp} &\approx x_{r,model} = x_r \\ m_{cyl,exp}[mg] &= m_{f,exp}[mg](1 + \alpha)(1 + x_r) \end{aligned} \quad (2.8).$$

It can be observed that the first method requires the mass of the fuel, while the second one is independent.

For the combustion problem the range between SA and EVO is observed, the following parameters are observed:

p_{peak} peak pressure [bar]

θ_{peak} peak angle [bar]

2 Experimental data

$MF B_{50}$ angle at which half of the fuel was burned [deg]

$MF B_{10-90}$ length of the interval from 10% to 90% of burned fuel [deg]

HR_{tot} total heat release [J]

2.2.1.2 Peak pressure, peak angle, mass fraction burned and heat release rate

The peak pressure and angle can be evaluated considering the maximum of the experimental line and the simulation line (CONVERGE save it in the thermo_region0.out file).

Manipulating the pressure data Heat release can be evaluated, considering losses thought the walls, it is quite important to separate Gross Heat release rate (HRR_{Gross}) and Net Heat release rate (HRR_{net}):

$$HRR_{Gross} = \frac{dQ_b}{d\theta} = \frac{k}{k-1} p \frac{dV}{d\theta} + \frac{1}{k-1} V \frac{dp}{d\theta} + \frac{dQ_l}{d\theta} \quad (2.9).$$

$$HRR_{Net} = \frac{dQ_b}{d\theta} - \frac{dQ_l}{d\theta} = \frac{k}{k-1} p \frac{dV}{d\theta} + \frac{1}{k-1} V \frac{dp}{d\theta} \quad (2.10).$$

The previous equations are got from the first principle for the close system considering a closes control volume (fig 2.3)

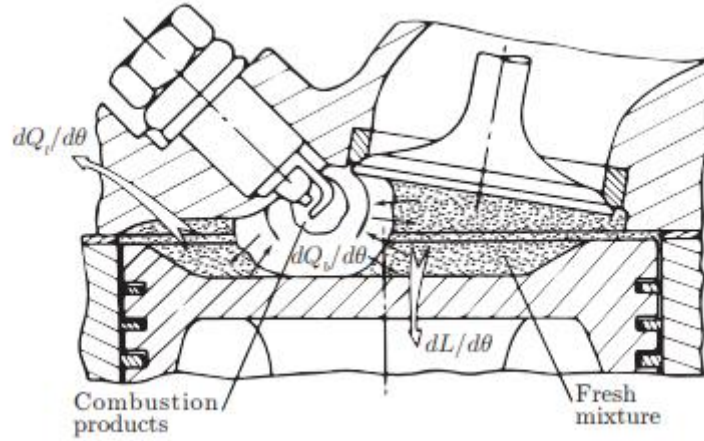


Figure 2.3: Combustion chamber of a Spark Ignition engine. $dQ_b/d\theta$ gross heat release rate supply by the burning fuel, $dQ_l/d\theta$ heat losses through the walls, $dL/d\theta$ work rate yield to the external system(piston) [3].

We use HRR_{net} to do our validation due to the impossibility to evaluate the losses rate experimentally. From now on we will call RR_{net} , HRR .

In addition we implement it using the methodology described by Michael F.J. Brunt [4], where the heat capacity ratio k is expressed by a quadratic polynomials:

$$HRR = \frac{dQ_b}{d\theta} - \frac{dQ_l}{d\theta} = \frac{k_{Br}}{k_{Br}-1} p \frac{dV}{d\theta} + \frac{1}{k_{Br}-1} V \frac{dp}{d\theta} \quad (2.11).$$

Integrating the 2.11 the total heat release is obtained:

$$HR_{tot} = \int_{\theta_{SA}}^{\theta_{EVO}} \frac{d(Q_b - Q_l)}{d\theta} d\theta \quad (2.12).$$

2 Experimental data

Since the total gross $HR Q_b$ is equal to the fuel mass times the low heating vale $mf \cdot H_l$, it is assumed that the heat release at the generic angle θ is proportional to the mass fraction burned MFB .

$$\begin{aligned} MFB(\theta) &= \frac{1}{m_f} \int_{\theta_{SA}}^{\theta_{EVO}} \frac{dm_f}{d\theta} d\theta = \frac{1}{(Q_b - Q_l)} \int_{\theta_{SA}}^{\theta_{EVO}} \frac{d(Q_b - Q_l)}{d\theta} d\theta \\ &= \frac{1}{HR_{tot}} \int_{\theta_{SA}}^{\theta_{EVO}} \frac{d(Q_b - Q_l)}{d\theta} d\theta \quad (2.13). \end{aligned}$$

A typical S-shape is found and, from it, MFB_{50} , MFB_{10} and MFB_{90} can be evaluated:

- $MFB_{50} = \{\theta \mid MFB(\theta) = 0.5\}$;
- $MFB_{10} = \{\theta \mid MFB(\theta) = 0.1\}$;
- $MFB_{90} = \{\theta \mid MFB(\theta) = 0.9\}$.

Finally MFB_{90-10} can be calculated as:

$$MFB_{90-10} = MFB_{90} - MFB_{10} \quad (2.14).$$

2.2.2 Data conditioning

To properly evaluate boundary conditions the pressure profile at inlet and outlet has to be calculated. In order to do it a Matlab script has to be used.

From Paolo De Angelis' thesis [2] the sampling frequency and the number of cycles recorded is obtained.

$$f_s = 120kHz \quad N_c = 100$$

After that all the data are collected in an array, then, since we use $\Delta\theta = 0.1^\circ$ we found the number of points per cycle:

$$N = \frac{720}{\Delta\theta} + 1 = 7201$$

Now it is possible to use the *Ensemble average* and we can evaluate the *mean pressure vector* $\langle\langle p \rangle\rangle_{int}$:

$$\langle\langle p \rangle\rangle_{int} = [\langle\langle p \rangle\rangle_{int,i}] = \frac{1}{N_c} \sum_{k=1}^{N_c} p_{Int}(\theta_i - 540 + 720k) \quad \text{for } i = 1, 2, \dots, N \quad (2.15).$$

Note that since we use the intake pressure at the cylinder 2, while our model refer to the cylinder 1, we need to shift rightward the pressure profile by a angle of 540° as show in Eq. (2.15) due the *firing order*.



Figure 2.4: firing order

2 Experimental data

Once we got the pressure profile for the single cycle we must remove all the high frequency noise due the previous process and other source in the experiment layout. We do this using a low-pass filter. The result of the process is that now the profile is smoother then the original one.

This array is now saved in a file [ORIGINAL NAME]-PINT.IN ready to be fed by CONVERGE.

This procedure was used for the intake pressure of the case 2000x14, however it can be used for the exhaust profile, following the same procedure.

Chapter 3

CFD Model setup

The section is dedicate to the discussion about all the tool used to setup the model. We will describe how to set BCs and ICs, then we will speak about CONVERGE meshing strategy and the setting that user have to change, focussing on the more interesting feature: Adaptive Mesh Refinement. About this latter we analyse in detail the algorithm describe in literature. After that we will analyze the combustion model and the source cell method.

3.1 Boundaries and initial conditions

First we define the control volume of this particular case Ω , dividing it in 3 particular regions:

- Ω_0 *cylinder* (Region 0), that is all the volume bounded by head, spark plug, liner, piston and intake valve bottom, and also when the valves are open we use a auxiliary surface that connect the valve edge to the its seat;
- Ω_1 *intake system* (Region 1), that is the volume delimited by intake runner, intake valve top and angle, and the inflow port;
- Ω_2 *exhaust system* (Region 2), that is the volume bounded by exhaust runner, exhaust valve top and angle, and the outflow port.

Therefore this 3 domain are linked by the following relation

$$\Omega = \Omega_0 \cup \Omega_1 \cup \Omega_2 \quad 3.1$$



Figure 3.1: Isometric axonometric projection of the Control Volume (cylinder, intake and exhaust runner)

3 CFD Model Setup

After that, the boundaries $\partial\Omega$ are defined: they are the surfaces that separates the CV from the environment. A mathematic definition of boundary is:

$$\partial\Omega = \{x \in R^3 \mid \forall \delta > 0 B(\delta, x) \cap \Omega \neq \emptyset \wedge B(\delta, x) \cap R^3 \setminus \Omega \neq \emptyset\} \quad (3.2)$$

Boundaries are necessary cause physical quantities ($\mathbf{v}, T, p, Y_{CH_4}$) have specific behaviours and values there. It is quite important to proper define a correct splitting of the boundaries:

- $\partial\Omega_0$ is the surface that include the piston head, liner, cylinder head, spark plug and valves bottom;
- $\partial\Omega_1$ is the surface of inlet runner and intake valve top and angle;
- $\partial\Omega_2$ is the surface of outlet runner and exhaust valve top and angle;
- $\partial\Omega_{in}$ is the inflow port ;
- $\partial\Omega_{out}$ is the outflow port.

After the geometry is defined, experimental data since the PDE problem to be “well-defined” require the boundary and initial condition (BCs and ICs). This have to be for all our equations such as momentum eq. (p, \mathbf{v}), energy eq. (T), continuity (Y_x).

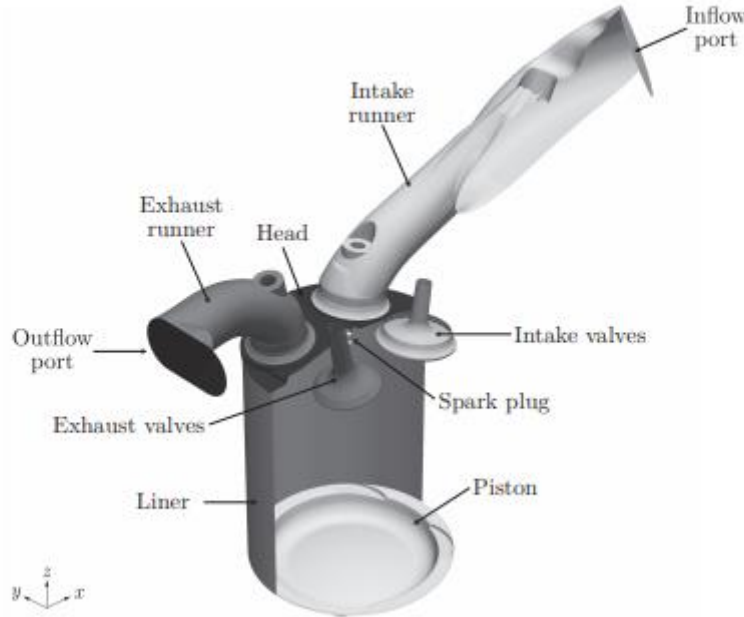


Figure 3.2: Control Volume boundaries and the nomenclature used

3.1.1 Initial conditions

- Energy equation
We set a constant temperature value for each main domain (intake, exhaust, cylinder):
 $T_{int}(\theta_0, \Omega_1)$ initial gases temperature in the intake runner [K];
 $T_{exh}(\theta_0, \Omega_2)$ initial gases temperature of the gases in exhaust runner [K];
 $T_{cyl}(\theta_0, \Omega_0)$ initial gases temperature in the cylinder [K].
- Momentum equation

3 CFD Model Setup

We the initial velocity field according to the piston and valves position at the starting time (e.g. if we are at the exhaust BDC we can set a null vector field in the two runners and a linear decreasing field $v = \left[0, 0, -\omega_0 \frac{x}{h}\right]^T$ in the piston).

- Continuity equation

We set the initial gas composition in the three domains, by using the A/F ratio, α , give to us by the lambda-sensors. Since in our case we start at the exhaust phase with the cylinder at BDC (180°), thus in the cylinder and in the outlet runner we impose the exhaust gas composition Eq. (3.4), while in the intake manifold we set the inlet mixture Eq. (3.3).

$$\begin{aligned} Y_{CH_4} &= \frac{1}{1+\alpha}; Y_{O_2} = \frac{\alpha}{1+\alpha} \frac{1}{1+3.77}; Y_{N_2} = \frac{\alpha}{1+\alpha} \frac{3.77}{1+3.77} \\ Y_{CO_2} &= \frac{1}{1+\alpha} \frac{M_{CO_2}}{M_{CH_4}}; Y_{H_2O} = Y_{CO_2} \frac{M_{H_2O}}{M_{CO_2}} 2; Y_{N_2} = \frac{\alpha}{1+\alpha} \frac{3.77}{1+3.77}; Y_{O_2} = \frac{\alpha}{1+\alpha} \frac{3.77}{1+3.77} - \\ &Y_{CO_2} \frac{M_{H_2O}}{M_{CO_2}} 2 \end{aligned} \quad (3.3)$$

where Y is the mass fraction, M is the molar mass, and 3.77 is the mean molar ratio of nitrogen over oxygen in the air ($\frac{N_2[mol]}{O_2[mol]} = 3.77$).

3.1.2 Boundary conditions

- Energy equation

We assume that the engine temperature has reached the steady state value, therefore we set a constant temperature on each boundary:

$TCyl(\partial\Omega_0)$ cylinder wall temperature2 . [K];

$Tint(\partial\Omega_1)$ intake duct wall temperature [K];

$Texh(\partial\Omega_2)$ exhaust duct wall temperature [K];

$Tin(\partial\Omega_{in})$ inlet temperature [K];

$Tout(\partial\Omega_{out})$ outlet temperature [K].

The last condition is replacd with an adiabatic boundary, eq (3.5) since we can assume that thermal phenomena are concluded:

$$\frac{\partial q}{\partial n} = 0 \quad (3.5)$$

- Momentum equation

The *no-slip* condition is used in all the boundaries except the inflow and outflow port, to do this as common practice is to use the *Law-of-the-wall*, were a semi-empirical law to simplify turbulent computation near the wall. While for the two port we set only the pressure using the value from the traducers installed in the runners.

$v(\theta, \partial\Omega_0)$ Law-of-the-wall (no-slip);

$v(\theta, \partial\Omega_1)$ Law-of-the-wall (no-slip);

$v(\theta, \partial\Omega_2)$ Law-of-the-wall (no-slip);

$pint(\theta, \partial\Omega_{in})$ intake pressure [Pa];

$pexh(\theta, \partial\Omega_{out})$ exhaust pressure [Pa].

- Continuity equation

The composition of the fresh charge is setted at the inlet, using the composition given by Eq (3.3), while at the exhaust there are combustion products; it is not necessary to use an equation.

3 CFD Model Setup

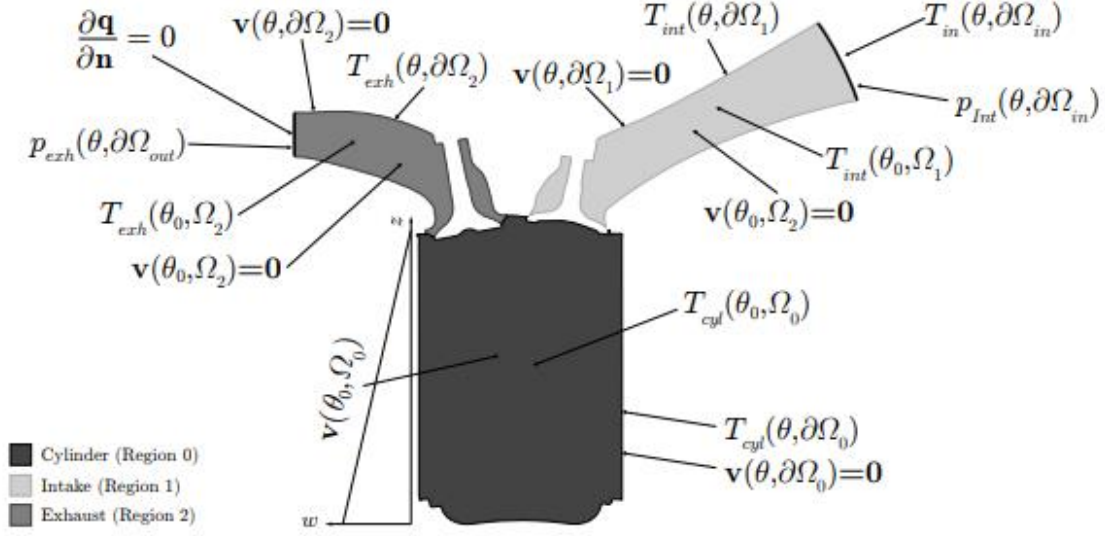


Figure 3.3: Boundary Conditions for energy and momentum equation

In Table 3.1 is reported the location or how to calculate the value for each BCs and ICs in the file with the experimental data.

Condition	How to evaluate the condition
$T_{int}(\theta_0, \Omega_1)$	T_AMAP (temperature in inlet manifold)
$T_{exh}(\theta_0, \Omega_2)$	T_ERun1 (temperature exhaust runner 1)
$T_{cyl}(\theta_0, \Omega_0)$	Since the simulation starts in the exhaust phase it is equal to T_exh
$T_{cyl}(\partial\Omega_0)$	It is considered constant and equal, for all the simulations, to the case 2000x12
$T_{int}(\partial\Omega_1)$	$T_{cyl}(\partial\Omega_0) - 50$
$T_{exh}(\partial\Omega_2)$	$T_{cyl}(\partial\Omega_0) + 50$
$T_{in}(\partial\Omega_{in})$	T_AMAP (temperature in inlet manifold)
$T_{out}(\partial\Omega_{out})$	T_ERun1 (temperature exhaust runner 1)
$p_{int}(\theta, \partial\Omega_{in})$	P_ARun22 (pressure in the intake run 2)
$p_{exh}(\theta, \partial\Omega_{out})$	p_ERun1 (pressure in the exhaust run 1)

3.1.3 Law of the wall (y+)

It is a phenomena that take place when a turbulent flow approach the wall of a duct, where the mean and fluctuating component of the speed, thus also k , vanishing causing a large gradient in the region. To better explain this let recall the Reynolds averaged Navier-Stokes Equation:

$$\frac{\partial}{\partial t} \rho \mathbf{v} + \nabla \cdot \rho \overline{\mathbf{v} \mathbf{v}} = -\nabla \bar{p} + \nabla \cdot \bar{\boldsymbol{\tau}} + \bar{\mathbf{f}}_b \quad (3.6)$$

3 CFD Model Setup

Where τ can be splitted in 2 parts:

$$\bar{\tau} = \underbrace{\mu \nabla \bar{v}}_{\text{laminar: } \tau_l} + \underbrace{-\rho \overline{v'v'}}_{\text{turbulent: } \tau_t}$$

For all the fluid that flow in a duct we can divide region according to the relative weight of this two, *Figure 3.4a*, we call *outer layer* the volume where turbulent shear stress prevail on the laminar one and thus can be neglected, and *inner layer*, also called boundary layer, where laminar part of the tensor is no more negligible. These last layers was deep studied during the first part of the 20th century, by L. Prandtl, his student T. Von Kármán, and C.B. Millikan using experiment and dimensional analysis (Buckingham π theorem). Prandtl in the 1930 conclude that velocity profile in the inner region is function of kinematic viscosity ν , fluid density ρ , wall shear stress $|\tau_w|$ and distance from the wall y :

$$u = f(\nu, \rho, |\tau_w|, y) \quad (3.7)$$

then he define the following dimensionless groups:

$$u^+ = \frac{|v - v_w|}{u_\tau} \text{ where } u_\tau = \sqrt{\frac{|\tau_w|}{\rho}} ; y^+ = \frac{d_\perp u_\tau}{\nu} \quad (3.8)$$

where u_τ is called the friction velocity or shear velocity, u^+ is the dimensionless velocity, $|v - v_w|$ is the magnitude of the relative velocity parallel to the wall, d_\perp is the normal distance to the wall, and y^+ is the normalized wall distance. Therefore the Eq. (3.7) became:

$$u^+ = F(y^+) \quad (3.9)$$

This relation it what Prandtl define as “**Law of the Wall**” expressed in inner variables, while Von Karman proposed a similar law but for outer layer call “*Velocity defect law*”. [2]

By using the y^+ is possible divide the inner layer in three regions:

- viscous sublayer $0 < y^+ \leq 5$;
- buffer sublayer $5 < y^+ \leq 30$;
- inertial sublayer $30 < y^+ \leq 200$.

The first is the region where only the stress tensor is present, the inertial is where the turbulent as a small influence and the buffer layer is where the two behaviour overlaps, show in *Figure 3.4a*.

For the first and last sublayer, between the 1930 an 1935, was proposed a empirical law that describe the speed profile. For the viscous layer the experiment show that Eq. (3.9) is linear, while for the inertial layer Von Karman and Millikan discover that the law of the wall assume a logarithmic trend, Eq. (3.10).

$$\begin{cases} u^+ = y^+ & \text{if } 0 < y^+ \leq 5 \\ u^+ = \frac{1}{k} \ln(y^+) + B & \text{if } 30 < y^+ \leq 200 \end{cases} \quad (3.10)$$

3 CFD Model Setup

where k and B are the Von Karman constant and is assigned the value $k = 0.41$ and $B = 5.25$, compute using Direct Numerical Simulation (DNS).

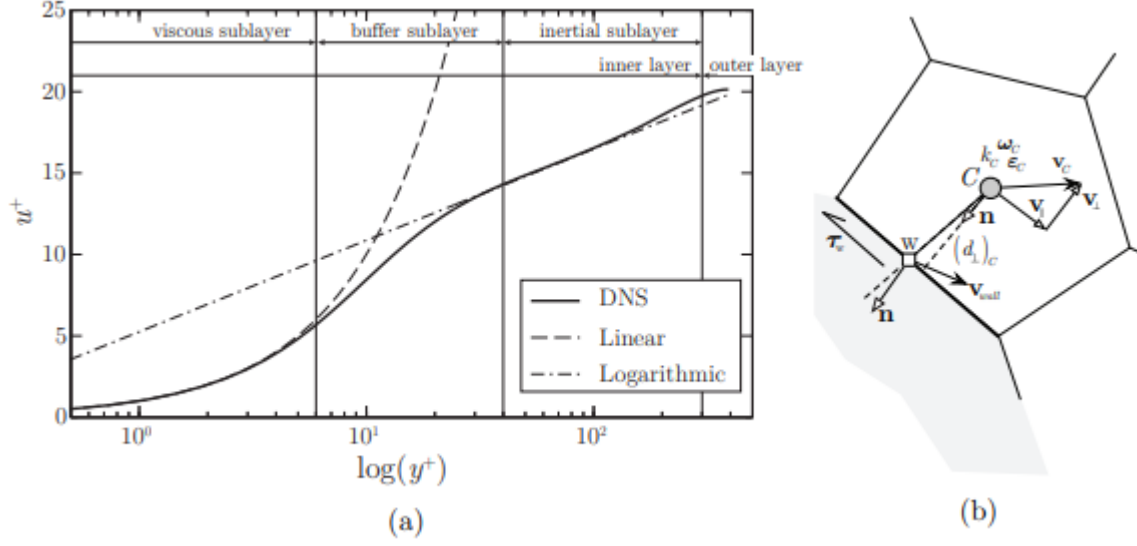


Figure 3.4: (a) velocity profile compared with linear and logarithmic approximation, $Re = 395$ [5]; (b) boundary control volume near the wall [6].

Boundary layer in CFD codes

What it described above show that a turbulent fluid that approach the wall undergo to a quick reduction since the relative speed is reduce to zero, thus the presence of high gradient made the discretization difficult, but at the same time, cause the relevance for thermodynamics problem of the stress tensor and of the heat exchange that take place in the wall, what happen in the boundary layer can not be neglected. Therefore for these needs the possibility are two. One solution is call “*Near wall model approach*” where to resolve the sublayer we increase the node number near the wall, usually this require 10-15 points in the sublayer $y^+ < 30$ and the distance of first grid point is $y^+ \approx 1$ or less. This solution require the use of a Low-Re-Model and a high numerical cost. The other solution is call “*Wall function approach*” (used in our model) where instead of to solve numerically the viscous sublayer we assume and superimpose the theoretical law of the wall, Eq. (3.10), Then we set the first node, Figure 3.4b, outside the inertial sublayer, i.e. $20 < y^+ < 200$, and we use the High-Re-Model to solve the discretization problem. Consequentially this approach reduce drastically the computational cost, but the main disadvantage is that this methodology is validated and justify for near-equilibrium condition boundary layer. Indeed the so call Standard Wall Function approach is valid only for near-equilibrium condition while the Improved Wall Function proposed by Launder and Spalding, extends the methodology also for the non equilibrium condition, but is not well-validated as the previous one.

3 CFD Model Setup

3.2 Meshing in CONVERGE

The commercial software used, CONVERGE, was developed with an autonomous meshing tool that removes the idle time spent to make and control the mesh, shaving a lot of time during the “pre-processing”, indeed the software motto is:

never make a mesh again.

Namely CONVERGE, starting from the surface of the CV stored in the .STL file, produce the structural mesh during the running time using a robust *meshing routine*, and also is recall at each time step to modify the mesh if there is a moveable component (e.g. valves and piston).

This meshing program, without going in detail, discretize the control volume starting creating a cube that includes all the CV, then the cube is discretized by dividing into small cells with the sizes (h_x, h_y, h_z) are user specified. Then the program save only cells which have the centre inside the CV forming the “**Base Mesh**”. Thanks the use of a *Cartesian structural mesh*, the softer easily handle the local refinement/coarsen of the mesh by using the “**Grid Scaling factor**” $GS \in \mathbb{Z}$. That is the number of times that the cell is divided or blended, i.e. if the GS is null the cell remains unchanged, if positive the cell is divided GS times, if negative will coarsen the base grid [7, p. 294], thus the resulting cell sizes change respect the base one as describe in Eq. (3.11).

$$h_x = \frac{h_{x,base}}{2^{GS}} \quad (3.11)$$

3.2.1 Fixed Embedding

Starting from the base mash, CONVERGE allow to specify local are where we can increase the number of cell, for example at the valve angle where the speed and pressure gradient are significant. All this localized refinement are call “Fixed Embedding”, and allow to use a coarse mesh in all the domain and refine only where is necessary, in this way we minimize the simulation time. This embedding can be also permanent, thus it is present during all the simulation, or time dependent to follow some phenomena. The software can deal only with a two-to-one connection between the cells, thus there is a transition zone between the coarse and fine area of the embedding where the grid scaling factor is progressively reduce.

The possible emending are:

Boundary;

Cylinder,Box;

Region;

Nozzle;

Injector Embedding.

Boundary embedding

It use to increase nodes in zones close to one of the CV boundary. It is always necessary, since, how explained in the subsection 3.1.3, the flow behaviour close to the wall is hard to compute, and if we want to use the wall function approach, we need that the first node falls in the buffer region. Therefore in all our models we set 2 boundary layer with the aim to have the

3 CFD Model Setup

Adimensional distance, y^+ between the wall and the first node not over $y^+ = 50$. Furthermore, we use this setting to increase more in the valve angle do guarantee that during the valve opening at least one node is present.

Cylinder, sphere and box embedding

Using this type of embedding is possible to define specific volume where we increase the grid resolution, by defining the center of the geometric figure and its main dimensions (e.g. diameter, side). The common practice in ICE models is to use the sphere embedding in the spark plug, to guarantee at least 5 nodes between the two electrodes, and the cylinder to refine the mesh in all the combustion chamber and last part of intake and exhaust manifold.

Region embedding

Like the previous tool we refine specific part of the volume, but instead of using a geometric figure we use a region of the CV define using the surface of the model and some auxiliary surface produce during the pre-processing using the software GUI: CSTUDIO. In our case, we define 3 regions, cylinder, intake and exhaust, and we refine specificity in the cylinder region, where happen the main phenomena which we are interested.

Nozzle and injector embedding

It is convenient tool specifically made for the direct injection engine, where the high pressure and speed that is present in this phenomena require a high resolution in this range. It is used for the DI model, since in this case it will be simulated a non-premixed engine.

3.2.2 Adaptive Mesh Refinement (AMR)

The Adaptive Mesh Refinement (AMR) is probably one of the most interesting provided by CONVERGE, it is the answer to the necessity of reducing the computational cost of the CFD models. Because to well resolve the velocity and temperature field we ideally need a very fine mesh or a high order interpolation, to reduce as much as possible the error introduced by the numerical approximation; while to speed up the simulation we have to reduce the degree of freedom of our problem, therefore we desire a coarse mesh and a linear interpolation (up-wind). Thus the AMR meets this necessity by reducing the mesh size only where the solution needs a refinement, e.g. where the error introduced by the approximation exceed a certain threshold, and leave or relax the grid outside this region. Since it is a new and innovative tool in the CFD studies, we made quite a deep study, to understand how it works, the advantage and the disadvantage. We will report a summary of all the mathematical theory behind it, and how the algorithm of CONVERGE work. About the first we know that the AMR is a concept that comes from the Finite Elements Methods (FEM), also call *Galerkin methods*, that are easier to handle mathematical, but fortunately can be proof that the Finite Volumes is a subset of the Discontinuous Galerkin (DG) method where the base function belong to the space X_h^0 [8, pp 47] [9, pp 220], therefore the concepts that we will explain soon refer to the FEM theory but can use as reference to understand the AMR algorithm.

3 CFD Model Setup

Model adaptivity

The aim of all the AMR is to reduce the numerical error:

$$||e_\varphi|| = ||\varphi - \varphi_h|| \quad (3.12)$$

where φ is a general scalar or vector field and φ_h is its numerical solution, and in our case φ can be the speed \mathbf{v} , the pressure p or the temperature T , e.g. $||e_v|| = ||\mathbf{v} - \mathbf{v}_h||$. To reduce it in the literature we can find many types of adaptive mesh algorithm, and they are collected in three main categories:

- **h-refinement:** refer to the techniques where we reduce the approximation error by locally reducing the maximum node distance h , thus increasing the number of node.
- **p-refinement:** refer to the techniques where the solution convergence is reached by increasing the polynomial order p of the base function, let's note the increasing the order means also that we need $p + 1$ point, otherwise the function is undetermined.
- **r-refinement:** refer to the techniques where the total node number is take constant, while the cell centre is move to increase the node density where the physical phenomena undergo to a rapid change.

The *r-refinement* is hard to apply both in the case of finite elements or volume and in case of complex shape the advantages quite disappear, without counting and also does not guarantee error reduction.

In case of *p-refinement* cannot be applied for what concerns the space discretization of FVM, since is the increase the base function order need to use the discontinuous *Galerkin theory*. In the FV we can only increase the time discretization order.

Therefore the only refinement technique applicable on the finite volume is the *h-refinement*. To increase locally the cell number in literature we find three main technique, with reference to *Figure 3.5a* where we highlight the cells where we have to apply the refinement, we will to a rapid review. The easier way is the, so call, “*Block-based*”, *Figure 3.5b*, where we split all the domain into subsets of cells with equal cardinality, called *blocks*, and thus we refine the blocks where the flagged cell fall. An alternative is the “*Patch-based refinement*”, *Figure 3.5c*, where refine the smallest block that includes all our underlined cells, then we have the “*Cell-based refinement*”, *Figure 3.5d*, where we refine only the selected cells.

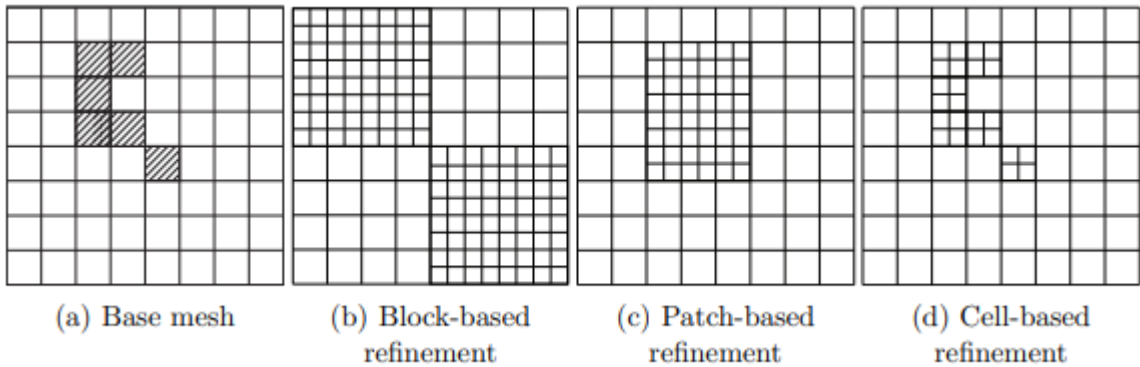


Figure 3.5: Comparison between the three typologies of AMR, the hatched cells in figure (a) indicate where have to be apply the refinement.

3 CFD Model Setup

Independently of what refinement method it is used, the usual practice to store and handle the new cell is the so call “quad-tree data structure”, *Figure 3.6*, that allows a to the storage of the neighbouring cells, the levels of refinement and level of refinement of neighbouring cells that are essential to writing the write the equilibrium equation in the discrete form. Namely this solution transform all the refined cells in a parent cell of other forth, making a refinement level, then at the new refinement round can happen that the cells refined before, became in turn parents of other 4 cell making a new level, and so on. In this way, we should have a progressive increasing density mesh in the critical zone of the domain.

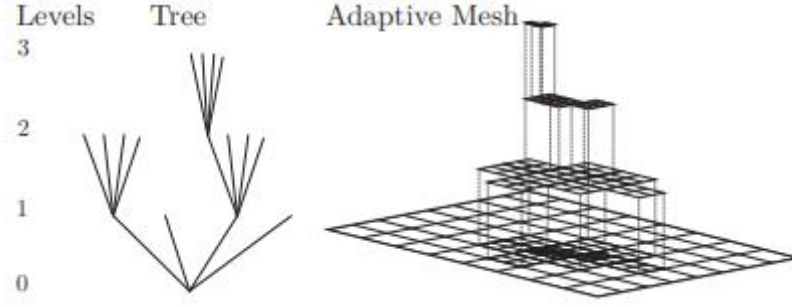


Figure 3.6: quad-tree structure of hierarchy refinement

Error estimation

At the base of all the model adaptivity technique is the error estimation, it is genary expressed, by the Eq. (3.13)

$$||\varphi - \varphi_h|| \leq C(h, \varphi, \varphi_h) \quad (3.13)$$

where φ is the exact solution and φ_h the numerical solution of the quantities studied, h is the characteristic length of our discretization and $C(h, \varphi, \varphi_h)$ is a general function that express the convergence of the model.

The RHS of Eq. (3.13 .) is what we use to do the refinement, and all the possible formulation of this function, that we can fine in literature, can be split in two main categories: a priori and a posteriori estimates.

In a *a priori* estimates, the RHS of Eq. (3.13) is function only of the mesh, h , and of the exact solution φ , but not φ_h namely:

$$||\varphi - \varphi_h|| \leq C(h, \varphi) \quad (3.14)$$

A example of this methodology is the “derivatives reconstructions” by using a approximated solution φ_h^* computed by using a attempt mesh of size h^* [22, pp. 100-113].

In a *a posteriori*, on the other and, the RHS of Eq. (3.13) is function only of the mesh, h , and the numerical φ_h but not φ .

$$||\varphi - \varphi_h|| \leq C(h, \varphi_h) \quad (3.15)$$

Thanks facility to implement this method in a program, also because the φ_h is the outcome of the simulation there fore starting from attempt mesh with characteristic length h^* that will be progressively refined.

3 CFD Model Setup

For the CFD codes the most use technique is the last, and in the last 10 years was proposed many formulation of the function $\mathcal{C}(h, \varphi_h)$, however we can discern in estimators base on the *residual*, that is a measure of how much the solution fulfil the differential problem. Then we have estimators base on the error call *goal-oriented*, where we try to minimize, no more all the function $\mathcal{C}(h, \varphi_h)$, but a new function define ad-hoc for the specific model.

AMR of CONVERGE

In light of the above we discusses we can conclude that the AMR proposed by is an *a posteriori, cell-based, adaptive mesh refinement*, where we can control the error in momentum, energy and chemical equation i.e. the error in the velocity field v , in the temperature T , and species mass fraction Y_x . The peculiarity of this a posteriori algorithm is the error estimate use, instead to use the residual, or the error of momentum equation; but they use a concept borrow from the Large Eddy Simulation (LES) turbulence model, the **sub-grid**, expressed by the Eq. (3.24).

$$\varphi' = \varphi - \bar{\varphi} \quad (3.16)$$

Where φ is vector or scalar field, $\bar{\varphi}$ is the field that outcomes from the filtered to remove all that fluctuation that has frequency over certain cut-off frequency that depend on the mesh size, that is the main difference with the RANS model, and φ' is the sub-grid, ie the remaining part of the field that was remove by then. Then to estimate the sub-grid we use the series expansion of Eq. (3.16) in terms of the complete field, also call Leonard's expansion [20], using the *Einstein tensor notation* we get:

$$\varphi' = -a_{[i]} \frac{\partial^2 \varphi}{\partial x_i \partial x_i} - \frac{1}{2!} a_{[i]} a_{[j]} \frac{\partial^4 \varphi}{\partial x_i \partial x_i \partial x_j \partial x_j} + o(h_i) \quad (3.17)$$

With

$$2a_{[i]} = \int_{-\infty}^{+\infty} x_{[i]} G(x) dx_{[i]} \quad (3.18)$$

where x_i can be the space vector, x , components h_i is the grid size along the x_i direction, $G(x)$ is *filtering function* and the where the indices is between the square brackets it means that the summation rule of Einstein notation is not applied. For the case of *box filtering function* the coefficient $a_{[i]}$ is equal to $\frac{h_i^2}{24}$. Then from Eq. (3.18), by cutting at the first term, using the numerical solution φ_h and converting it in classical notation we get the following error estimator:

$$\eta = \frac{1}{24} ||[hx, hy, hz]^T \cdot \nabla^2 \cdot \varphi_h||$$

for the case of isometric Cartesian structural mesh ($h = hx = hy = hz$) became:

$$\eta = \frac{h^2}{24} \sqrt{\left(\frac{\partial^2 \varphi_{h,x}}{\partial x^2}\right)^2 + \left(\frac{\partial^2 \varphi_{h,y}}{\partial y^2}\right)^2 + \left(\frac{\partial^2 \varphi_{h,z}}{\partial z^2}\right)^2} \quad (3.19)$$

3 CFD Model Setup

Thus the algorithm of the software, using the user-defined tolerance ε , divides or releases the grid if Eq. (3.20) is not satisfied by the mesh.

$$\frac{1}{5} \varepsilon \leq \eta \leq \varepsilon \quad (3.20)$$

3.2.3 Mesh adopted

The mesh used has its main characteristics exposed in table 3.1. Since the aim of my thesis was to validate a model of H2 ICE, the mesh used is quite coarse. In fact in this thesis we have run a lot of simulations for the same case.

Time discretization scheme	1.5 order (up-wind blended)
Base mesh [hx, hy, hz]	[4 4 4] mm
AMR	3 (max embedding level)
velocity tol. ε_v	3 m/s
temperature tol. ε_T	5 K
y+ embedding	2 layers with grid scale 2
Fixed embedding	
cylinder	2 mm
intake	4 mm
exhaust	4 mm

3.3 Combustion model

In this thesis we have used the combustion model ISSIM and ECFM.

3.3.1 ISSIM (Imposed Stretch Spark Ignition Model)

The Imposed Stretch Spark Ignition Model (ISSIM), it is a evolution of the AKTIM and are both developed by the *Institut Français du Pétrole - Energies nouvelles* with the aim to model the ignition phase. It is available in CONVERGE 2.3[7] and in others newer versions. It is able to model multi-ignition starting from the spark, flame kernel production and growth since it was developed to work in symbiosis with the Flame Surface Density (FSD) equation.

The model can be divided in four sub-models:

- A model that describes the circuit of the secondary side of electrical inductance system of the spark plug, that is the same used in the AKTIM [11];
- A model that describe the spark growth, that is necessary to correctly modelling the voltage between the electrodes.
- One manages the flame kernel initialisation, base on the one used in the AKTIMeuler [12];
- Last model drive the flame growth, and it is the main difference with the AKTIM [13], this is based on the modification of FSD equation.

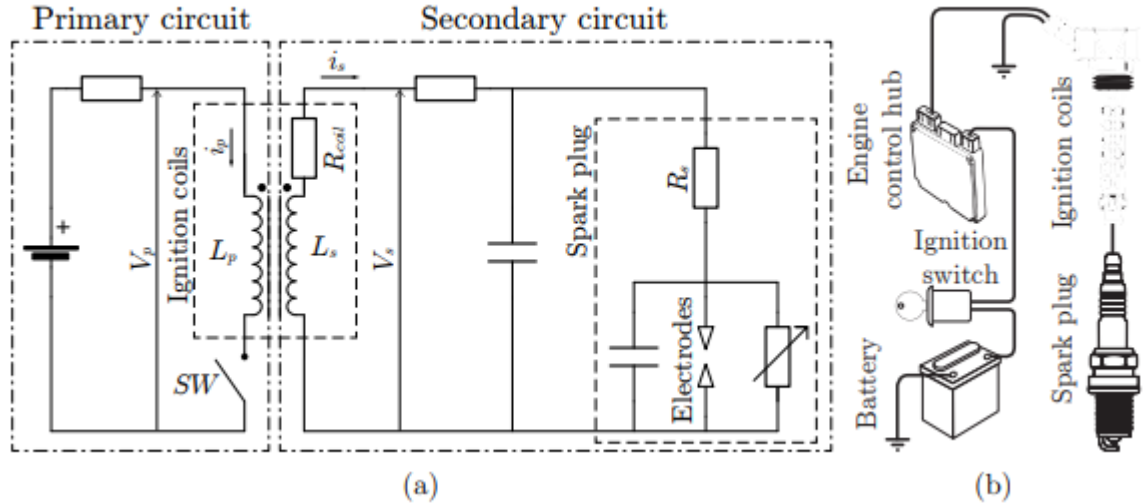


Figure 3.7: Simplified scheme of inductive ignition system: (a) electric circuit used in the ISSIM model [11] (during spark discharge); (b) ignition system of FIAT FIRE 1.4 TJET engine.

Electric circuit model

It is a “0D” model with aim the representing of secondary circuit of inductive ignition system show in Figure 3.7 to reproduce the energy deposit in the gas during spark discharge. In the modern SI engine the ignition system, Figure 3.7a, we have an electrical power source a engine hub that control the switch, i.e. the spark timing that represent the primary circuit; then we have for each cylinder a ignition coils which consist of a primary and secondary coils, the latter is connected to the spark plug. of a primary ans secondary coils, the latter is connected to the spark plug. During the dwell time shortly before the ignition time, $t = 0^-$, the switch SW is closed

3 CFD Model Setup

for few milliseconds during which is stored in the primary inductance L_p the magnetic energy $E_{mag,prim} = \frac{1}{2} L_p i_p^2$ due the DC current that through the coils and usually reach values about 40-100 mJ [14, pp 143]. Then at the SA ($t = 0^+$) the switch is turned off, we have a rapid variation in the magnetic field in the coils (break down), that induces the voltage of primary circuit up to 400 V [14, pp 143]. Now from “coupled inductors” laws we have:

$$V_p = L_p \frac{di_p}{dt} - \frac{M di_s}{dt}, V_s = L_s \frac{di_s}{dt} - \frac{M di_p}{dt} \quad (3.21)$$

Where M is the “mutual inductance” that considering a ideal case can be expressed as $M = \sqrt{L_p L_s} = k N_p N_s$ while the inductance are proportional to the square of coils number. At the begging current in secondary circuit is null ($i_s = 0$) then the Eq. 3.21 became:

$$V_p = L_p \frac{di_p}{dt}, V_s = -M \frac{di_p}{dt} = -\sqrt{\frac{L_s}{L_p}} V_p = -\frac{N_s}{N_p} V_p \quad (3.22)$$

Therefore, since a common value for the coil ratio is $\frac{N_s}{N_p} = 75$ the secondary coils voltage is 30 kV, the high voltage between the spark electrode cause the ionization of gas and an ignition spark begin.

Now, Focusing on the spark life, this can be split in 3 phases: breakdown or *spark initiation*, arc and glow discharge, as show in *Figure 3.8*, the first two are very quickly usually lasts few μs , thus they are neglected; while the spark glow phase, also called *spark duration*, it is the visible spark observed in the experiment lasts 1-2.5 ms [11] depending to the energy supplied by the primary circuit.

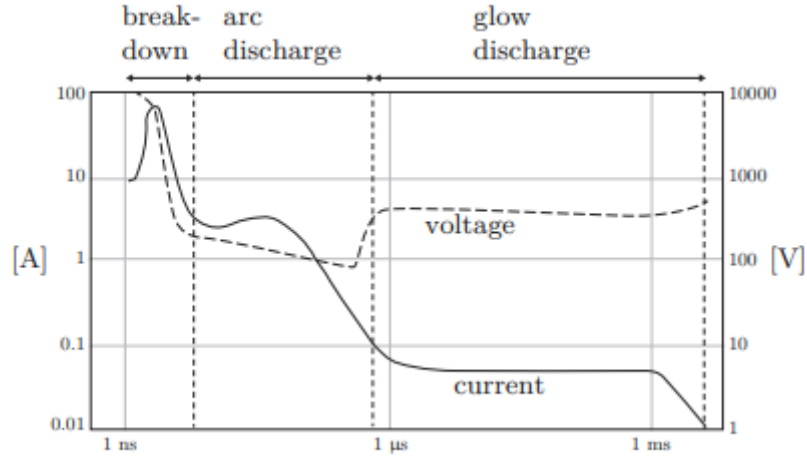


Figure 3.8: Phases of ignition [14, 144]

Therefore the model will represent only the time evolution of the glow phase by studding the phenomena from a energy point of view, indeed is assumed that at the SA in secondary inductance is transferred only the 60% of energy from the primary (to taking into account dissipation in the secondary inductance), therefore we have as initial condition:

$$E_s(0) \approx 0.6 E_{mag,prim} \quad (3.23)$$

3 CFD Model Setup

That is given as input parameter. To take into account the breakdown and arc discharge it is assumed a instantaneous energy deposit in the gas E_{bd} [11]:

$$E_{bd} = \frac{V_{bd}^2}{C_{bd}^2 d_{ie}} \quad (3.24)$$

where, C_{bd} is a constant, d_{ie} is the inter-electrode distance and V_{bd} is the breakdown voltage given by the Paschen's law:

$$V_{bd}(pd_{ie}) = \frac{Bpd_{ie}}{\ln(Apd_{ie}) - \ln[\ln(1 + \frac{1}{\gamma_{se}})]} \quad (3.25)$$

where A and B are constants that depend on the characteristic of the gas, γ_{se} is the secondary electron emission coefficient (the number of secondary electrons produced per incident positive ion) and depend on the geometry and material of the electrodes. During the glow phase the voltage between electrodes is made by three terms, namely:

$$V_{ie}(t) = V_{cf} + V_{af} + V_{gc} \quad (3.26)$$

with V_{cf} and V_{af} are the cathode and anode falling voltage, respectively, and V_{gc} is the gas column voltage along the spark path, and is give by the semi-empirical relation [15]:

$$V_{cg} = 40.46 l_{spk} i_s^{-0.32} p^{0.51} \quad (3.27)$$

where l_{spk} is the spark length, p the pressure and i_s the current in the secondary circuit and depend from the energy stored in the inductance:

$$i_s = \sqrt{\frac{2E_s}{L_s}} \quad (3.28)$$

Now by making a energy balance of the secondary circuit we obtain the non-linear ODE that governs the model.

$$\frac{dE_s}{dt} = -R_s i_s^2 - V_{ie} i_s \quad (3.29)$$

where dE_s/dt is the changing rate of the energy stored by the magnetic field that is the sum of two sink terms, i.e. the power dissipate for Joule's effect $R_s i_s^2$ and the power dissipate by the spark $V_{ie} i_s$.

Then replacing the Eq. (3.27) into Eq. (3.28) we explicit the energy:

$$\frac{dE_s}{dt} = -2 \frac{R_s}{L_s} E_s - V_{ie} \sqrt{\frac{2E_s}{L_s}} \quad (3.30)$$

From the Eq. (3.26), Eq. (3.27) and Eq. (3.30) we deduce that the model needs data about the pressure, the circuit parameters and the spark length. About the first it is got from the CFD code, while for the second, since the it is hard to measure directly the electrical parameters (cause the presence of diodes and transistor in the modern ignition system) we use values found in literature, they are listed in *Table 3.2*. For the spark plug length it is given by another sub-model of the ISSIM, explained in the next subsection.

Table 3.2: Electrical parameters of the spark plug used in the ISSIM.

3 CFD Model Setup

Secondary inductance L_s	38 H
Secondary resistance R_s	13300Ω
Inter electrodes distance d_{ie}	0.8mm
Electrodes radius r_{ie}	0.3mm
Initial secondary circuit energy, $E_s(t = 0)$	70mJ

Spark model

This model describe the spark growth during the glow phase, taking into account the velocity field, the turbulence and the voltage close to the spark. At the breakdown instant ($V_{ie} > V_{bd}$) it is assumed that the spark length is equal to the gap between electrodes, i.e $l_{spk}(0^+) = d_{ie}$. The spark during a glow phase is a arc of plasma, i.e. a ionized molecules through by current, that is convected and stretched by the velocity field, *Figure 3.9b*, therefore $l_{spk}(t) > d_{ie}$ [11]. The spark is stretched by the local turbulence field, and it is modelled by introducing the spark wrinkling factor Ξ .

$$l_{spk} = l_{spk} \Xi_{spk} \quad (3.31)$$

where Ξ depend on wrinkling K_t that is modelled using the RANS as ECFM:

$$\frac{\Xi_{spk}}{dt} = K_t(t, x) \text{ with } K_t = \frac{\varepsilon}{k} \cdot f\left(\sqrt{\frac{2k}{3}} S_L, \frac{L}{l_F}\right) \quad (3.32)$$

while with the mean length, l_{spk} , the model take into account the growth due to convection. It is assumed that during the growth phase mean length have a rectangular shape as in *Figure 3.9a*, where the vertical side is transported by the flow leading the spark, that is why we have 2 that multiply the velocity in Eq. (3.33):

$$\frac{l_{spk}}{dt} = 2\bar{u} \quad (3.33)$$

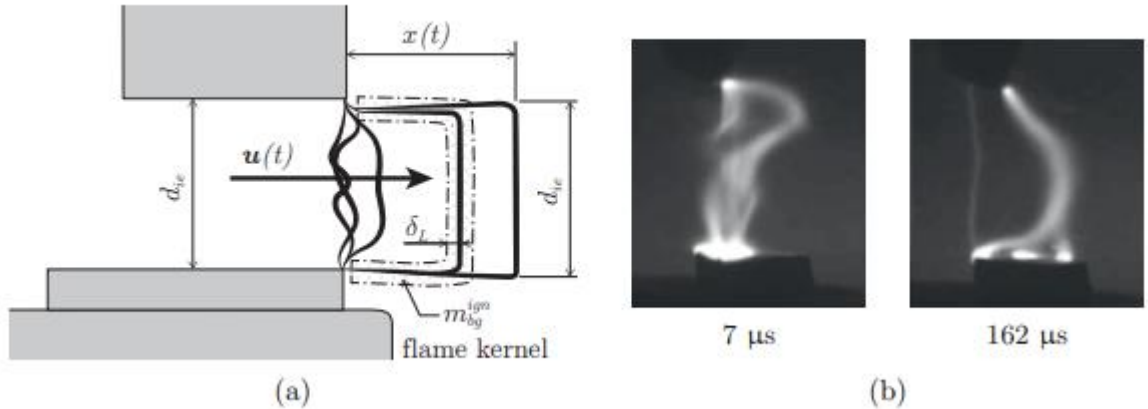


Figure 3.9: Glow discharge shape of the spark: (a) simplified shape of glow discharge in convective flow field [15]; (b) Photographs of spark evolution after breakdown ($t = 0 \mu s$) with chamber pressure of 700 kPa and a camera exposure time of $100 \mu s$ (Images from F.A. Soldera et al., Description of the discharge process in spark plugs and its correlation with the electrode erosion patterns[16]).

In case of strong convection the spark grow really fast and can be many time longer that d_{ie} , and as shows in Eq. (3.27) it causes a directly increase of the voltage between electrodes V_{ie} even up to reach again the breakdown voltage V_{bd} . If this happen we have a the formation of a

3 CFD Model Setup

new spark, i.e. the spark length is resetted at the initial spark gap distance $l_{spk} = d_{ie}$ thus $l_{spk} = d_{ie}E_{spk}$, which cause a fall in the voltage as show in *Figure 3.10*.

Therefore the model is able to handling multiple breakdown.

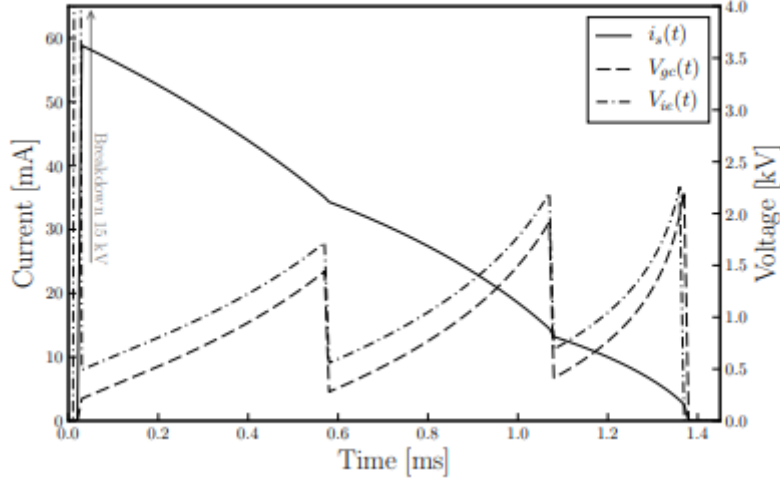


Figure 3.10: Current i_s and voltage between the electrodes of spark plug, V_{ie} , and through the gas column, V_{gc} , predicted by the ISSIM model in CONVERGE

Initial gas kernel

The previous two model, as we have seen, govern the energy release from the ignition system to the gas, i.e. E_{ign} , which is the sum of part of the breakdown energy, Eq. (3.24), and energy received during the glow phase, thus for $t > t_{spk}$ the ignition energy can be write as:

$$E_{ign} = 0.6E_{bd} + \int_{t_{spk}}^t V_{gc} i_s dt \quad (3.34)$$

Then if the energy in the gas go above the critical energy E_{crit} , defined in Eq. (3.35) where δ_L is the laminar flame thickness and k the gas adiabatic index, the gas ignition take place.

$$E_{crit} = 4 \frac{k}{1-k} l_{spk} p \pi \delta_L^2 \quad (3.35)$$

When this happen a mass of burned gases, m_{bg}^{ign} , is deposited, since the flame kernel is physically locate near the spark, it is assumed that the volume of gas involved is equal to a cylinder along the spark with a radius equal to δ_L as in Figure 3.9, which lead that m_{bg}^{ign} is determined by:

$$m_{bg}^{ign} = \langle \rho_u l_{spk} 4\pi \delta_L^2 \rangle \quad (3.36)$$

with ρ_u the density of unburned gas and the brackets means that the values are computed as average in the cells within a sphere of radius twice the spark gap. According to experimental observation the initial kernel does not depend on the composition of gas but rather on amount of energy deposited [7], then CONVERGE modified the Eq. (3.36) as follow

3 CFD Model Setup

$$m_{bg}^{ign} = C_{bg} \left\langle \frac{E_{ign}}{C_p \Delta T_{ign}} \right\rangle \quad (3.37)$$

where $\Delta T_{ign} + T_u$ is the characteristic temperature of the plasma, since it decreases very quickly after break down, it is impossible to define with accuracy, thus it is chosen a arbitrary value of 20 000 K; and the parameter C_{bg} is defined by the user to correct the initial deposited mass (in our model we left the default value $C_{bg} = 1$). Up to now, we have describe how the ISSIM model convert the energy supply to the spark plug in energy to the gas and therefore the mass burned by the plasma during spark glow phase, therefore we have been dealing with 0D model. Now all this have to be translate to the ECFM model. This issue is solved by using the *volume progress variable* \bar{c} of ECFM model. During the spark, at the ignition time, i.e. when the Energy go above the critical one Eq.(3.35), this progressive variable is “spread through” the 3D domain following a Gaussian distribution, that impose the initial burned gas volume fraction, c_{ign} , that is given by

$$\bar{c}_{ign}(\mathbf{x}, t_{ign}) = c_0 \cdot e^{-\frac{||\mathbf{x} - \mathbf{x}_{spk}||}{0.5d_{ie}}} \quad (3.38)$$

where \mathbf{x} is the cell coordinate, \mathbf{x}_{spk} spark plug position, d_{ie} inter electrode distance, and c_0 has to satisfy the Eq. (3.39), a example of mass fraction burned at the ignition is show in *Figure 3.11a*.

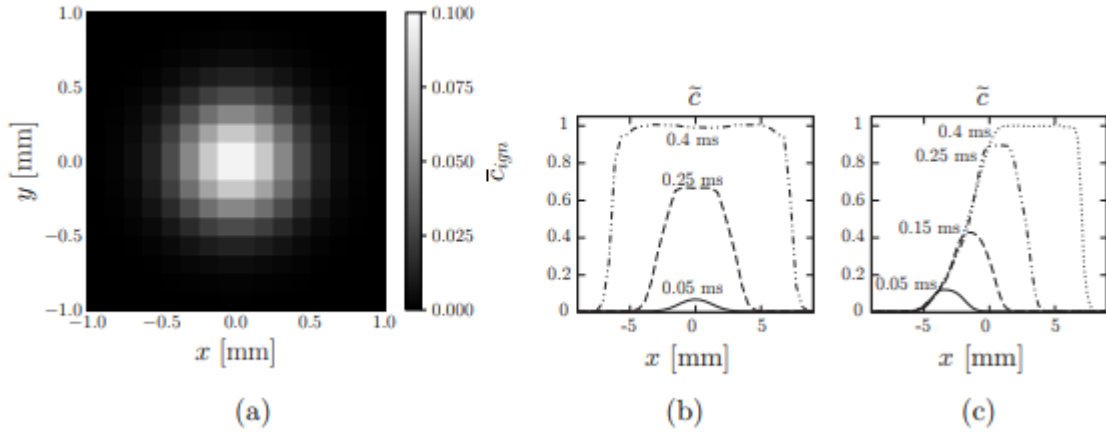


Figure 3.11: Initial burned gas volume fraction: (a) Example of initial burned gas volume fraction at the ignition $c_{ign}(\mathbf{x}, t_{ign})$, in a 2D domain with cell size (0.125 mm, 0.125 mm) and spark plug gap 0.8 mm; (b) Evolution of burned gas mass fraction, without convection [13]; (c) Evolution of burned gas mass fraction with convection speed $u_{conv} = 30$ m/s [13].

$$\int_D \rho_b \bar{c}_{ign} \rho_b dV = \int_D \bar{\rho}_b \bar{c}_{ign} \rho_b dV = m_{bg}^{ign} \quad (3.39)$$

and its time evolution depend on the reaction rate $\frac{\partial \bar{c}_{ign}}{\partial t} = \bar{r}_c$

$$\bar{r}_c = \max(\rho_u S_L \bar{\Sigma}_{\bar{c}}, \frac{\rho_b(\bar{c}_{ign} - \bar{c})}{dt}) \quad (3.40)$$

Now this evolution parameter has to be converted in a flame surface density (FSD) to complete the communication chain, Figure 3.12, between ISSIM and ECFM. As describe in the previous section the FSD is the ration between flame front and a sphere with a radius that depend of the volume of burned gases. Recalling the formula for sphere volume:

3 CFD Model Setup

$$V = \frac{4}{3} \pi r^3 \rightarrow r = \sqrt[3]{3/4\pi V}$$

Therefore

$$r_b^{ign} = \left(\frac{3}{4\pi} \int_D \bar{c}_{ign} dV \right)^{1/3} \quad (3.41)$$

then the FSD is defined as:

$$\Sigma_{ign} = C_{surf} \frac{3\bar{c}}{r_b^{ign}} \quad (3.42)$$

where C_{surf} is a user-specified parameters that correspond to the initial wrinkling value that is use to take into account the not perfect sphericity of the flame kernel, i.e. it is 1 if *laminar ignition* > 1 if it is turbulent ignition. This parameter strongly affect the combustion rate at the beginning and consequentially all the combustion phase.

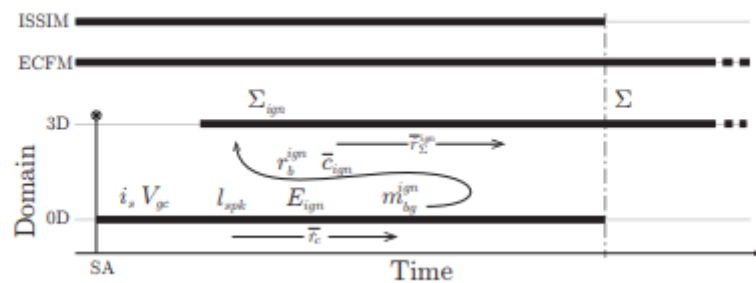


Figure 3.12: Timeline chart that reassume how the ISSIM and ECFM models dialogue at the beginning of the combustion

And similarly to the burned fraction volume, the reaction rate is defined as:

$$\dot{r}_{\Sigma}^{ign} = \max(\frac{\Sigma_{ign} - \Sigma_c}{dt}, 0) \quad (3.43)$$

Study of Electrical circuit model

How we explained in previous subsections it is impossible to get experimentally the electrical parameters of secondary circuit (R_s , L_s , E_s), cause the complexity of modern ignition system, thus to study the influence of this parameters and to have a deep knowleg of ISSIM model a 0D model was developed in the Paolo De Angelis thesis [2]. To have more information about this study, read the subsection 4.1.4 in this particular thesis.

3 CFD Model Setup

In this thesis we will show the result of this work:

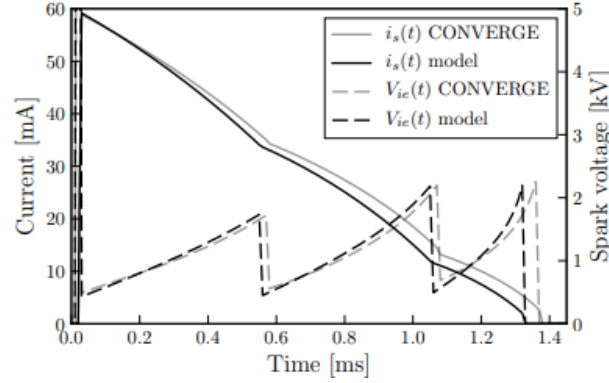


Figure 3.13: Current and Spark voltage comparison between result of CONVERGE and the model used.

Thanks this model it was possible to predict the behaviour of ISSIM, i.e. duration, current and energy of spark. In Figure 3.14 is shown the result of this study by varying E_s , R_s , L_s and \bar{u} .

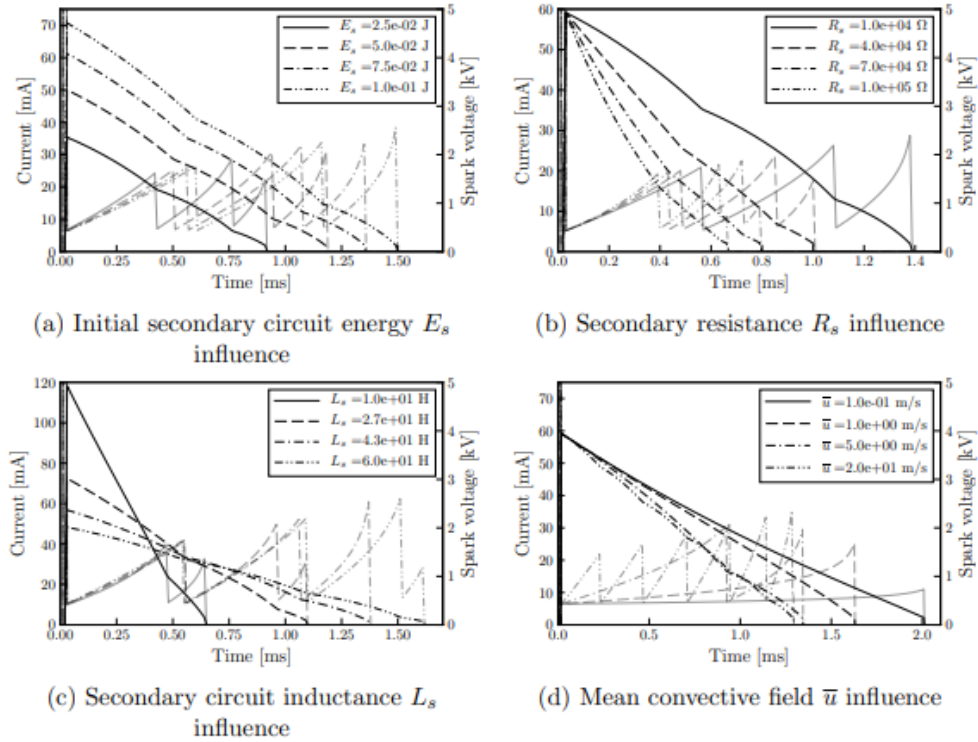


Figure 3.14: Influence of the electrical circuit parameter (user-specified) and convective field on OD model of ISSIM, where the black lines is current of spark during glow phase, i_s , while the grey lines is potential difference between electrodes V_{ie} .

- a) How shown by the Figure 3.14a, the energy strongly affect the model since increase both duration and current similar to a scaling process, indeed $E_s \approx \int i_g V_{ie} dt$ and the voltage is independent by circuit energy, therefore we can say that the energy is proportional to the area below the current curve.

3 CFD Model Setup

- b) In *Figure 3.14b*, is showed the effect of the resistance, the peak of current is independent from R_s for Eq. (3.28), but increasing the resistance we increase the dissipation in the circuit for Joule's effect, so it reduce the energy fraction that goes to the gas. Therefore by changing R_s is possible to reduce the spark duration without reducing the voltage peak.
- c) The inductance, L_s , strongly affect the behaviour of model since the power realised by the spark depend on it, indeed how the *Figure 3.14c*, show how increasing L_s the peak reduce according Eq. (3.28), and the spark duration increase since the inductance opposes the current variation.
- d) Last image shows how the convective flow affect the voltage, since it force the spark to growth until the new break down, but this effect is evidence if the speed is few m/s while for speed higher of 8-10 m/s increase the velocity show a more sparks release but the effect on current is negligible since the spark new discharge increase in number but this introduce more irregularity in current discharge but the effect on duration is negligible.

3.3.2 ECFM (Extended Coherent Flamelet Model)

In our model we use the model base on the surface density theory, i.e. ECFM-3Z proposed by Colin and Benkenida [17], this model is based on the hypothesis of the flamelet of other model like the G-Equation model [18] but try to use physical observation to write its definition and governing equations. This model is a extension of the CFM, Coherent Flame Models, which was well developed for the pre-mixed combustion of gasoline engine, where show a good prediction of the real combustion, thus starting from the semian hypothesis the ECFM try to reproduce the combustion also in unmixed case as direct injection engine. The peculiarity of the ECFM proposed by Colins et al [17] is the use of 3 Zones: unmixed air zone, the unmixed fuel zone and the mixed zone.

Flame Surface Fensity models

The Flame Surface Density, Σ , is base on the concept of the flamelet models, i.e we assume that the reaction rate is infinite so the flame zone thickness is infinitesimal thus can be handle as a surface. Starting from this hypothesis we define the flame surface density as the flame front surface per unit volume of burned gas, Eq. (3.44).

$$\Sigma = \frac{S_{flame}}{V_{burned}} \quad (3.44)$$

e.g. the laminar combustion the flame front of a combustion with punctual source we obtain $\Sigma = \frac{3}{r_f}$, this value is the minimum possible FSD for a certain burned gas, thus for high Σ at a given position means that the turbulent field strongly stretched the flame. Thanks this definition we easily modelled the flame stretching due the turbulence. The main hypothesis of the FSD model is that considering a infinitesimal area of the flame surface it is planar thus, introducing the local combustion rate for flame area, $0 \langle s_c \rangle_s$, we write the reaction rate using Eq.(3.45), which is quite similar to the reaction rate for laminar combustion.

$$\bar{\omega} = \rho_0 \langle s_c \rangle_s \Sigma \quad (3.45)$$

3 CFD Model Setup

where ρ_0 is the density of unburned gas, $\langle s_c \rangle_s$ is the average flame consumption speed.

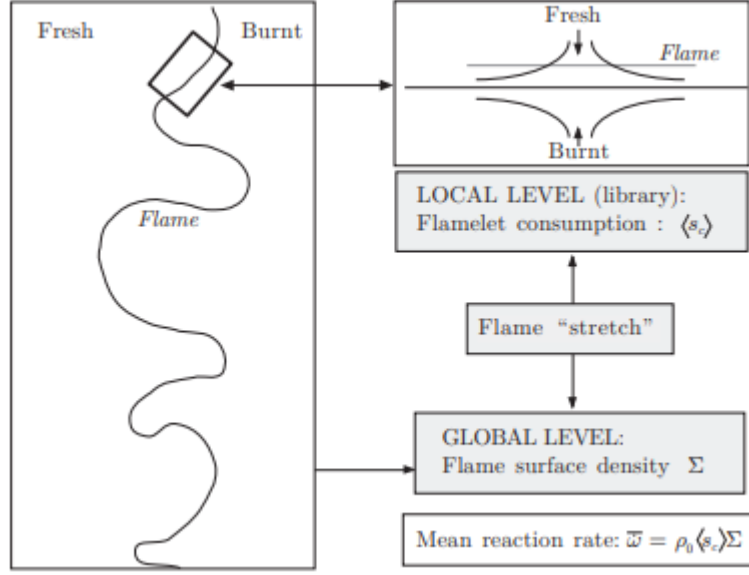


Figure 3.15: Flame surface density algorithm chart, for turbulent premixed flames [18]

This latter is computed using a weighed mean using the probability function $p(\kappa)$ that give us the odds to have a stretch rate κ on the flame surface, in many practical case it is used the Diract distribution $p(\kappa) = \delta(\kappa - \kappa_0)$. Since the consumption rate is not well know respect other chemical parameter as the laminar flame speed, s_L , we introduce the “stretch factor” I to link the two parameter, defined as show in Eq. (3.46)

$$\langle s_c \rangle_s = I s_L \quad \text{where} \quad I = \frac{1}{s_L} \int_0^\infty s_c(k) \delta(\kappa - \kappa_0) d\kappa \quad (3.46)$$

The DNS simulation shows that the “stretch factor” oscillate about the unit value therefore we can introduce the simplification $\langle s_c \rangle_s = s_L$. Thus the Eq. (3.47) became:

$$\bar{\omega} = \rho_0 s_L \Sigma \quad (3.47)$$

From the last equation highlight the main advatage of this method, indeed the raction is described only by thw parameters s_L and Σ , the first collect all the complex chemistry characteristics, while the second take into account the flame interaction with the velocity field. Thus now the problem is to produce a model that provide the equation that describe the evolution of the laminar speed and FSD.

UDF for laminar speed

To compute the Laminar Flame Speed we can use a semi-empirical relation or table where we store the value for thifferent state variable. In CONVERGE its use the first, it compute s_L using the Gulder correlation (1984) [7, pp 439-440], where it is given starting from a reference value compute as follow:

$$s_{L_{ref}} = \omega \varphi^\eta e^{-\xi(\alpha-1.075)^2} \quad (3.48)$$

3 CFD Model Setup

where ω , η and ξ are user-specified constants function of the mixture used, that can be derivated by the experimental data. The Eq. (3.48) is referred to a constant pressure and temperature of the reference point, $(p_{ref}, T_{u,ref})$, of unburned gas. Than we can compute it for all the pressure and temperature that we have during the combustion using the following relation:

$$s_L = s_{L,ref} \left(\frac{T_u}{T_{u,ref}} \right)^\gamma \left(\frac{p}{p_{ref}} \right)^\beta (1 - 2.1Y_{dil}) \quad (3.49)$$

where T_u and p_u is unburned gas temperature and pressure, and Y_{dil} is the mass fraction of dilution species, while the temperature and pressure exponent is function fo the equivalent ratio as show in Eq. (3.50).

$$\gamma = \gamma_{ref} - 0.8(\varphi - 1) \quad \text{and} \quad \beta = \beta_{ref} + 0.22(\varphi - 1) \quad (3.50)$$

In CONVERGE we specify the $\omega, \eta, \xi, \gamma$ and β [7] that usually is take from the literature or experimental value.

The laminar flame speed table used was obtained in a previous thesis [19] using the 0D and 1D chemical simulator DARS, that is a commercial stand-alone software where, by building the reduction mechanism, is possible to reproduce the reaction in detail and thus obtain a set of combustion parameter among which the laminar speed. During this study it was analysed and validated 3 kinematic mechanisms, *GRI Mech 3.0* for methane, *GRI Mech 3.0* and *USC Mech II* for CNG. At the and of the analysis it was observed that *USC Mech II* gives better prediction than those of *GRI Mech 3.0* model in the fuel rich mixture, but it was decided to use the *GRI Mech 3.0* because more stable thus give use more point where we get convergence. After that the outcome of this mechanism and the prediction of the Gulder relation were compared, this letter under predict at both lean and rich mixtures and over predict near stoichiometric and also provides a rough estimate for considering the residual fraction effect on the laminar flame speed.

In light of this work a laminar flame speed table was created by Paolo and his teammates [2].

ECFM 3-Z

The 3 Zone Extended Coherent Flame Model start from the definition of the balance equation of the FSD. In literature there are many proposes, the most common is the one base of the “reduced temperature” Θ [18], where its definition is reported in Eq. (3.51):

$$\Theta = \frac{T - T_1}{T_2 - T_1} = 1 - \frac{Y_f}{Y_{f,1}} \quad (3.51)$$

where T_1 and T_2 is the initial and final temperature, and Y_f is the fuel mass fraction and $Y_{f,1}$ is its initial value. Θ goes from 0 in the fresh gases to 1 in the burned gases and is the progress variable of the combustion. The balance equation base on Θ is expressed by:

$$\frac{\partial \Sigma}{\partial t} + \nabla \cdot (\langle \mathbf{v} \rangle_s \Sigma) - \nabla \cdot [\langle s_L \mathbf{n} \rangle_s \Sigma] = \underbrace{\langle (\mathbf{I} - \mathbf{nn}^T) : \nabla \mathbf{v} \rangle_s \Sigma + \langle s_L \nabla \cdot \mathbf{n} \rangle_s \Sigma}_{\langle \kappa \rangle_s \Sigma} \quad (3.52)$$

3 CFD Model Setup

where $n = -\frac{\nabla\theta}{\|\nabla\theta\|}$ is the flame front normal, thus the flame curvature is $\nabla \cdot n$, and $\langle \cdot \rangle_s$ is the “surface averaged operator” defined as:

$$\langle \varphi \rangle_s = \frac{\varphi \Sigma}{\Sigma} \quad (3.53)$$

The last two term on LHS of Eq. (3.52) is the advective term and the normal propagation of the flame, while on the RHS we have the the stretch rate κ is compose by the sum of tangential strain rate and the curvature effects. Then we explicit the turbulence using RANS model ($v = \bar{v} + v'$) the advective term became:

$$\nabla \cdot (\langle v \rangle_s \Sigma) = \nabla \cdot (\langle \bar{v} \rangle_s \Sigma) + \nabla \cdot (\langle v' \rangle_s \Sigma)$$

and the tangential flame stretching term became:

$$\langle (\mathbf{I} - \mathbf{nn}^T) : \nabla \mathbf{v} \rangle_s = \underbrace{\langle (\mathbf{I} - \mathbf{nn}^T) : \nabla \bar{\mathbf{v}} \rangle_s}_{\kappa_m} + \underbrace{\langle (\mathbf{I} - \mathbf{nn}^T) : \nabla \mathbf{v}' \rangle_s}_{\kappa_t}$$

Thus introducing this term in Eq. (3.52) and also we introduce a function D that express the flame destruction (otherwise the flame grows to the infinite), and we get:

$$\frac{\partial \Sigma}{\partial t} + \nabla \cdot (\bar{v} \Sigma) = -\nabla \cdot (v' \Sigma) + \kappa_m \Sigma + \kappa_t \Sigma + \langle s_L \nabla \cdot n \rangle \Sigma - D \quad (3.54)$$

This last is the base expression from with all the FSD model are derived, and all the various expression proposed are reported in [18, pp 231]. In CONVERGE Eq. (3.54) became:

$$\frac{\partial \Sigma}{\partial t} + \nabla \cdot (\bar{v} \Sigma) = \nabla \cdot \left(\frac{\nu_t}{S_c} \nabla \Sigma \right) + \underbrace{\alpha_\Sigma \frac{\varepsilon}{k} K_t \Sigma}_{S_1} + \underbrace{\frac{2}{3} \nabla \cdot \bar{v} \Sigma}_{S_2} + \underbrace{\frac{2}{3} s_L \frac{1 - \Theta}{\Theta} \Sigma^2}_{S_3} - \underbrace{\beta s_L \frac{1 - \Theta}{1} \Sigma^2}_D + S_k \quad (3.55)$$

where ν_t is the turbulent kinematic viscosity, S_c is the Schmidt number, and α_Σ and β are user-specified coefficient. The equation show also all the sources terms of the FSD during the combustion, namely S_1 is the FSD turbulent stretch that converge modell using the Intermittent Turbulent Net Flame Stretch (ITNFS) [7, pp 248], S_2 is the source term due the flame curvature, S_3 the flame production due to the fuel consumption, and S_k is the flame production from ISSIM model that we describe in Section 3.3.1.

3-zones method

Now all the model expressed above are was build under the ipothesis of premixed fuel combustion, indeed the reduced temperature Θ that is the progressive variable is compute assuming the initial temperature T_1 and composition $Y_{f,1}$ equal and constant in all the domain, therefore in case of direct inject ICE the model fail. Thus to extend the field of case that can be model with the FSD model, Colins et al [17], proposed the *ECFM-3 Zones* model where each cell of the domain is split in 3 zones:

- A is the unmixed zone containing the air and EGR;
- F is the unmixed fuel zone;
- M is the mixed fuel zone where there is air, fuel and EGR.

3 CFD Model Setup

In *Figure 3.16*, is shown a schematic draw of how the model describe the combustion for a typical cell.

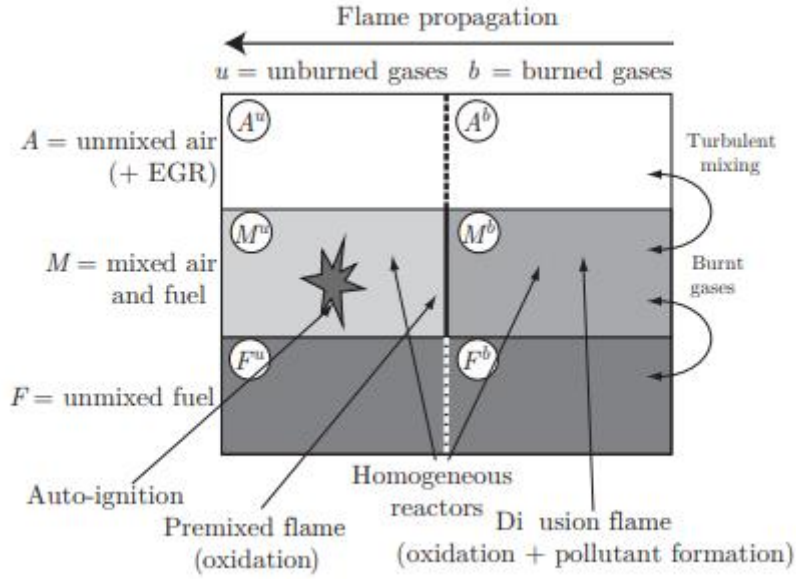


Figure 3.16: Schematic representation of ECFM-3Z model [17]

To understand how work the model we can observe four phases. The first is the cell initialization where in the cell is stored in the zones F^u and A^u the value of the mass fraction of the various species (YCH_4 , YO_3 , etc.), *Figure 3.17b*, that are given by the momentum and continuity equation; then mixing sub-model compute the zone M, *Figure 3.17b*, where reductants and oxidants are progressively transfer using convection–diffusion equation [17, pp 599] forming the region M_u .

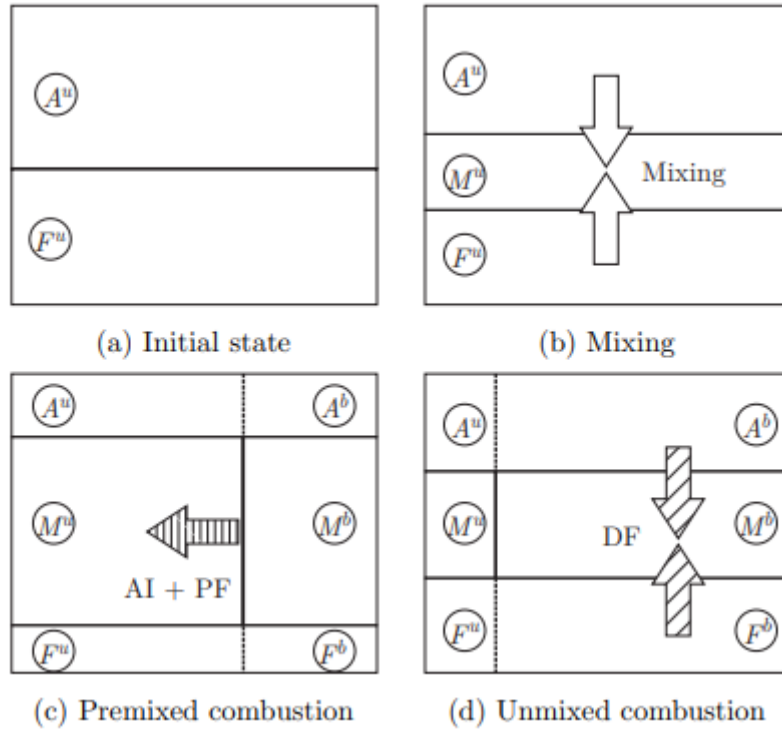


Figure 3.17: ECFM-3Z phases during combustion [17]

3 CFD Model Setup

Now we can have two possibility, one is the auto-ignition, in this case the region M_u is quickly consumed; the other is that the mixture is progressively burned by the FSD, Figure 3.17c. The last phase is the post-flame kinetic, Figure 3.17d, where simple Arrhenius model compute the remaining possible reaction as fuel combustion in very rich mixture the NOx formation, CO equilibrium etc. In this way we obtain a precise gases temperature as well as a prediction of the pollution concentration.

3.4 Injector Model (Source cell method)

In order to proper simulate a DI ICE without specifying the geometry of the injecto, it was necessary to use the source modeling. In CONVERGE this was possible creating a source.in file. The source/sink volumes are defined by specifying the shape of the source (i.e., box, sphere, cylinder, region, line, circle, boundary, or proximity). The source.in file also contains information regarding the strength of the source, the start and end times of the source, and the motion of the source (if any) [20, pp 532].

In our case we need to model a species (CH4), the species transport equation is given by:

$$\frac{\partial \rho_m}{\partial t} + \frac{\partial \rho_m u_j}{\partial x_i} = \frac{\partial}{\partial x_j} \left(\rho D \frac{\partial Y_m}{\partial x_j} \right) + S_m, \quad (3.56)$$

where

$$\rho_m = Y_m \rho$$

and where u is velocity, ρ is density, ρ_m is the density of the species m , Y_m is the mass fraction of species m , D is the mass diffusion coefficient, and S_m is the species source term of species m .

After specified a particular species CONVERGE automatically calculates additional source terms for the energy and momentum equations. These additional sources account for the energy and momentum of the species source and are calculated based on the *source > species_control > temp and source > species_control > velocity* parameters in source.in. These parameters apply only to species sources, for which they are required.

Source.in created

In this part of the thesis we analyze the creation of the source.in file.

First we have chosen the species generated (CH4). After that the amount of CH4 injected was evaluated. It was calculated from the mass flow rate \dot{m}_{CH4} :

$$m_{CH4} = \frac{\dot{m}_{CH4} 60}{n} \frac{inj_{degrees}}{360^\circ} \quad (3.57)$$

Where n is the engine velocity and $inj_{degrees}$ is the duration of the injection.

A temperature of 350 K was estimated in the rail of the powertrain, using the equation of a sonic nozzle, the temperature of the injected fuel was obtained. Finally the velocity of the species injected in the cylinder was obtained considering sonic velocity at the calculated temperature (303 K). It was also decided that the direction of the species was in line with the

3 CFD Model Setup

cylinder axis. After that the *SOI* (start of injection) and *EOI* (end of injection) was specified; these values were chosen from GT-POWER analysis (see subsection 5.4).

The screenshot displays the 'General' tab of a source specification window. On the left, a 'Sources' list contains 'hole_inj' with a green 'SPE' button next to it. The main panel has tabs for 'General', 'Shape', and 'Motion'. Under 'General', the 'Source' is set to 'Species' and 'CH4'. 'Source units' are 'Species mass'. The 'Value' is '4.15e-05' kg, with a 'Use file' checkbox. 'Max mass fract.' is '1.0'. 'Temperature' is '303.0' K. 'Velocity' is set to three components: '-3.16', '0.0', and '-453.59' m/s. The 'Mode' is 'CYCLIC'. 'Start time' is '566.0' deg, 'End time' is '660.0' deg, and 'Period' is '720.0' deg. At the bottom, 'Source time-step multiplier' is '1.0' units. Buttons for 'Add', 'Delete', and a copy icon are at the bottom left.

Parameter	Value	Unit
Source	Species	
Species	CH4	
Source units	Species mass	
Value	4.15e-05	kg
Max mass fract.	1.0	-
Temperature	303.0	K
Velocity (x, y, z)	-3.16, 0.0, -453.59	m/s
Mode	CYCLIC	
Start time	566.0	deg
End time	660.0	deg
Period	720.0	deg
Source time-step multiplier	1.0	units

Figure 3.18: general specification in the file source.in

The shape of the source was a thin cylinder placed right under the cylinder head.

3 CFD Model Setup

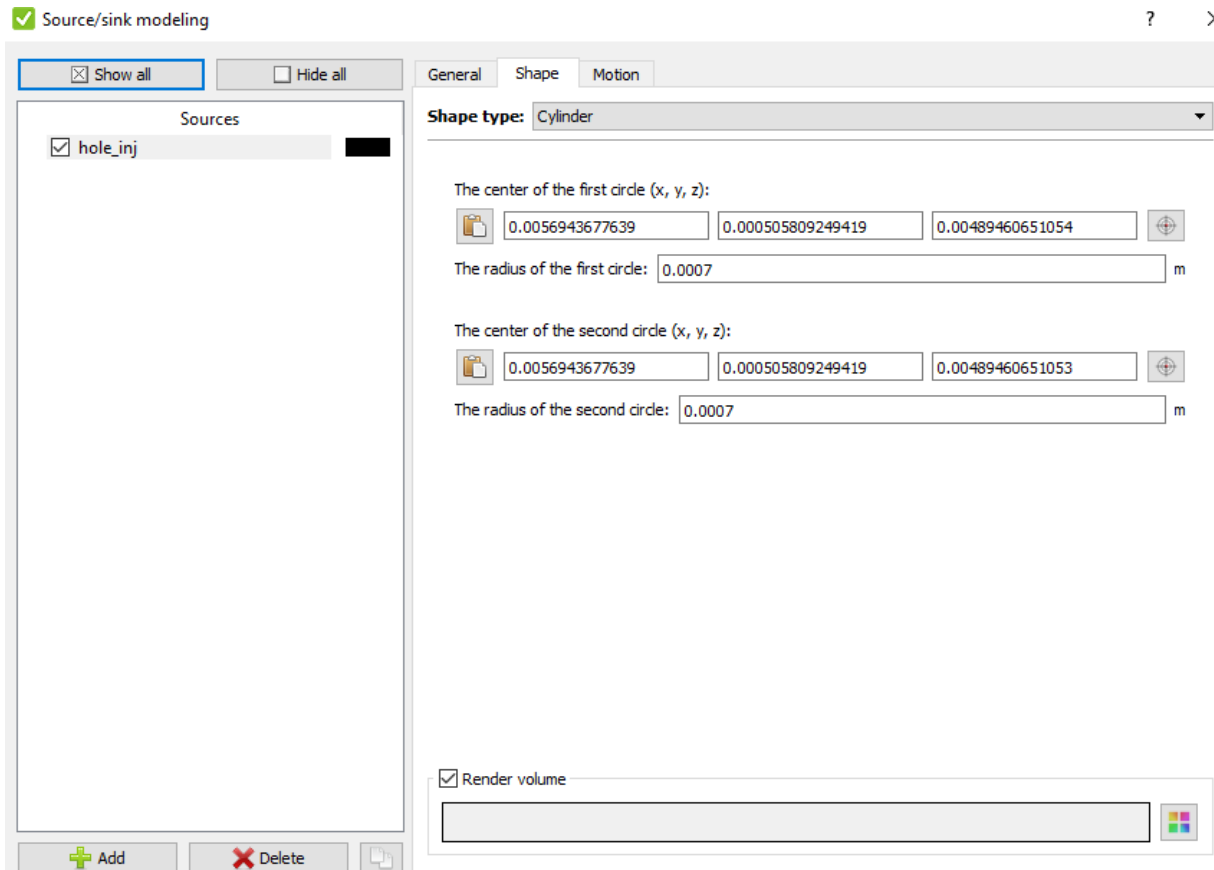


Figure 3.19: shape specification in the source.in file

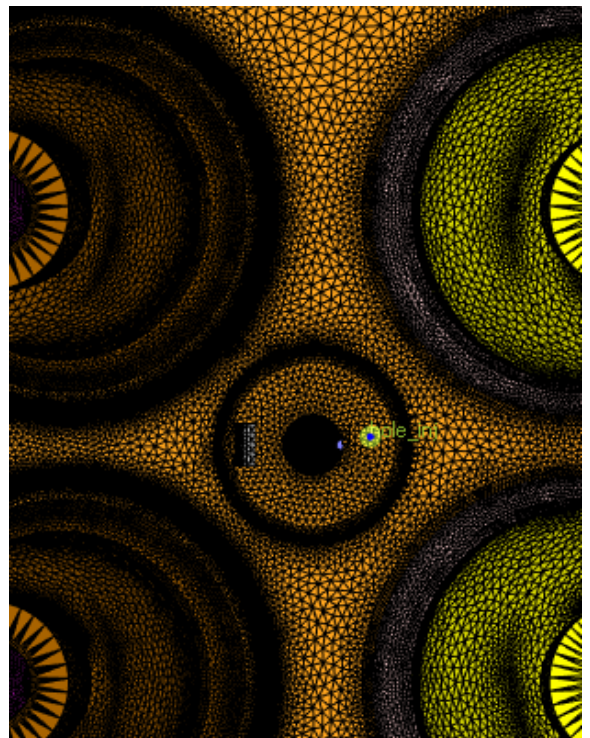
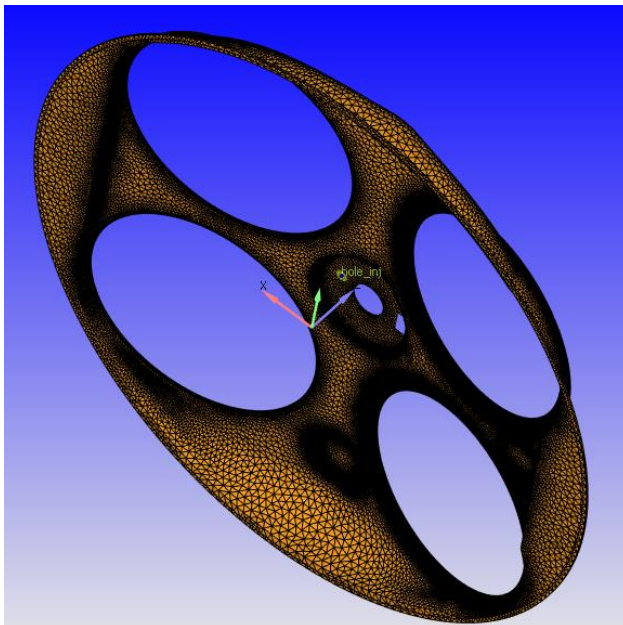


Figure 3.20: position of the injector hole

3 CFD Model Setup

It is a mandatory to specify that an embedding was added in this model. In fact it is necessary to proper modify the embedding in order to simulate the injection accurately.

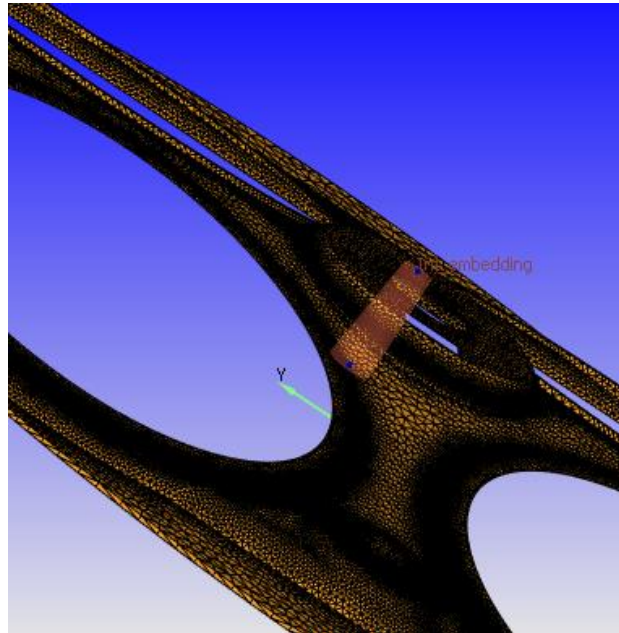


Figure 3.21: hole embedding

Chapter 4

GT-POWER Model Setup

The section is dedicate to the discussion about all the tool used to setup the GT-POWER model. We need to increase the engine load to the maximum as possible, but we have no eexperimental data, so we have to manually increase the load: To do this we have chosen a1D 0D software called GT-POWER. We will describe environments used and some characteristics of the software. After that we will analyze the trasformation of the engine into a DI engine.

4.1 Editing of the previous PFI model

The aim of this thesis is to compare a H2 engine with a CNG engine which has already a validated model both in CONVERGE and GT-POWER. First of all it was conduced and analysis on the old PFI model which simulates all the components (from the intake system to the aftertreatment system). We have tried to increased the load without changing anything, however the model was created to follow the experimantal data, so it was impossible to obtain a good result. In *figure 4.1* we can see the main problem of this analysis.

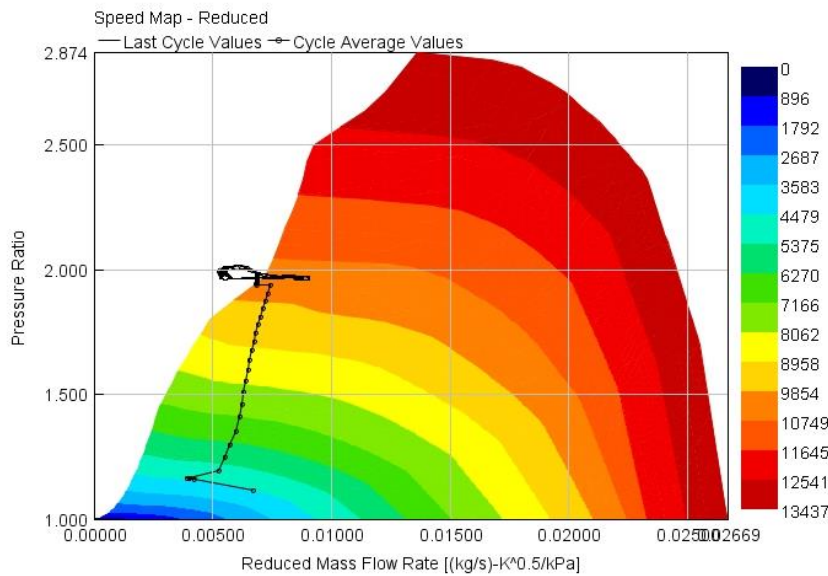


Figure 4.1: surge of the compressor

After this analysis we decided to cut all the elements upstream the compressor and downstream the turbine. We replaced them with two end enviroments (*figure 4.2*) that are objects which describe temperature, pressure and composition of a specific environment [21].

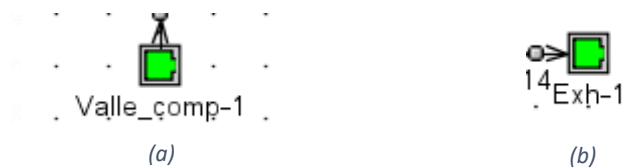


Figure 4.2: (a) endenvironment upstream the compressor (b) endenvironment downstream the turbine

4 GT-POWER Model Setup

In fig 4.3 we can see the model itself.

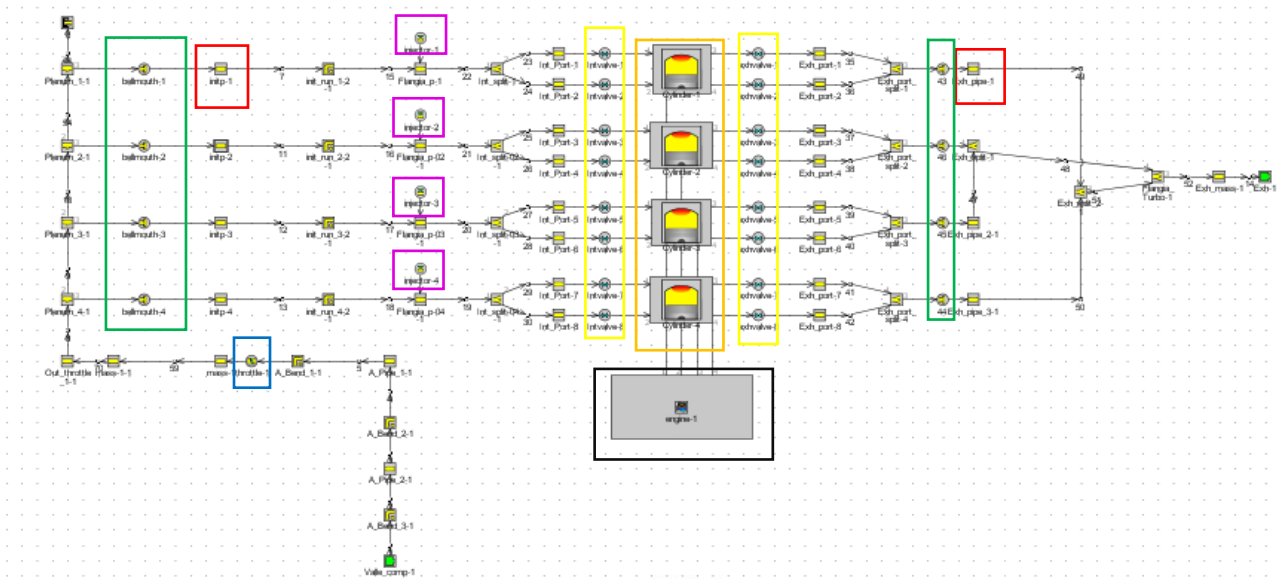



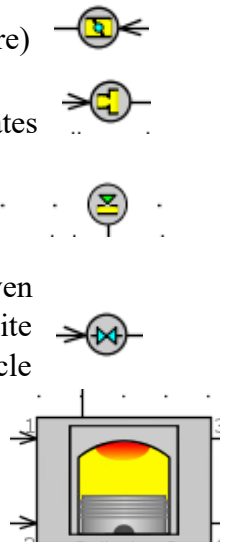
Figure 4.3: GT-POWER PFI model

From this model we have obtained dynamic intake and exhaust pressures, objects from which this information is taken are highlighted with a red square.

These components are called *PipeRound - Round Pipe with Bend*, () they are used to simulate pipes that have a round cross-section and an optional bend. In this case it is necessary to specify basic geometric characteristics and initial conditions. Other *PipeRound - Round Pipe with Bend* are not highlighted.

In the model we can see:

- *ThrottleConn*: this object simulates the throttle valve (highlighted in a blue square) [21];
- *OrificeConn - Orifice between two flow components*: this component simulates the plane connecting two flow components (highlighted in a green square) [21];
- *Injector*: simulates the PFI injector (highlighted in a pink square) [21];
- *Intake and exhaust valves*: This object defines the characteristics of a cam-driven valve including its geometry, lift profile, and flow characteristics. It is quite important to say that values of the angle lift should be consistent with the cycle (highlighted in a yellow square) [21];
- *Cylinder*: This object is used to specify the attributes of engine cylinders. It is quite important to remember that cylinder geometry is specified in the EngineCrankTrain (highlighted in an orange square) [21];



4 GT-POWER Model Setup

- *EngineCrankTrain*: this component is used to model the kinematics and rigid dynamics of common reciprocating IC engine cranktrain configurations. The rigid-dynamic model translates phased pressure forces acting on each piston to torques at crankpins, which are in turn added to produce total engine torque. The resulting engine torque is reported at various "stations" (cylinder, crankpin, shaft, brake). The net torque acting on the engine (after inertia and friction) may also be used (along with external load torques) to calculate acceleration of a free engine cranktrain ("load" mode). It is highlighted with a black square [21];
- *Links*: this component is used to connect all the elements, they are necessary in order to use GT-POWER properly.



Now, it is quite clear that all the data that have been introduced are too many to be written in every single elements, so several parameters (such as p_{amb} as ambient pressure) were created. This is quite useful since the model could be edited in a easy way.

Also, in this model we have to specify the initial conditions:

- *FluidInitialState - Initial Fluid State*: it specifies the initial conditions in flow components, in our case the state *init* is reported in fig 4.4.

Attribute	Unit	Object Value
Pressure (Absolute)	See Case S... ▾	[p_amb] ...
Temperature	See Case S... ▾	[T_amb] ...
Composition		air ...

Figure 4.4: initial state on GT-Power

- T_{exh} : temperature of exhaust gasses;
- P_{out_comp} : pressure boost, in our case, this is not only the boost pressure, but it is also the pressure at the inlet of the turbine;
- T_{runner} : temperature of the intake runner;
- T_{port_int} : temperature of the intake port;
- T_{coll_exh} : temperature of the exhaust collector.
- T_{port_exh} : temperature of the exhaust port.

In order to increase the engine load we have changed the pressure in the environment $Valle_comp_1$, in fact this pressure ($p_{out_compressor}$) is the boost pressure.

Now some restrictions have to be followed in order to increase the load:

- Mechanical restriction: The engine could not support a pressure that is higher than 90 bar, so boost pressure can't be increased as we want;
- Thermal restriction: in order to increase the bmep, it is possible to delay the combustion process, however since the engine analyzed is a turbocharged engine we should consider the temperature in the exhaust pipe which is right before the turbine. This component is made with a super alloy which could resist to temperatures up to 1000°C.

4 GT-POWER Model Setup

It is now a mandatory to properly define the combustion process, since the previous model used experimental data (pressure data) in order to perform the combustion. In our case the aim isn't study a detailed combustion process in GT-POWER but obtaining dynamic pressures, so we will use a combustion model using Wiebe function. In the four cylinders was created a function called *comb_full_load*. This function was *EngCylCombSIWiebe - SI Wiebe Combustion Model* which imposes the combustion burn rate for spark-ignition engines using a Wiebe function and it can be used with any type of injection. In *figure 4.5* specific values of parameters can be seen.

Attribute	Unit	Object Value
Anchor Angle (def = 50% burn)		[mfb_50] ...
Duration (def = 10% to 90%)		19 ...
Wiebe Exponent		def (=2.0) ...

Figure 4.5: specific values of the function *comb_full_load*

Where:

- The first parameter is the MFB50 which is not constant, infact it is used to calibrate simulations (see subsection 5.2);
- The second parameter is the duration of the combustion process ($MFB_{90} - MFB_{10}$), it is costant and equal to the case 2000x14;
- The last one is the Wiebe exponent and it is equal to its default value 2.

Changing MFB50 and boost pressure, different cases were analyzed and they will be discussed in chapter 5.2.

Also another tool of GT-POWER was used: the optimization tool. We used it in order to find the best IVO in order to obtain the best *bmp*. To do this we used the *direct optimizer tool* provided by GT-POWER; in particular we maximized the *btq:engine1* (i.e. the engine torque) using the *Fase_B* (IVO).

Single Objective Setup		
Dependent Variable RLT		btq:engine-1 ...
Objective	Maximize	...
Maximum Number of Iterations		20 ...

(a)

Attribute	Unit	1
Parameter to be Varied		FASE_B ...
<input checked="" type="radio"/> Parameter Range		40.0 ...
Lower Value of the Range		0.5
Upper Value of the Range		1.5
Resolution (% of Range)		2.0 ...

(b)

Fig 4.6: parameters used in the direct optimizer

The results of these studies were examined in GT-POST, the tool used by GT-POWER for the post-processing and will be discussed in the chapter 5.

4 GT-POWER Model Setup

4.2 DI model

Transforming the GT-POWER PFI model into a DI model was pretty easy in GT-POWER, infact only the *injector* was edited: it was disconnected by the intake port and it was connected to the cylinder. The new model is shown in *fig 4.7*.

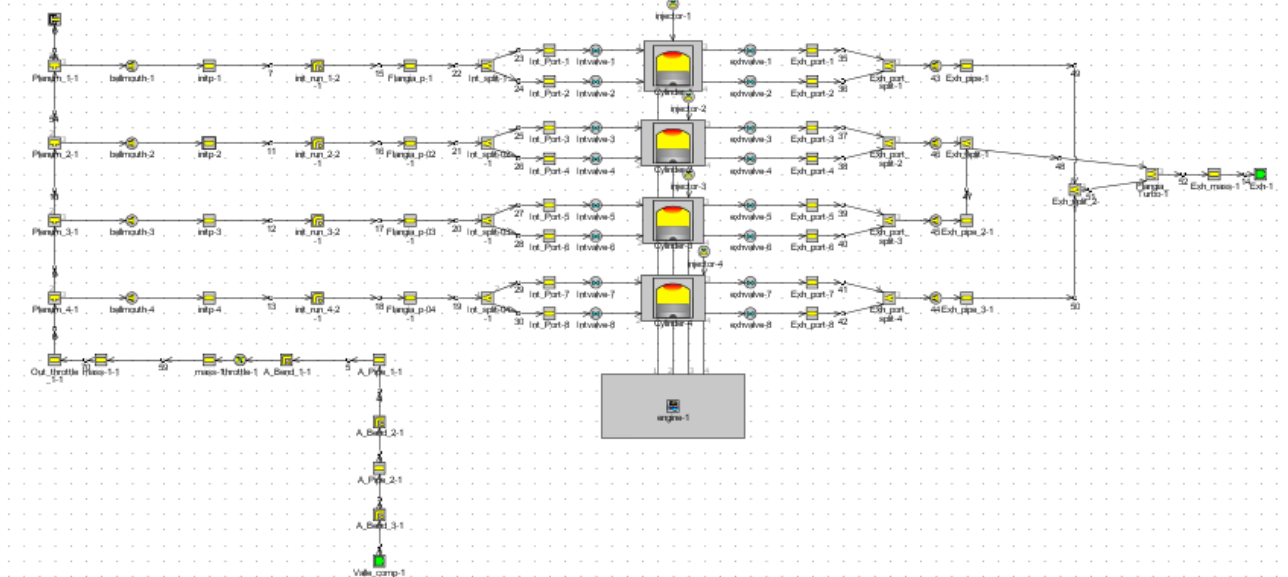


Figure 4.7: DI model in GT-POWER

After the model was ready several initial conditions has to be modified:

- The injection rate was modified, infact this model is a DI model and the injection pressure in this type of engines could be equal to 20 bar [22], so the injection rate was tripled, except in the case in which the injection rate is the variable examined;
- In all the cases examined the SOI was delayed in order to improve the volumetric efficiency and consequently the power density;

Also the geometry of the injector hole was established: it was a single hole injector with a diameter of 0.7mm . It is quite important to highlight that this value will be used also in CONVERGE.

<input checked="" type="checkbox"/> Rate <input checked="" type="checkbox"/> Timing-General <input checked="" type="checkbox"/> Initialization <input checked="" type="checkbox"/> Nozzle (DI Only)		
Attribute	Unit	Object Value
Nozzle Hole Diameter	See Case S... ▾	[diameter] ...
Number of Holes per Nozzle		1 ...
Nozzle Discharge Coefficient		def (=0.7) ...

Figure 4.8: definition of the nozzle diameter; in this case it is equal to [diameter] is equal to 0.7 mm

4 GT-POWER Model Setup

Sweep of the start of injection and of the end of injection

After these general changes, several cases were created in order to evaluate the SOI (*start of injection*) and its influence on the power density. First of all on the characteristics of the injector the *Fase_B* (EOI) was delayed.

Attribute	Unit	Object Value
Injector Delivery Rate	See Case S...	[delivery]...
Fuel Ratio Specification	Air-to-Fuel	
Fuel Ratio		[dosatura]...
Air Mass Flow Rate Sensor		
Part Name		
Improved Calculation of Stoich. AFR		<input type="checkbox"/>
RLT		fav:A_Bend_1-1...
Number of Injectors per Sensor		4...
Apply Engine Trapping Ratio to Air Mass Flow Rate		<input type="checkbox"/>

Attribute	Unit	Object Value
Source of Angle		
Attached Cylinder		
Part on Map		*...
Driver Reference Object		
Injection Timing Angle	See Case S...	[Fase_B]...
Injection Timing Flag		Injection-end
Injector Location (Pipes only)		0.9...
Injected Fluid Temperature	See Case S...	[Ing_temp]...
Fluid Object		methane-vap...
Vaporized Fluid Fraction		1...

Figure 4.9: parameters of the injector, FASE_B can be changed in the case setup

As for the PFI model the *boost_pressure* and the *MFB50* were used as calibration parameters.

Sweep of the injection rate

In this particular analysis the injection rate (*delivery*) was used as parameter evaluated.

As explained in the PFI case (subsection 4.1), the parameter *delivery* was changed in the case set up. In particular it was reduced up to be double respect to the PFI value and 2,5 times respect to the PFI value.

Parameter	Unit	Description	Case 1	Case 2	Case 3
Case On/Off		Check Box to Turn Case On	<input checked="" type="checkbox"/>	<input checked="" type="checkbox"/>	<input checked="" type="checkbox"/>
Case Label		Unique Text for Plot Legends	2000X20	2000X20	2000X20
delivery	g/s		5.3...	3.5...	4.5...

Figure 4.10: values of the delivery in the case set up of GT-POWER

Sweep of the compression ratio

In this particular case the object *EngineCrankTrain* was modified; infact, changing the compression ratio, is equal to modify the geometry of the engine (*geom*).

Attribute	Unit	Object Value
Bore	mm	72...
Stroke	mm	84...
Connecting Rod Length	mm	129...
Compression Ratio		[CR]...
TDC Clearance Height	mm	1.7...

Figure 4.11: template of the engine geometry

4 GT-POWER Model Setup

Now, a new parameter called *CR* was created in the case set up and values are reported in the *table 4.1*.

	Case 1	Case 2	Case 3	Case 4	Case 5
CR	9.8	11	12	13	14

All of these three cases will be discussed in the next chapter.

Chapter 5

Simulation results

The section is dedicate to the discussion about the numerical results. In particular we will analyze the CH₄ engine model that will be compared to the H₂ engine model that will be created in the future.

5.1 2000x12 and 2000x14 simulations

It is quite important to understand that no experimental results are available for the Full Load of PFI engine, so we need to obtain the two parameters α and C_{sf} using old simulations of Paolo De Angelis thesis and simulations at an higher load 2000x12 and 2000x14. After the calibration of these two simulations we will interpolate all the results of α and C_{sf} and we will use the mas parameters for the Full Load PFI case.

Results for 2000x12 were already investigated in the Paolo De Angelis thesis, however they weren't so accurate; in particular the CA of maximum pressure was retarded and its own value was too high. Starting from his old results we calibrate the particular case and the following results were obtained (fig 5.1 and 5.2). It is necessary to observe that only two cycles were simulated, since it was observed that starting from the second cycle the simulation was stable.

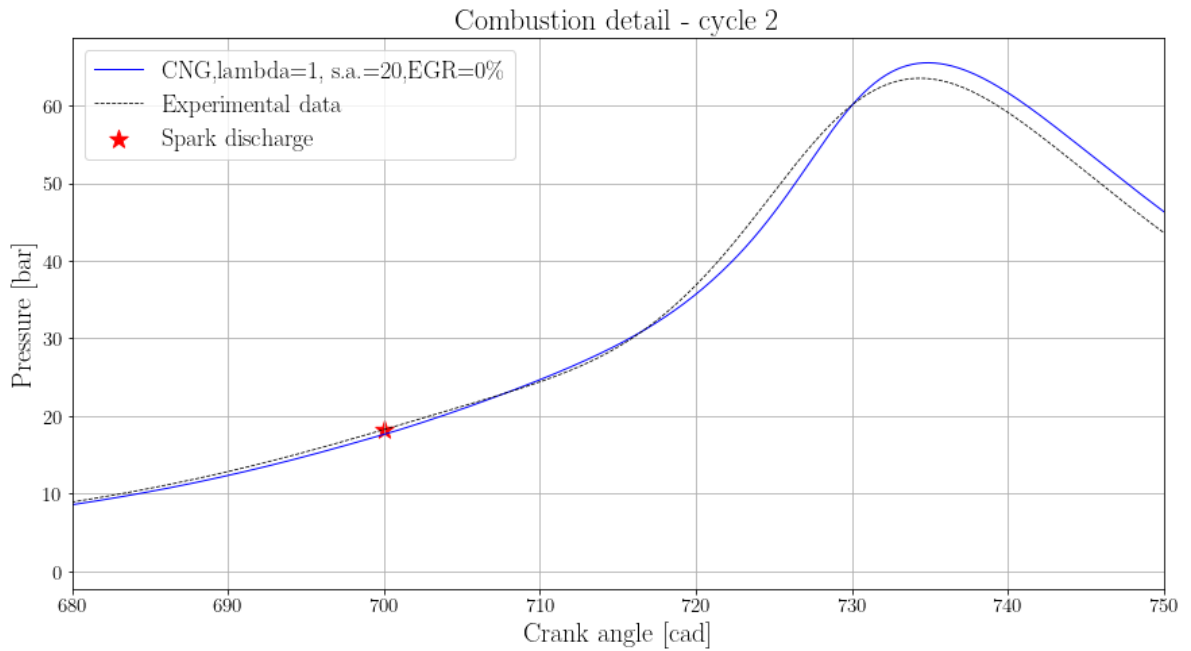


Figura 5.1: Combustion detail of the second cycle of the simulation 2000x12

5 Simulation results

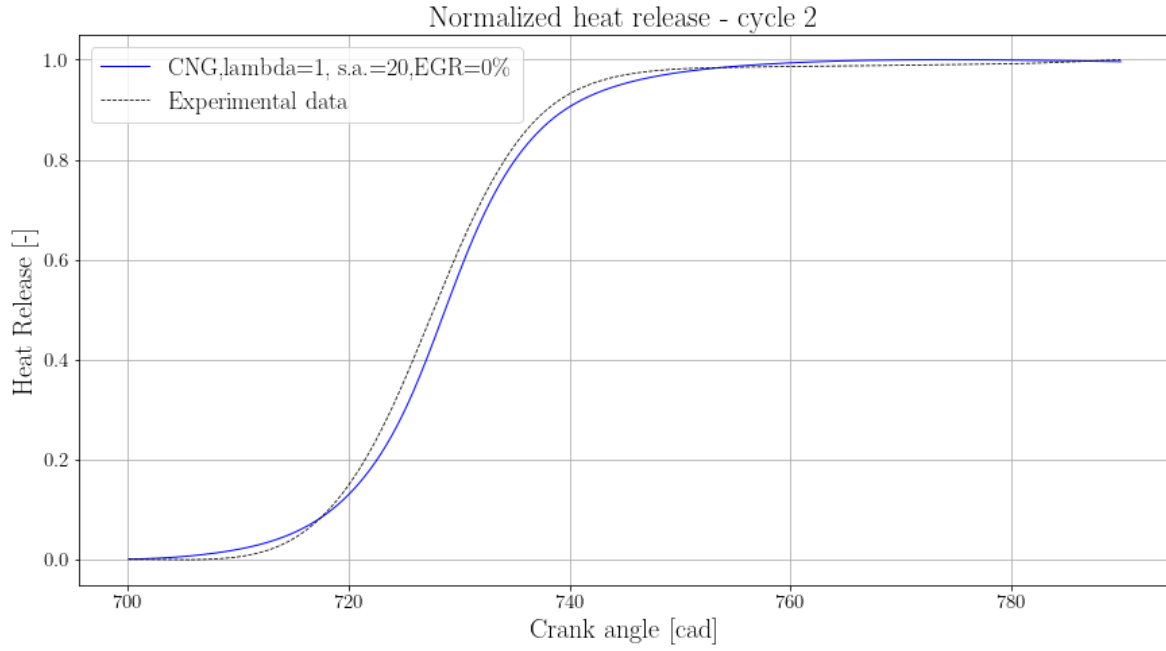


Figure 5.2: Normalized heat release of the second cycle of the simulation 2000x12

Now it is required to say that the main aim of this part of the work is to obtain quite good values of parameters α and C_{sf} , not to calibrate perfectly the simulation.

Results for 2000x14 case were investigated for the first time in this thesis. Firstly it was necessary to manipulate data from experimental results using Matlab following the procedure explained in the subsection 2.2.2 of this thesis. After the dynamic pressure of the intake manifold and the dynamic pressure of the exhaust manifold were manipulated in order to be written from CONVERGE, initial values for α and C_{sf} were chosen and the first simulation was run.

5 Simulation results

The final results of this case are reported in *fig 5.3 fig 5.4*.

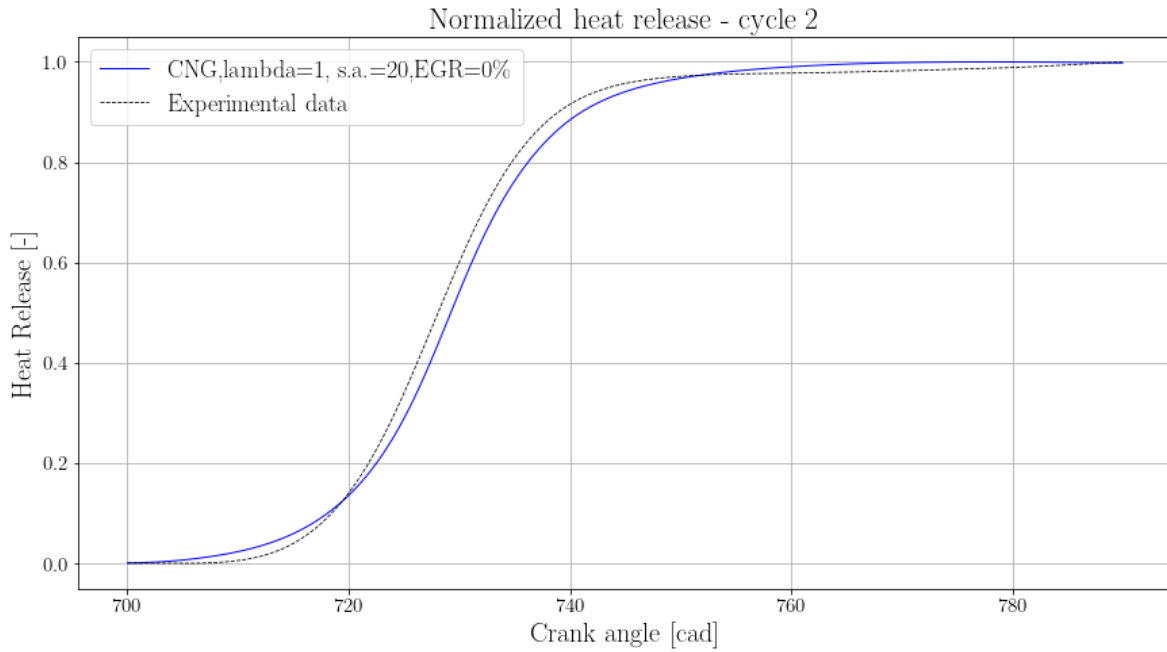


Figura 5.4: Normalized heat release of the second cycle of the simulation 2000x14

In the table 5.1 are reported values of α and C_{sf} regarding old simulations in the Paolo De Angelis thesis and for the simulations 2000x12 and 2000x14.

Simulation	α	C_{sf}
2000x3.6	2.5	12
2000x6.2	1.7	14
2000x7.9	1.6	16
2000x12	1.5	16
2000x14	1.05	15.5
2000xFULL (intepolated)	0.75	16

The interpolation used was a logarithmic regression, we used this particular regression because the behaviour of α and C_{sf} wasn't linear. Infact, for the case of C_{sf} , an asymptote can be observed.

5 Simulation results

5.2 PFI engine load increase on GT-POWER

Since no experimental data are available, it was impossible to use the procedure of the subsection 2.2.2. In order to properly increase the load limit values for maximum pressure in the combustion chamber and in the exhaust pipe were used:

$$p_{max} = 90 \text{ bar} \quad T_{exh} = 1000^\circ\text{C}. \quad (5.1)$$

In order to reduce the degree of freedom of the problem a 1D 0D software was used. GT-POWER was not only used to obtain dynamic pressures, but it was useful to obtain a value of M_{FB50} and a first value of the b_{mep} of the engine at full load (useful for the interpolation).

In order to increase the load, the combustion process was retarded. However the longer delay, the higher exhaust temperature was obtained, so it was important to evaluate all the of the problem.

To focus only on the increase of the load a simple wiebe function was used on GT-POWER; following this procedure, only two parameters were used in order to obtain this new model:

- the pressure at the outlet of the compressor;
- the value of M_{FB50} .

Two cases were analyzed:

- $p_{out} = 2.2 \text{ bar}$ $M_{FB50} = 18.5^\circ$ (fig 5.5)

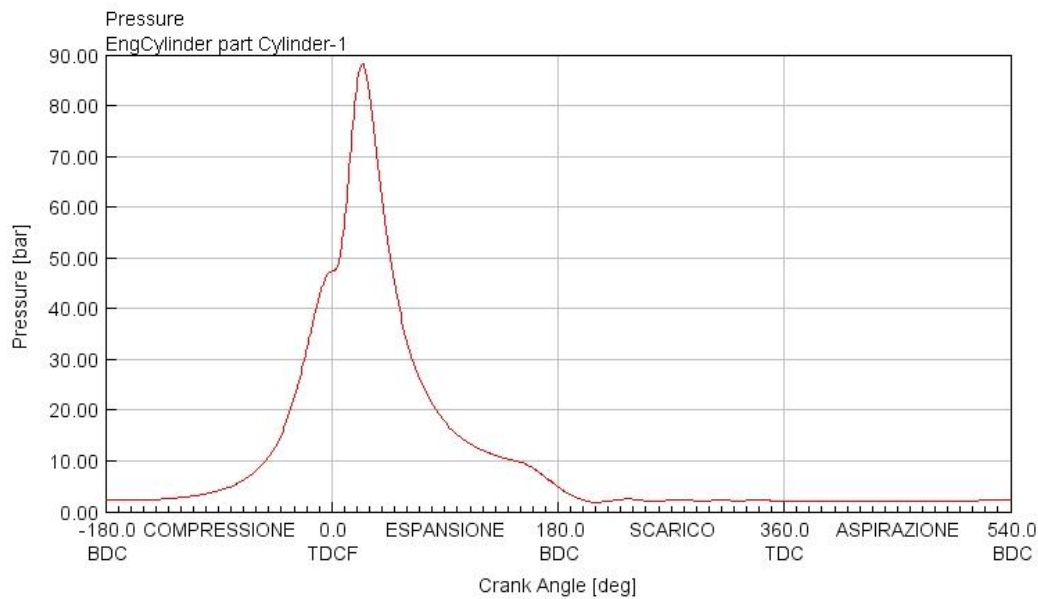


Figura 5.5: pressure of the combustion chamber of the case 1

5 Simulation results

- $p_{out} = 2.3 \text{ bar}$ $M_{FB50} = 20^\circ$ (fig 5.6)

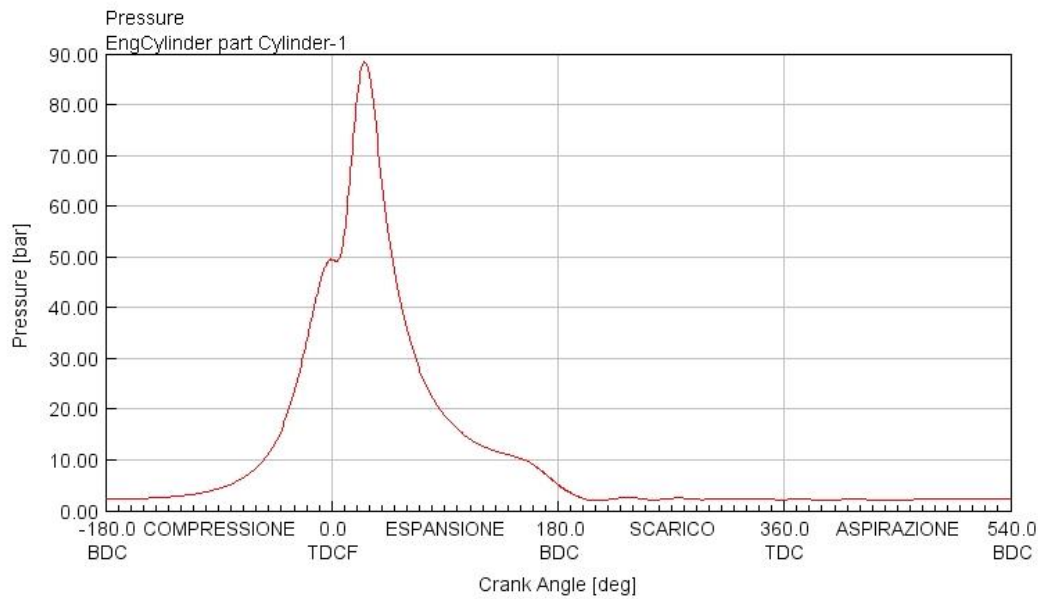


Figura 5.6: pressure of the combustion chamber of the case 2

As can be seen both cases have the maximum pressure below 90 bar, also the temperature of exhaust gasses is below 1000°C :

$$T_{exh1} = 977^\circ\text{C}$$

$$T_{exh2} = 990^\circ\text{C}$$

As a result we have a *bmep* of:

$$bmep_1 = 20.5 \text{ bar}$$

$$bmep_2 = 21.3 \text{ bar}$$

In order to have the highest power density the case 2 was chosen. The dynamic pressures of this case were exported from GT-POWER and manipulated in order to be fed by CONVERGE.

Secondly, another study of the PFI engine model was done. Since the engine had not a VVT, an optimization of openings and closures valves was conducted. Using the tool optimization offered by GT-POWER it was possible to obtain an optimized lift (fig 5.8)

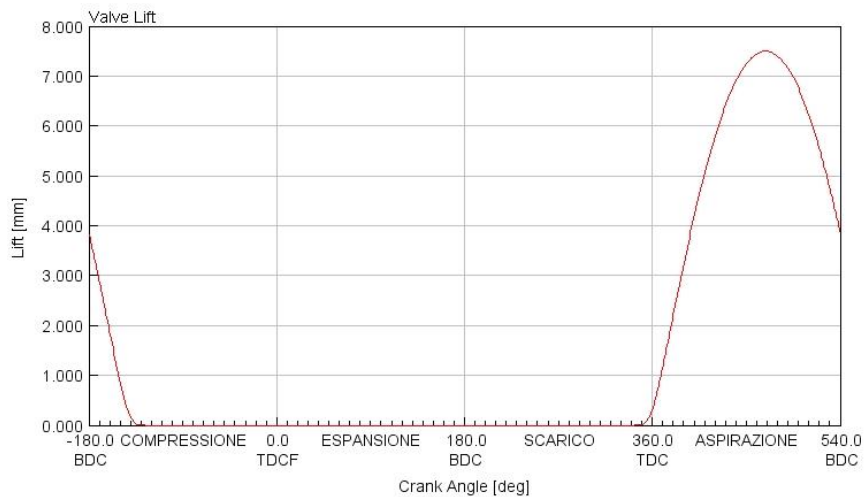


Figura 5.7: standard lift

5 Simulation results

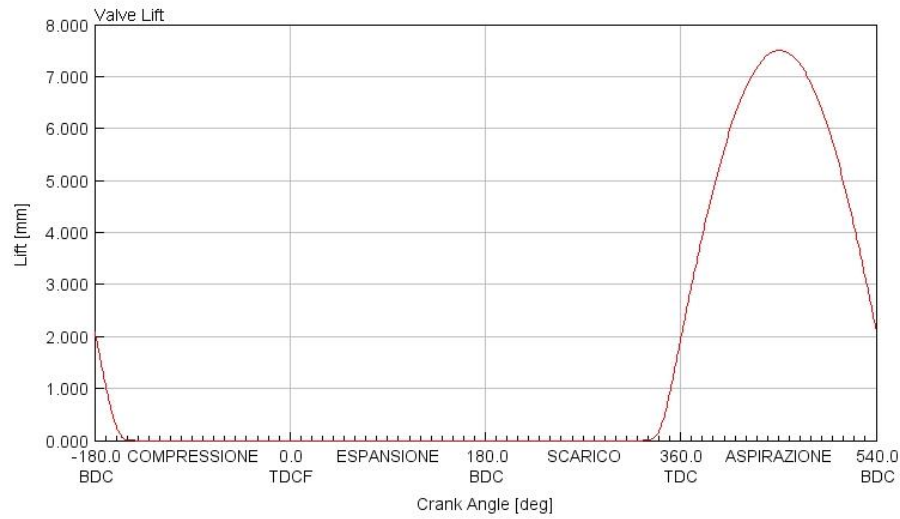


Figura 5.8: optimized lift

Three cases were analyzed with the optimized lift:

- $p_{out} = 2.2 \text{ bar}$ $M_{FB50} = 19^\circ$ (fig 5.9)

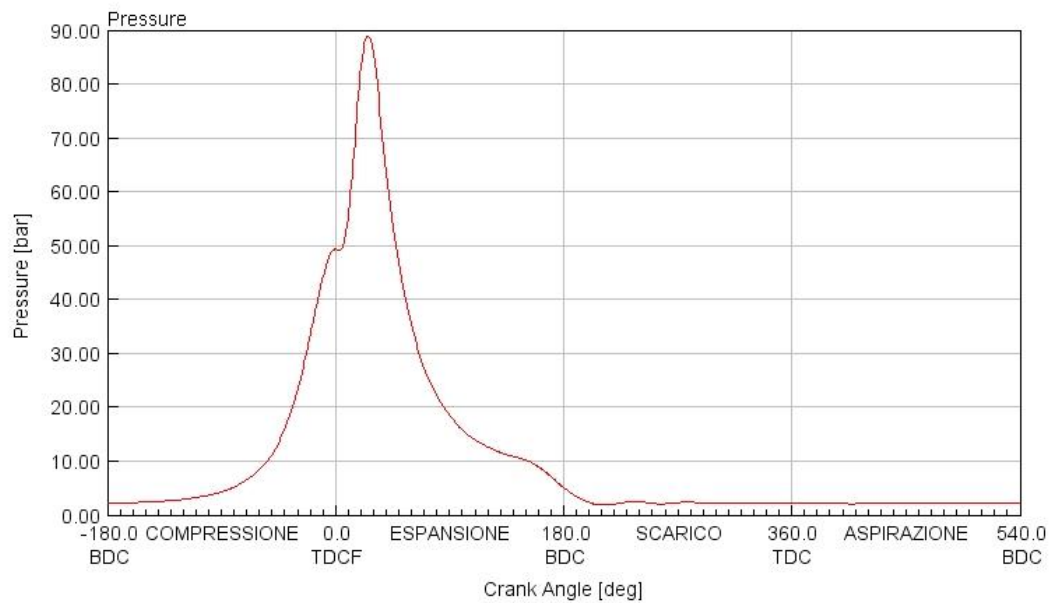


Figura 5.9: pressure of the combustion chamber of the case 1

5 Simulation results

- $p_{out} = 2.1 \text{ bar}$ $M_{FB50} = 18^\circ$ (fig 5.10)

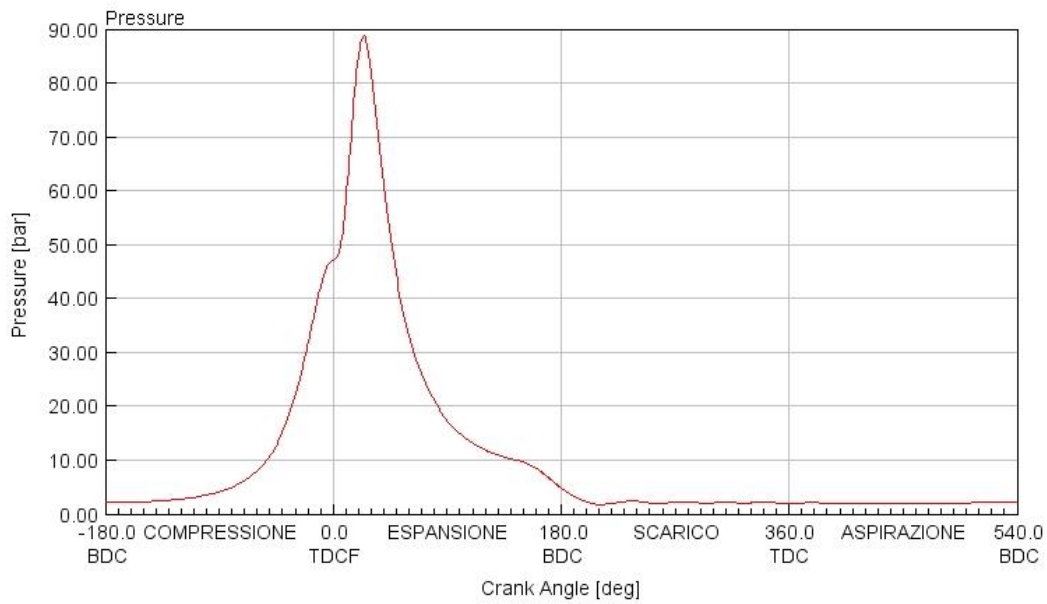


Figura 5.10: pressure of the combustion chamber of the case 2

- $p_{out} = 2.25 \text{ bar}$ $M_{FB50} = 20^\circ$ (fig 5.11)

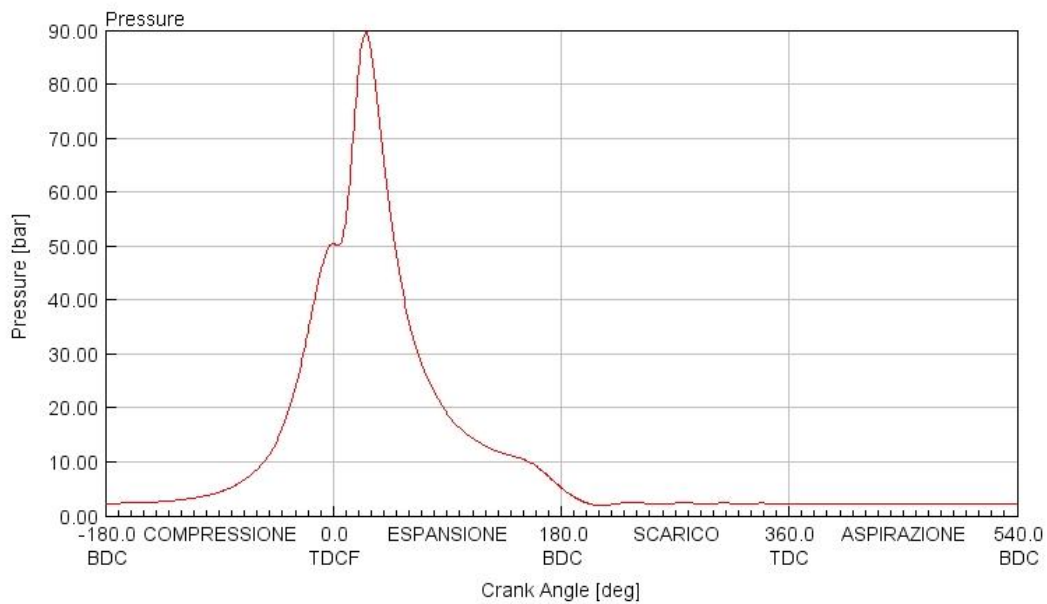


Figura 5.11: pressure of the combustion chamber of the case 3

Now this three different cases has the following values of b_{mep} :

$$b_{mep_1} = 21 \text{ bar} \quad b_{mep_2} = 20.4 \text{ bar} \quad b_{mep_3} = 21.5 \text{ bar}$$

It is a mandatory to say that this study was not investigated anymore because in modern engines valve overlap is minimum, while with this particular choice it was not negligible. An engine with a large overlap produces an amount of pollutant that is too high for the 2021's rules.

5 Simulation results

All in all this study was usefull, because thanks to it, it was possible to see how, with a smaller boost it was possible to obtain equal or higher values of b_{mep} .

5.3 PFI Full load simulation

Once all the dynamic pressures were obtained and after the interpolation was done, the full load case can be studied using CONVERGE. In this type of simulation the parameter used for calibrate the case was the spark advance and not α and C_{sf} (blocked parameters found with the interpolation). Infact the aim was to obtain a value of about $M_{FB50} = 20^\circ C$ (found in GT-POWER) using a proper SA.

Firstly, it is important to change some parameters, that are necessary for the stability of the simulation:

- The embedding of the spark plug must to be retarded, since the combustion process is retarded itself.

Without changing this parameter the simulation is highly unstable as can be seen in *fig 5.12*

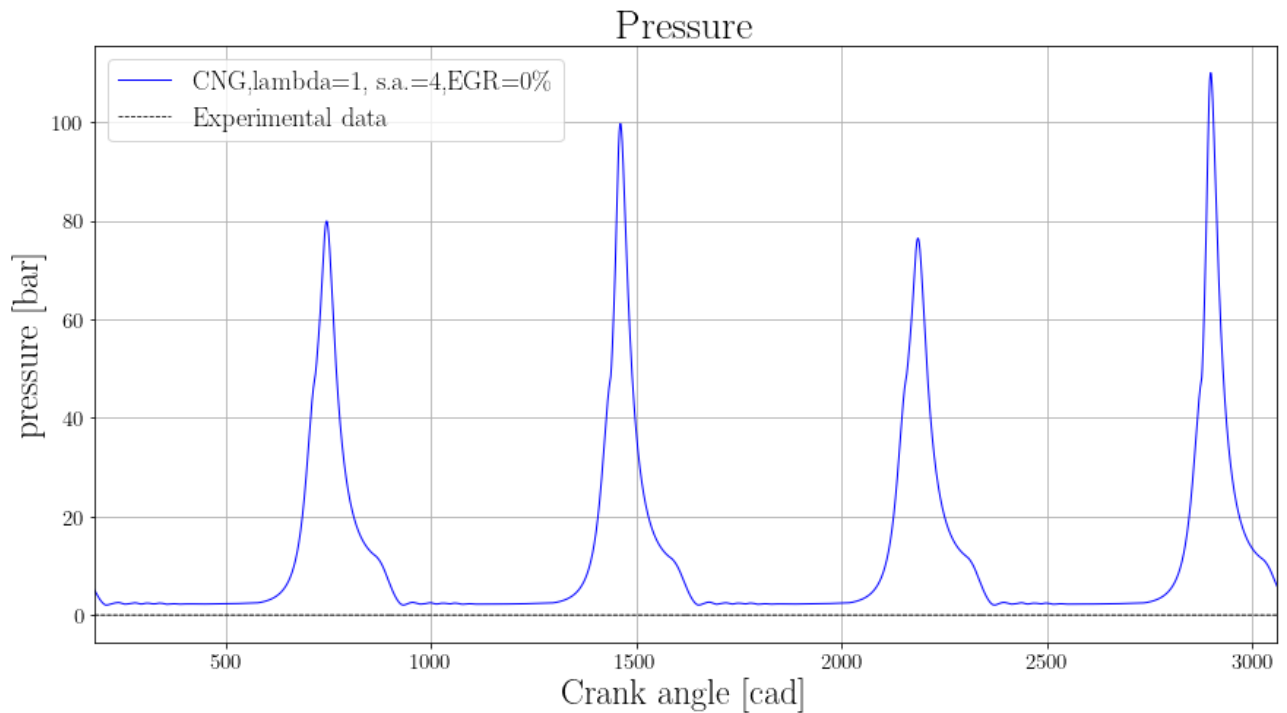


Figure 5.12: pressure of the 4 cycles simulated.

This unstable behaviour happens due to a not well refined mesh during the spark advance.

5 Simulation results

However, fixed this problem, the simulation will be stable again, as can be seen in *fig 5.13*.

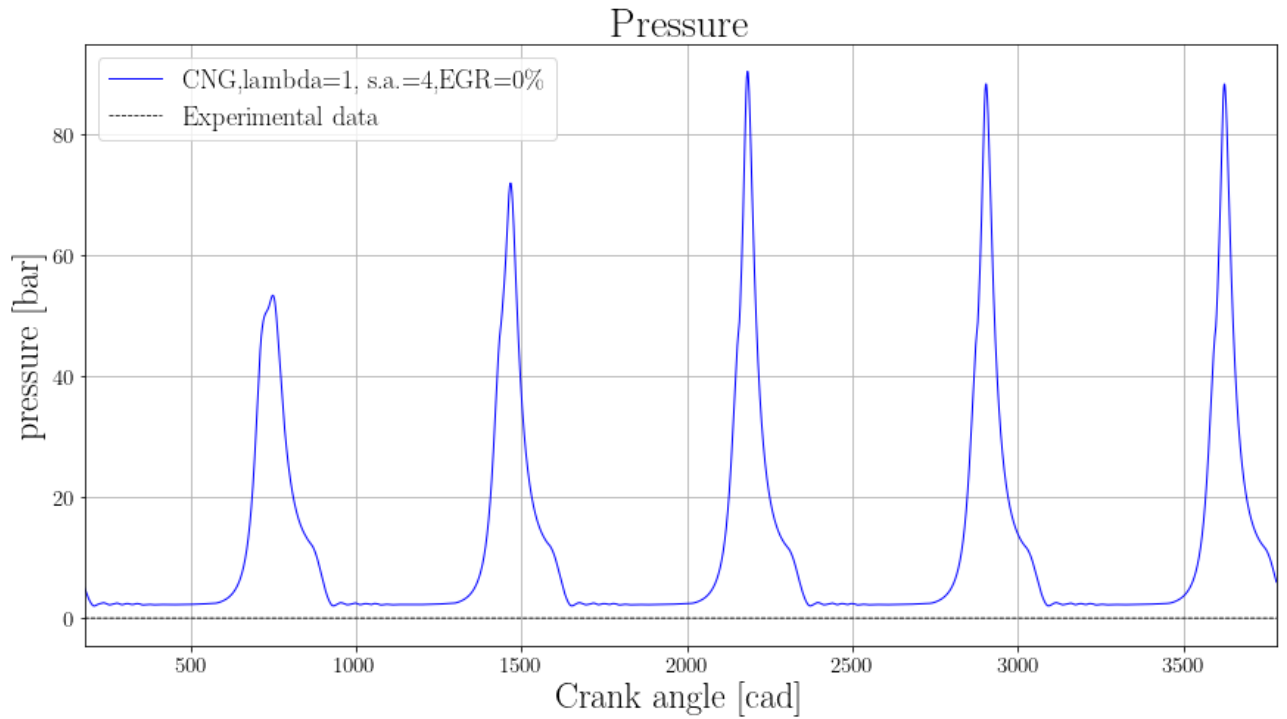
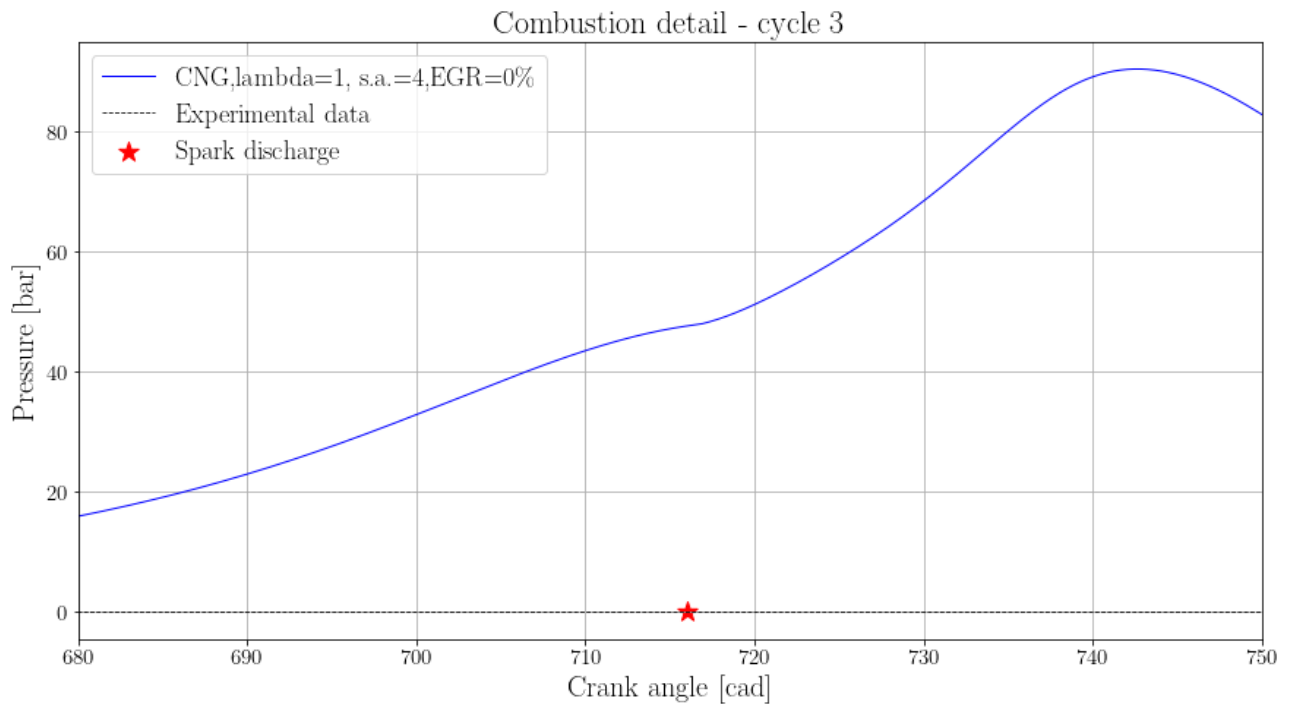


Figure 5.13: pressure of the 4 cycles simulated.

In this particular case the stability of the simulation is reached after two cycles and not only one, as in the previous cases. The cause of it is probably the high value of the load, CONVERGE spent two cycle in order to guarantee the stability.

The combustion detail of the three stable cycles is shown in *fig 5.14*



5 Simulation results

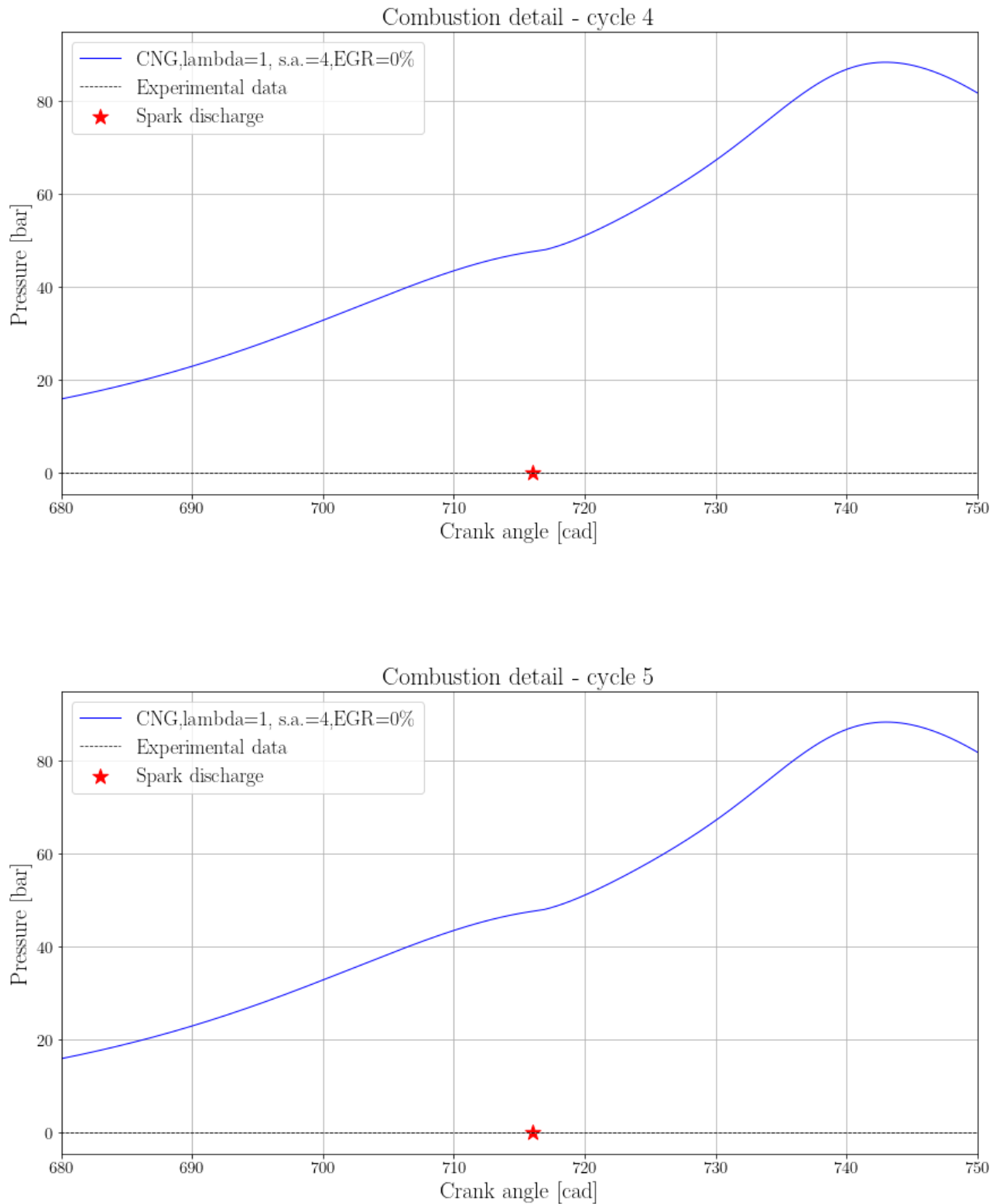
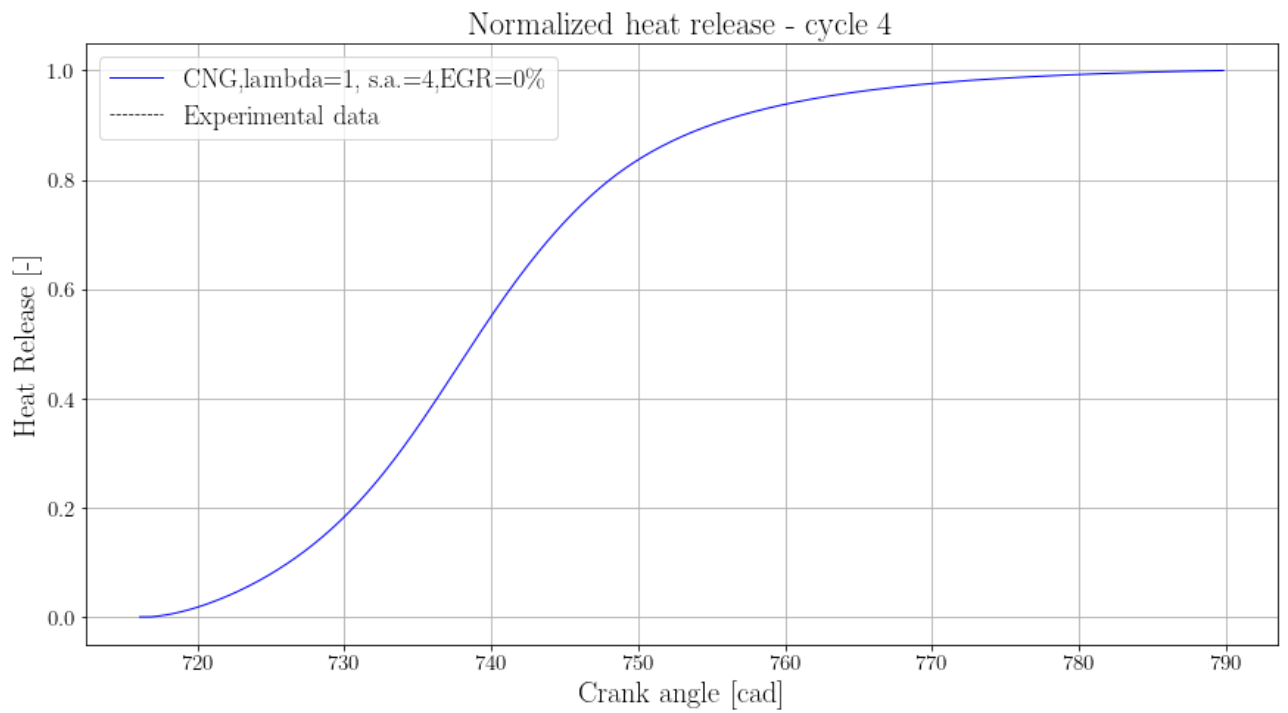
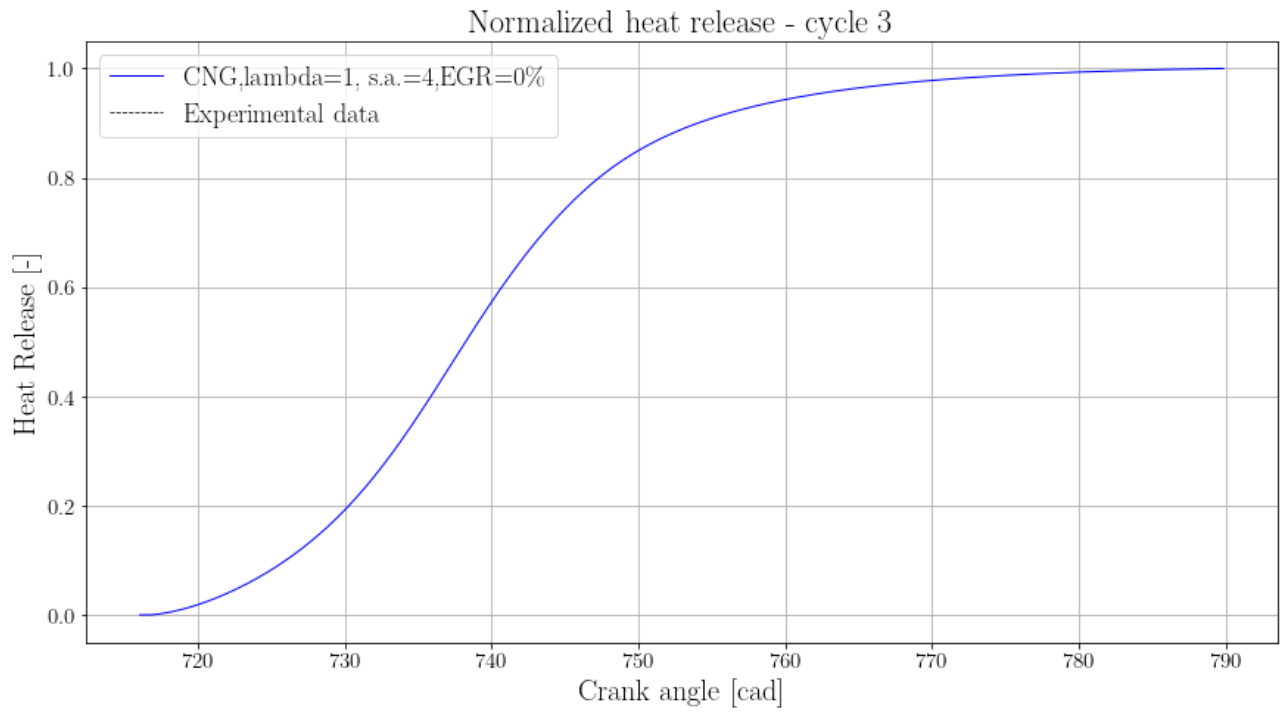


Figure 5.14: combustion details of cycle 3-4-5

As can be seen the spark advance chosen is 4. Also, the maximum pressure is under the limit of 90 bar.

5 Simulation results

In the following figures the M_{FB50} can be evaluated (*fig 5.15*).



5 Simulation results

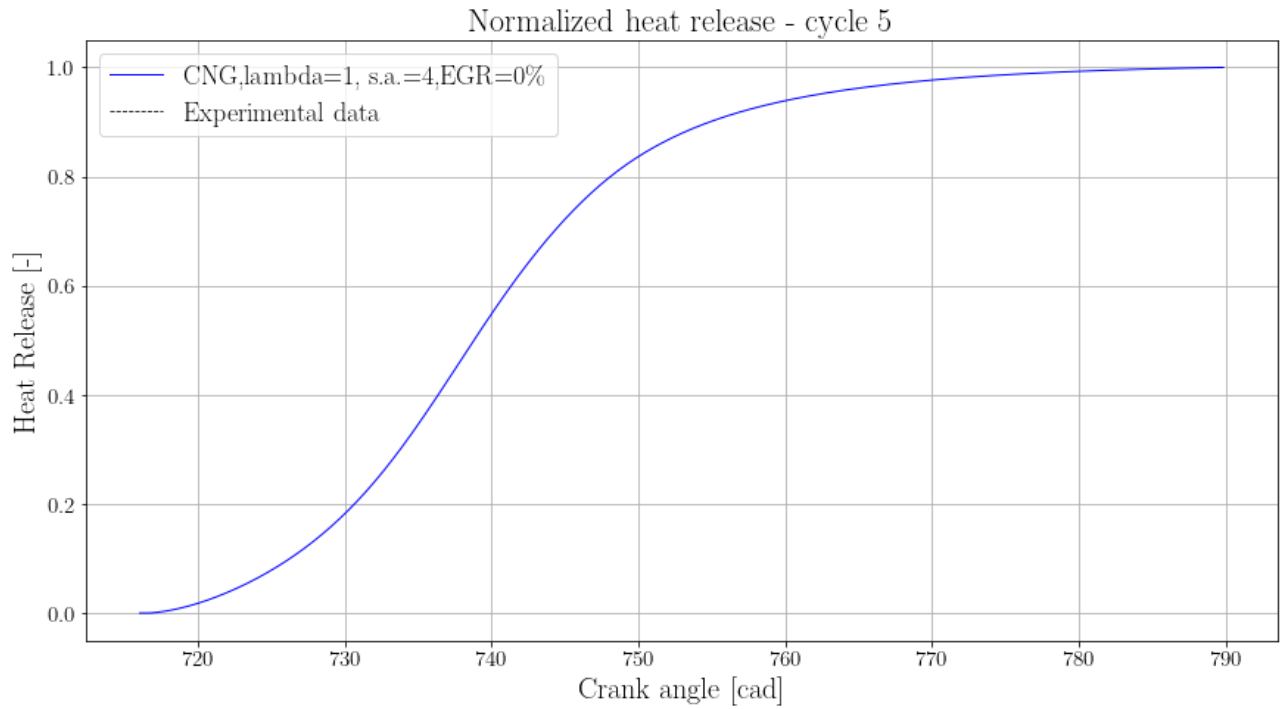


Figure 5.15: Normalized heat release of the 3-4-5 cycles of the simulation 2000xFULL

The M_{FB50} obtained is about 20° (values from 18.75° to 19.65°), that was the aim of the simulation.

This case is the base case of CH4 PFI engine that will be compared with the H2 PFI engine.

The table 5.2 reports some of the main characteristics of these three cycles.

	Max pressure (bar)	CA of max pressure ($^\circ$)	MFB_{50} ($^\circ$)	MFB_{10-90} ($^\circ$)
Cycle 3	89.45	742.66	739.25	28.06
Cycle 4	88.39	742.97	739.76	28.66
Cycle 5	88.36	742.98	739.77	28.56

5 Simulation results

5.4 DI engine studies on GT-POWER

Now, following the procedure that was done for the PFI engine, it is necessary to start the investigation of the direct injection from a zero-D 1-D simulation.

Since GT-POWER do not require specifications for the geometry of injector in some models, we decided to use a very simple injector, in which only the hole dimension was specified.

$$d_{hole} = 0.7mm$$

It is now clear that the injector has got a single hole. Also, for GT-POWER, the position of the injector is not important: basically we have just linked the injector to the engine.

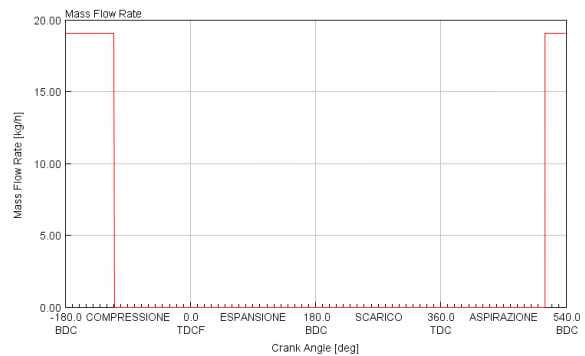
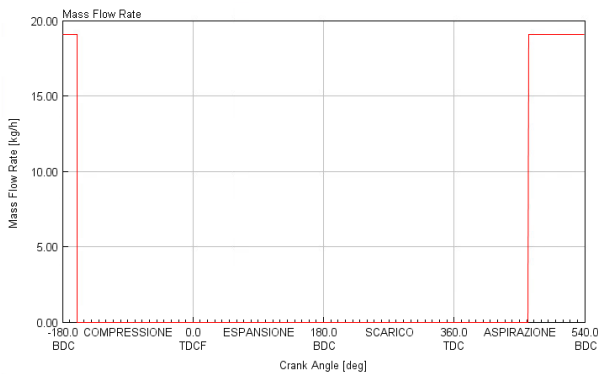
Several studies were conducted in order to rudimentally understand what direct injection is and what are the major changes in the engine:

- Variation of the injection timing;
- Variation of the compression ratio;
- Variation of the injection rate.

Now it is a mandatory to specify that on the CFD simulation in CONVERGE we will focus particularly on the first aspect.

For the first analyses we studied five different cases with the following SOI:

- $SOI = 466CA$;
- $SOI = 516CA$;
- $SOI = 566CA$;
- $SOI = 606CA$;
- $SOI = 626CA$;



5 Simulation results

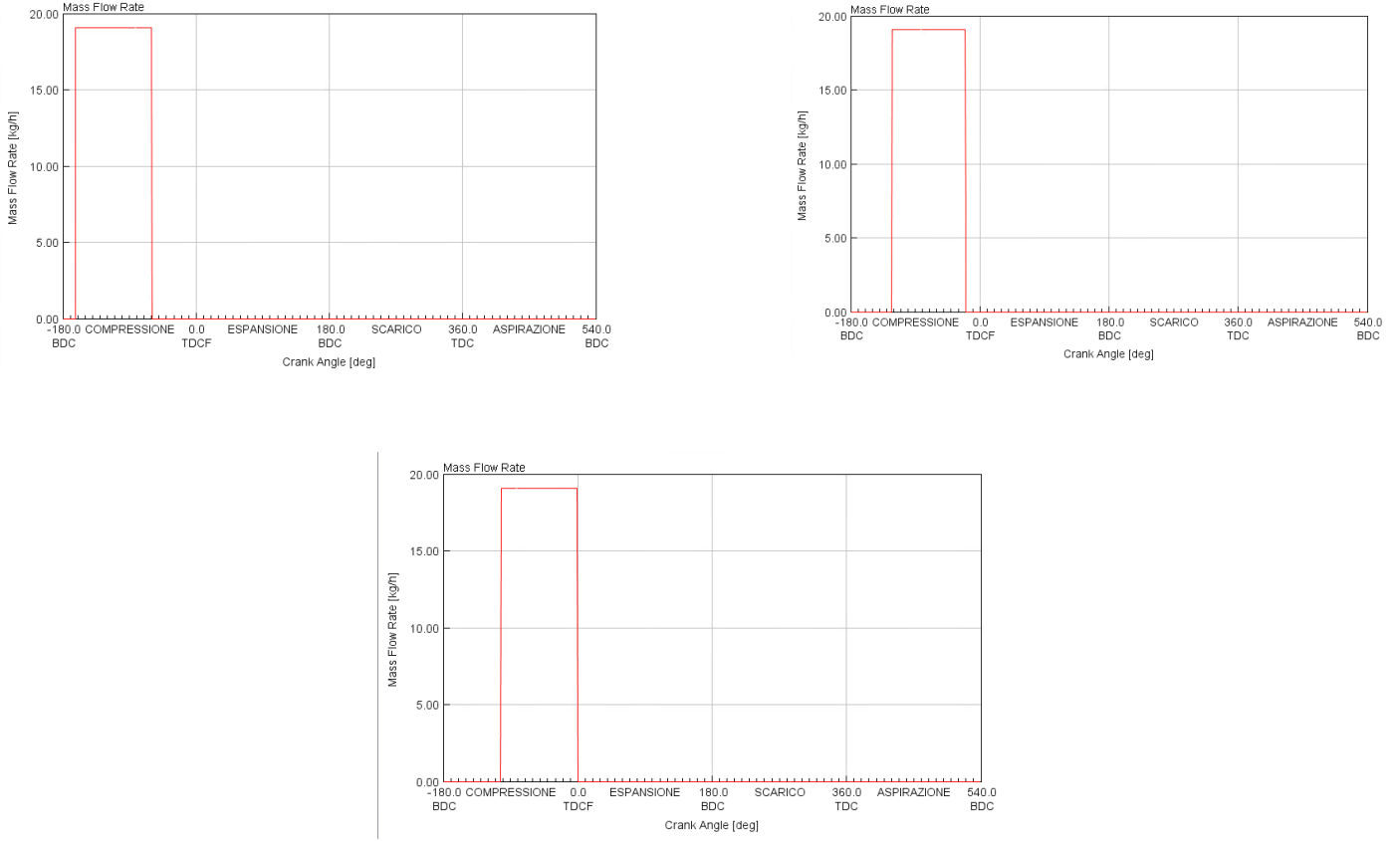


Figure 5.16: different injection timings

In the figures it can be seen that the injection rate adopted was constant and equal to three times of the value used for the PFI case.

$$inj_{rate} = 5.3 \frac{g}{s}$$

Also, in order to well understand effects of direct injection we used the same conditions of the PFI case chosen and described in the subsection 5.2:

$$p_{out} = 2.3 \text{ bar} \quad M_{FB50} = 20^\circ$$

The first important effect of shifting the injection timing was an increase of the volumetric efficiency as can be seen in *fig 5.17*.

5 Simulation results

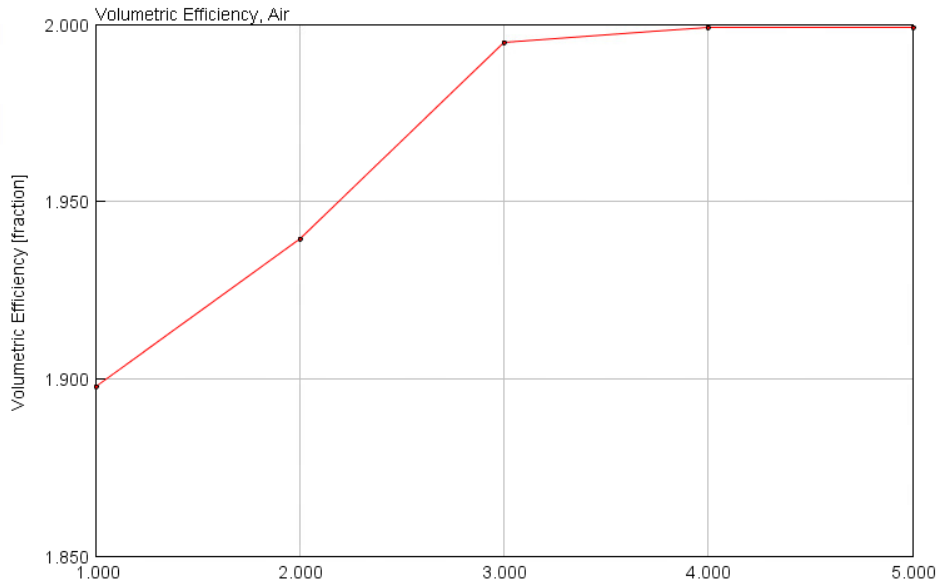


Figure 5.17: values of the volumetric efficiency in the five cases.

It can be observed that delaying the injection the volumetric efficiency will increase until it reaches an asymptote. This can be easily explained considering the valves lifts:

- Injection in case 1 and case 2 happens when intake valves are still opened, so part of the space in the combustion chamber is occupied by CH₄;
- Injection in case 3 4 and 5 happens when intake valves are closed, so it is obvious that the efficiency increases and that it is practically constant, this happens because during the intake phase only air was present in the chamber.

It is also clear that the volumetric efficiency is higher respect to the PFI one (1.84).

The behaviour of the *b MEP* is the same of the volumetric efficiency as can be seen in *fig 5.18*. Shifting the injection timing the volumetric will increase and so the *b MEP*. However, it is important to remember that all these cases exceeds the limit of maximum pressure (90 bar). After we have seen the effects of the direct injection we will calibrate these five cases in order to choose the best one that will be used as first step for the CONVERGE simulation.

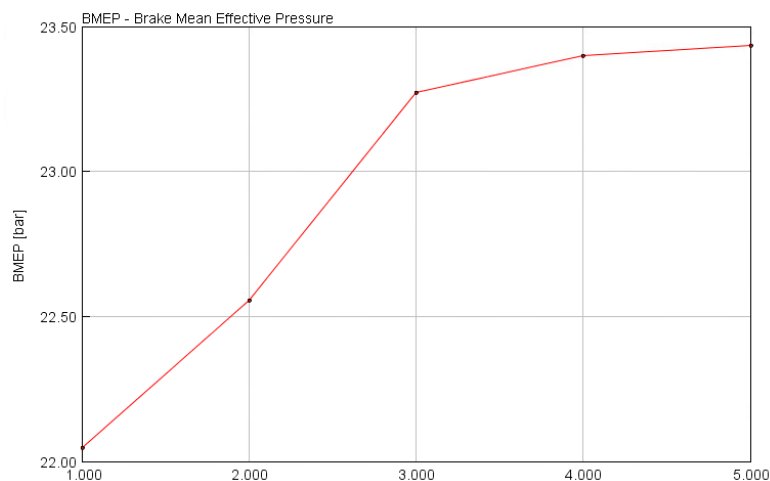


Figure 5.18: *b MEP* of the five cases

5 Simulation results

After the calibration considering the two limits exposed in the subsection 5.2 (maximum pressure and temperature of exhaust gasses) the *b MEP* of these five cases is shown in *fig 5.19*.

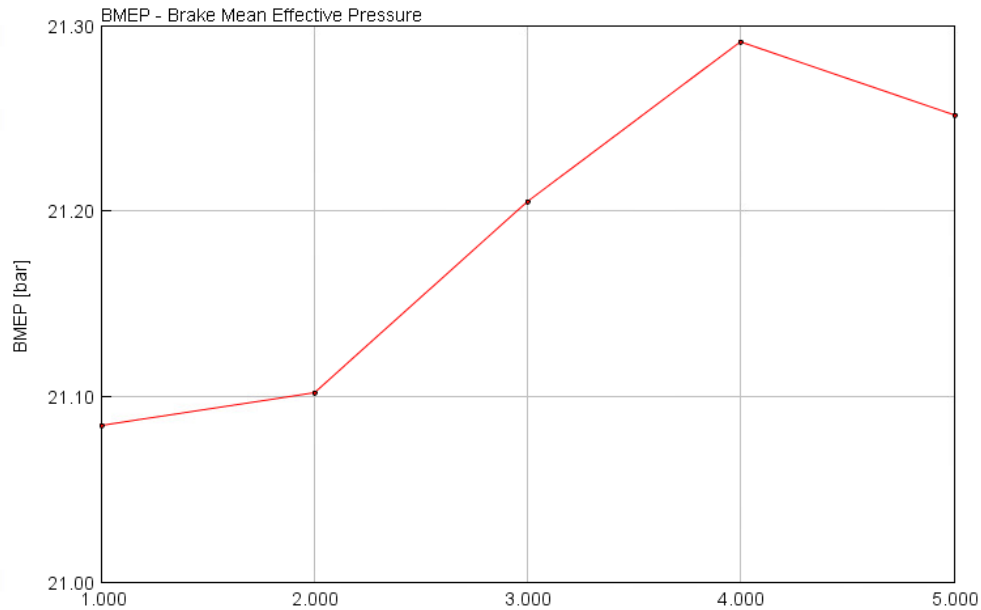


Figure 5.19: *b MEP* after considering the two limits

It is clear that the case with the best power density is the case #4, however it is a mandatory to remember that this simulation is quite rudimental and it is impossible to describe the mixing process, so it is not safe to assume this case as the best one because the EOI is too near to the TDCF (20° from TDCF). A safer choice is the case #3 where the EOI is 60° before the TDCF. This case has the following characteristics:

$$p_{out} = 2.1 \text{ bar}$$

$$M_{FB50} = 19.5^\circ$$

In *fig 5.20* the pressure in the combustion chamber for case 3 is shown.

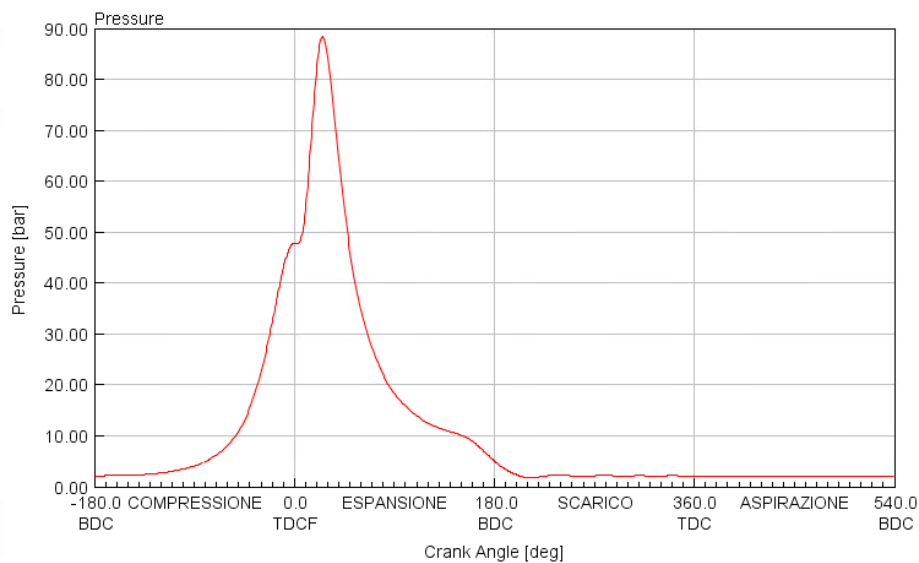


Figure 5.20: pressure in the combustion chamber for case 3

5 Simulation results

The dynamic pressures of this case will be used for the simulation in CONVERGE; also values for SOI and EOI of this case will be the first step for the CONVERGE simulation.

The second study focuses on the variation of the compression ratio. We created five different cases which have the same SOI, EOI, injection rate, boost pressure and MFB50 of the case #3 recently presented. The five compression ratios (CR) considered are:

- $CR = 9.8$ (standard);
- $CR = 11$;
- $CR = 12$;
- $CR = 13$;
- $CR = 14$.

First of all we analyzed effects of an increase of the CR . It is obvious that the higher CR , the higher the maximum pressure of the chamber as shown in *fig 5.21*

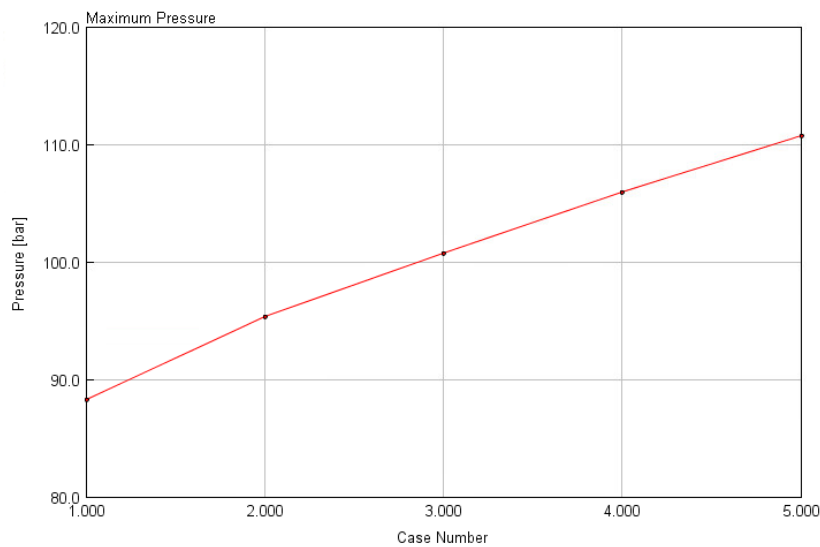


Figure 5.21: maximum pressures

Another interesting trend is the increase of the efficiency of the engine and, consequently, the decrease of the temperature of the exhaust gasses as shown in *fig 5.22 and 5.23*.

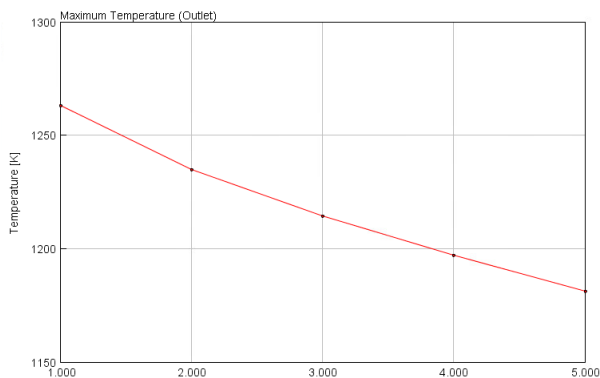


Figure 5.22: maximum temperature at the outlet

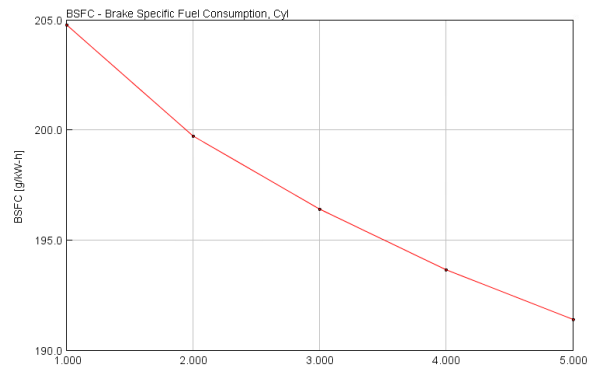


Figure 5.23: bsfc of the engine

5 Simulation results

The *b MEP*, also, increases as shown in *fig 5.24*.

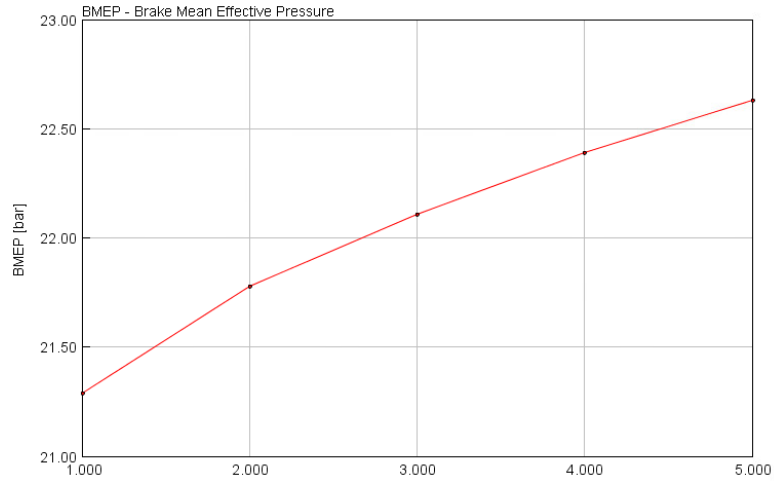


Figure 5.24: *b MEP* of five cases

Now that we have observed the effects of CR we will calibrate these cases. One of the interesting results of the calibration is the longer and longer delay of the combustion process if the CR is bigger. We will report the M_{FB50} of these five cases:

- $CR = 9.8$ $M_{FB50} = 19.5^\circ$;
- $CR = 11$ $M_{FB50} = 22.5^\circ$;
- $CR = 12$ $M_{FB50} = 24.5^\circ$;
- $CR = 13$ $M_{FB50} = 26.0^\circ$;
- $CR = 14$ $M_{FB50} = 27.0^\circ$;

A giant delay reduces the *b MEP* of the engine, so having a big CR do not guarantee a bigger power density as shown in *fig 5.25*.

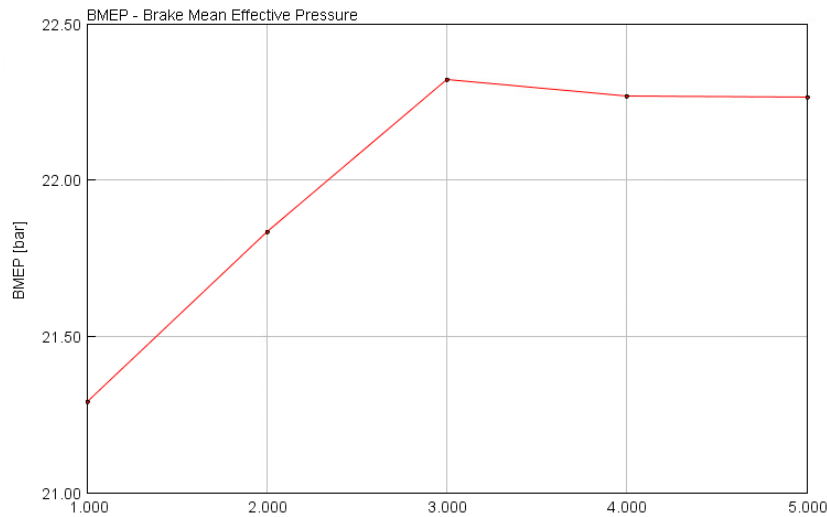


Figure 5.25: *b MEP* after the calibration

This big increase of the delay was possible thanks to the high efficiency of the engine.

5 Simulation results

The third analysis was focused on the injection rate. All cases present the same EOI (20CA before the TDCF), the same boost pressure (2.1 bar) and the same MFB50 (19,5°). We consider three different cases:

- $inj_{rate} = 5.3 \frac{g}{s}$ (value choosen for the other two studies);
- $inj_{rate} = 3.5 \frac{g}{s}$;
- $inj_{rate} = 4.5 \frac{g}{s}$.

In the *fig 5.26* the injection shape is shown:

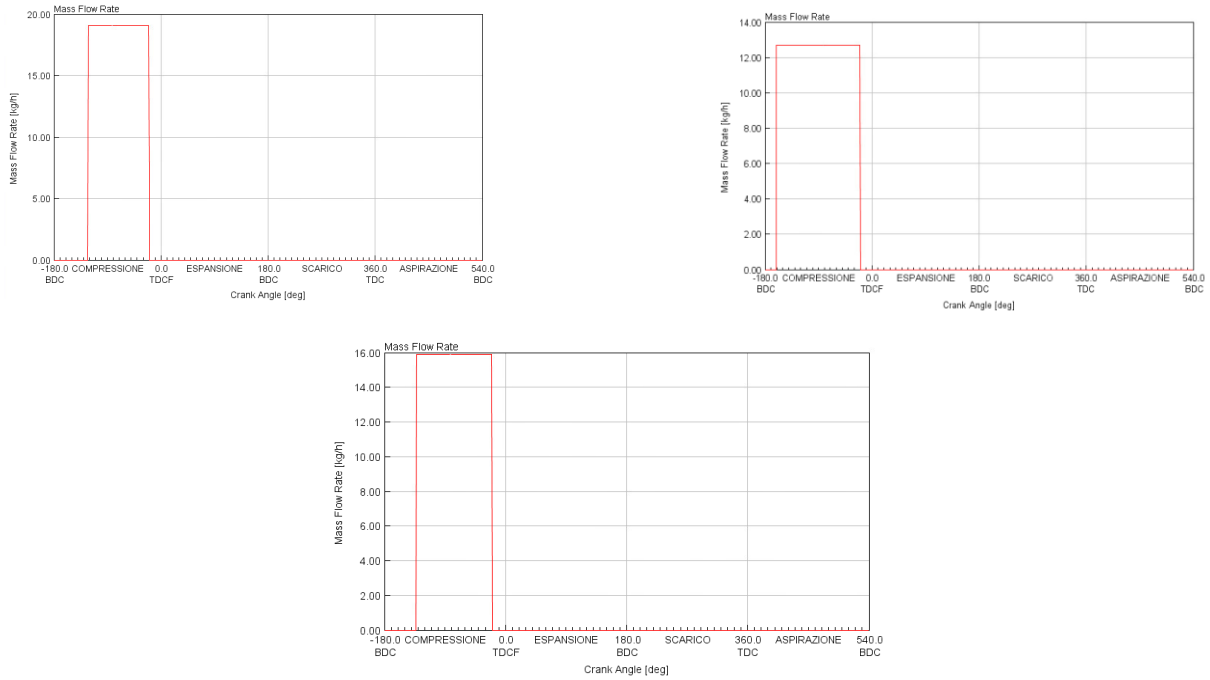


Figure 5.26: injection shapes

In this third part of the analysis the *bme_p* has not a great variation (about 1%) as shown in *fig 5.27*

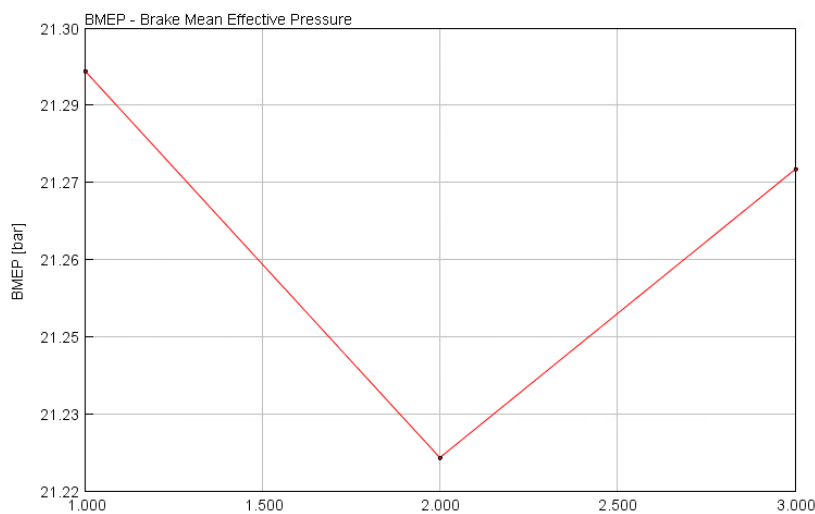


Figure 5.27: bme_p of cases studied

5 Simulation results

Also, the volumetric efficiency is constant if the injection rate is reduced as shown in *fig 5.28*.

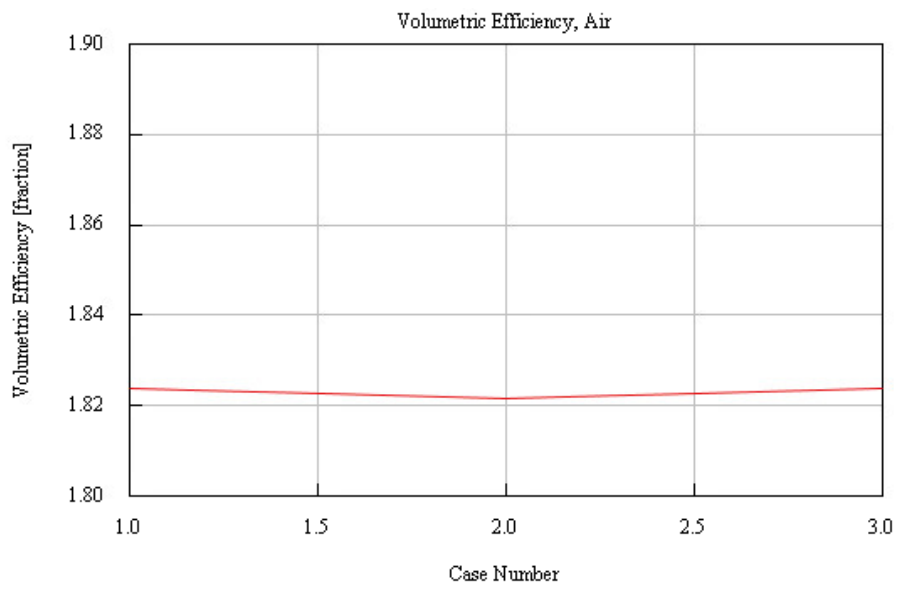


Figure 5.28: volumetric efficiency

Chapter 6

Conclusions

In this thesis we ran a lot of simulation both in GT-POWER and in CONVERGE. This thesis was really useful because we verified that the ECFM+ISSIM method could be used even at higher load points with good results (at least in the PFI). Also, using the 1D simulation in GT-POWER it was possible to analyze the effect of different parameters in the engine (both in the PFI simulation and in the DI simulation). In this study we also started investigating the source cell method and how to generate a virtual injector in CONVERGE: this will be particularly usefull in H₂ DI engine, since there are a lot of issues in the realization in the hydrogen injector. The method i salso quite interesting, because the CAD of the engine have not to be modified, so for the future analysis only the fuel and its property will be changed. Also thanks to this thesis two CH₄ engine models (PFI and DI) were created; in the future, this setups will be used in comparison with a pure H₂ or a CNG-H₂. Finally a usefull procedure was tested when no experimental data are avaiable, these can be used in the future study of H₂ engine and even in other type of engines.

Nomenclature

ACRONYMS

A/D	Analog to Digital converter
A/F	Air to Fuel ratio [-]
AKTIM	Arc and Kernel Tracking Ignition Model
AMR	Adaptive Mesh Refinement
BC	Boundary Condition
BDC	Bottom Dead Center
C2C	Cycle to Cycle
CAD	Crank Angle Degree
CFD	Computational Fluid Dynamics
CFL	Courant-Friedrichs-Lewy number
CNG	Compressed Natural Gas
COV	Coefficient of Variation
CR	Compression Ratio
CRF	Centro Ricerche Fiat
DAQ	Data Acquisition
DENERG	Dipartimento Energia Politecnico di Torino
DG	Discontinuous Galerkin
DI	Direct injection
DIFF	Differential connection
DNL	Differential Non-Linearity
ECFM	Extended Coherent Flame Model
ECFM-3Z	3-Zones Extended Coherent Flame Model
EEM	Explicit Euler method
EEMS	Electronic Engine Management System
EGR	Exhaust Gas Recirculation
EOI	End of injection
EVC	Exhaust Valve Closing
EVO	Exhaust Valve Opening
FFT	Fast Fourier Transform
FIFO	First In First Out
FSD	Flame Surface Density $[m^2/m^3]$
FSO	Full Scale Output
GUI	Graphical User Interface
HF	High Frequency
HR	Heat Release [J]
HRR	Heat Release Rate $[J\ deg^{-1}]$
HWA	Hot Wire Anemometer
IAC	Idle Air Control
IC	Initial Condition
ICE	Internal Combustion Engine
ICN	Implicit Crank-Nicolson method
IMEP	Indicated Mean Effective Pressure
ISSIM	Imposed Stretch Spark Ignition Model
IVC	Intake Valve closing
IVO	Intake Valve Opening
LF	Low Frequency

LHS	Left Hand Side
MFB	Mass Fraction Burned [–]
NRSE	Single Ended Nonreferenced
ODE	Ordinary Differential Equation
RHS	Right Hand Side
SA	Spark Advance
SOI	Start of injection
STL	StereoLithography file
TDC	Top Dead Centre
TDMS	Technical Data Managment Streaming
TKE	Turbulent Kinetic Energy [J kg ⁻¹]
TPS	Throttle Position Sensor
UDF	User Defined Function
UEGO	Universal Exhaust Gas Oxygen
VI	Virtual Instrument
VTG	Variable Geometry Turbocharger

SYMBOLS

α	Air to fuel ratio	[–]
α_Σ	Turbulent flame stretching coefficient	
$\Delta\theta$	Crank angle increment [deg]	
δ_L	Laminar Flame Thickness	[m]
\dot{m}_a	Air mass flow rate	[kg s ^{−1}]
\dot{m}_f	Fuel mass flow rate	[kg s ^{−1}]
η	Error estimate function	
η_t	Kolmogorov length scale	[m]
λ_v	Volumetric efficiency	
q	Heat flux per unit area	[W/m ²]
\mathbf{v}	Velocity vector field	[m s ^{−1}]
M_x	Molar mass of componet X	[mol]
ν	Kinematic viscosity	[m ² /s]
Ω	Control volume	[m ³]
\bar{r}_Σ^{ign}	Ignition FSD reaction rate ($\partial\Sigma_{ign}/\partial t$)	[s ^{−1}]
\bar{r}_c	Burned gas volume fraction reaction rate ($\partial c/\partial t$)	[s ^{−1}]
$\partial\Omega$	Control volume boundary	[m ²]
Φ	Air to fuel equivalence ratio a/a_{st}	[–]
Σ	Flame surface density models	[m ² /m ³]
Θ	Reduced temperature	[–]
θ	Crank angle	[deg]
ε	Turbulence dissipation	[J kg ^{−1} s ^{−1}]
C_{surf}	Wrinkling parameters initial flame kernel	
f_c	Cut-off frequency	[Hz]
f_s	Sampling frequency	[S/s]
G_a	Air mass flow rate	[kg h ^{−1}]
G_f	Fuel mass flow rate	[kg h ^{−1}]
GS	Grid scaling factor	
h	Grid lenght	
h_v	Valve lift	[m]
γ	Heat capacity ratio (cp/cv)	[–]
k	Turbulence kinetic energy	[J kg ^{−1}]
n	Engine speed	[rpm]
p	Pressure	[Pa]
s_L	Laminar flame speed	[ms ^{−1}]
S_c	Schmidt number	[–]
T	Temperature	[K]
u^+	Dimensionless velocity	[–]
u_t	friction velocity	[m s ^{−1}]
y^+	Normalized wall distance	[–]
Y_x	Mass fraction of componet X	[–]

NOTIFICATIONS

<i>a</i>	Scalar (lightface italic letters)
$\langle \ \rangle$	Weighted arithmetic mean
$\langle\langle \ \rangle\rangle$	Ensemble Average
$[\]$	Use to denote that what is inside is a vector
<i>a</i>	Vector (lower boldface Roman letters)
A	Matrices (upper boldface Roman letters)
α	Tensors (boldface Greek letters)
$\overline{\quad}$	Reynolds mean value
\prime	Reynolds fluctating value
<i>T</i>	Transpose
\parallel	Parallel projection
\perp	Normal projection
<i>h</i>	Numerical solution

Bibliography

- [1] Marco Mina. “*Allestimento e strumentazione di un banco prova, sviluppo di un programma di acquisizione dati ed analisi sperimentale della combustione in un motore “downsized” a gas naturale*”. Italian. diploma thesis. Politecnico di Torino.
- [2] Paolo De Angelis. “*Simulation of the ensemble and cycle-resolved combustion processes in a NG-H2 engine*”. Italian. diploma thesis. Politecnico di Torino.
- [3] G. Ferrari. “*Motori a combustione interna*”. Italian. Il capitello, 1996. isbn: 9788874889716.
- [4] Michael F. J. Brunt and Andrew L. Emtage. “*Evaluation of Burn Rate Routines and Analysis Errors*”. In: SAE Technical Paper. 970037. SAE International, Feb. 1997. DOI: 10.4271/970037. Url: <https://doi.org/10.4271/970037>.
- [5] Robert D. Moser, John Kim, and Nagi N. Mansour. “*Direct numerical simulation of turbulent channel flow up to $Re_\tau = 590$* ” DOI: 10.1063/1.869966.
- [6] F. Moukalled, L. Mangani, and M. Darwish. “*The Finite Volume Method in Computational Fluid Dynamics. An Advanced Introduction with OpenFOAM and Matlab*”. Springer International Publishing, 2015. ISBN: 978-3-319-16873-9. doi: 10.1007/978-3-319-16874-6
- [7] Convergent Science. “*CONVERGE v2.3 Manual*”. URL: <https://convergecf.com/>
- [8] Susanna Carcano “*Finite Volume methods and discontinuous galerkin methods for numerical modelling of multiphase gas-particle flow*”. Ph.D. thesis. Politecnico di Milano.
- [9] Alfio Quarteroni “*Modellistica Numerica per Problemi Differenziali*”. Italian. 6th. Springer International Publishing, 2016. isbn: 978-88-470-5780-7. doi: 10.1007/978-88-470-5782-1.
- [10] Eric Pomraning. “*Development of Large Eddy Simulation Turbulence Models*” Ph.D. thesis. University of Wisconsin – Madison. doi: 10.13140/2.1.2035.7929 .
- [11] J.M. Duclos and O. Colin. “*Arc and Kernel Tracking Ignition Model for 3D Spark-Ignition engine calculations*”. Ed. by Kinji Tsujimura et al. Vol. 01.204. July 2001, pp. 343–350. doi: 10.1299/jmsesdm.01.204.1.
- [12] S. Richard et al.” *Proceedings of the Combustion Institute*” Vol. 31. 2005, pp. 3059–3066.
- [13] O. Colin and K. Truffin. “*A spark ignition model for large eddy simulation based on an FSD transport equation (ISSIM-LES)*”. In: vol. 33. 2. 2011, pp. 3097–3104. doi: 10.1016/j.proci.2010.07.023.
- [14] *Combustion Engines Development. Mixture Formation, Combustion, Emissions and Simulation*. Ed. by G.P. Merker. Ed. by C. Schwarz. Ed. by R. Teichmann. Springer Berlin Heidelberg, 2012. isbn: 978-3-642-02951-6. doi: 10.1007/978-3-642-14094-5.
- [15] Jaehong Kim and Richard W. Anderson. “*Spark Anemometry of Bulk Gas Velocity at the Plug Gap of a Firing Engine*”. In: SAE Technical Paper. SAE International, Oct. 1995. doi: 10.4271/952459.
- [16] F. A. Soldera et al. “*Description of the discharge process in spark plugs and its correlation with the electrode erosion patterns*”. In: IEEE Transactions on Vehicular Technology 53.4 (July 2004), pp. 1257–1265. issn: 0018-9545. doi: 10.1109/TVT.2004.830977.

- [17] Colin O. and Benkenida A. “*The 3-Zones Extended Coherent Flame Model (Ecfm3z) for Computing Premixed/Diffusion Combustion*”. In: Oil & Gas Science and Technology-revue De L’Institut Francais Du Petrole - OIL GAS SCI TECHNOL. Vol. 59, pp. 593–609. doi: 10.2516/ogst:2004043.
- [18] T. Poinso and D. Veynante. “*Theoretical and Numerical Combustion*”. Edwards, 2001. isbn: 9781930217058. url: <https://books.google.it/books?id=HMvCQgAACAAJ>.
- [19] Prashant Goel. “*3D-CFD Simulation of the Combustion Process in a NG Engine by Adopting a LFS Submodel from Detailed Kinetic Mechanism*”. Master’s thesis. Politecnico di Torino.
- [20] Convergent Science. “*CONVERGE v3.0 Manual*”. URL: <https://convergecf.com/>
- [21] GT-SUITE. “*Help in the GT-Suite template*” URL: <https://www.gtisoft.com/>
- [22] Stefania Zanforlina and Alberto Boretti “*Numerical analysis of methane direct injection in a single-cylinder 250 cm³ spark ignition engine.*” In: ScienceDirect Paper. 2015